PB 296211

REPORT NO.
UCB/EERC-78/27
NOVEMBER 1978

EARTHQUAKE ENGINEERING RESEARCH CENTER

CYCLIC LOADING TESTS OF MASONRY SINGLE PIERS VOLUME 1 – HEIGHT TO WIDTH RATIO OF 2

by

PEDRO A. HIDALGO
RONALD L. MAYES
HUGH D. McNIVEN
and
RAY W. CLOUGH

Report to:

National Science Foundation
Masonry Institute of America
Western States Clay Products Association
and the
Concrete Masonry Association of California and Nevada

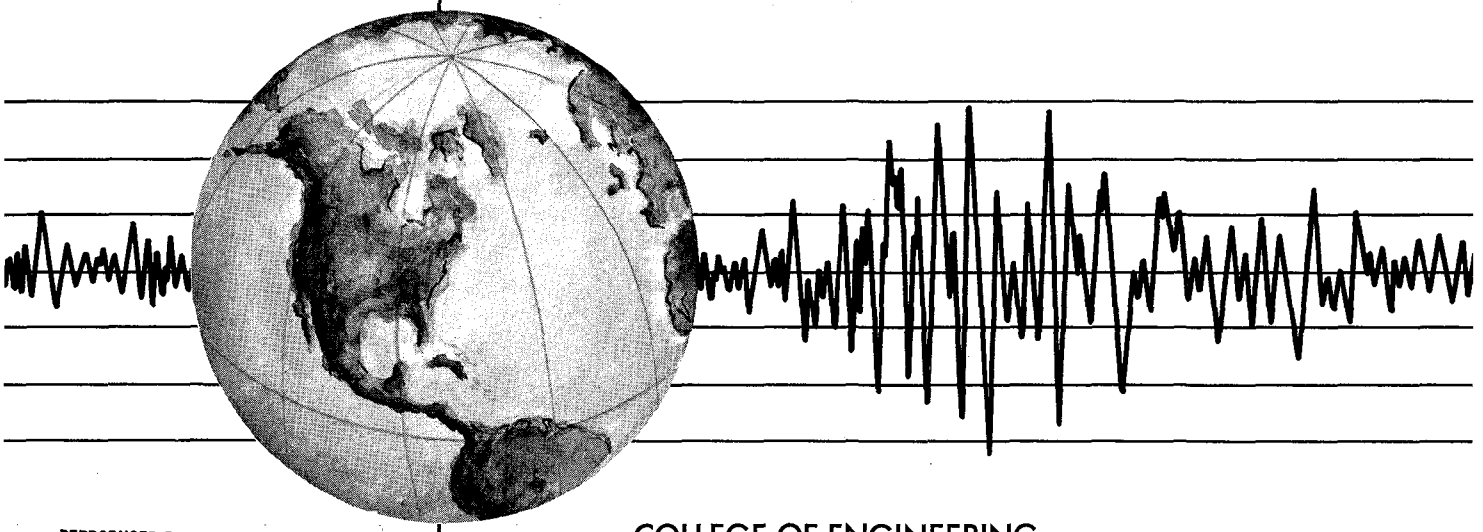

COLLEGE OF ENGINEERING

UNIVERSITY OF CALIFORNIA · Berkeley, California

CYCLIC LOADING TESTS OF MASONRY SINGLE PIERS
VOLUME 1 - HEIGHT TO WIDTH RATIO OF 2

by

Pedro A. Hidalgo

Ronald L. Mayes

Hugh D. McNiven

and

Ray W. Clough

Report to

National Science Foundation
Masonry Institute of America
Western States Clay Products Association
Concrete Masonry Association of California and Nevada

Report No. UCB/EERC-78/27

Earthquake Engineering Research Center
College of Engineering
University of California
Berkeley, California

November 1978

ABSTRACT

This report presents the results of fourteen cyclic, in-plane shear tests on fixed ended masonry piers having a height to width ratio of 2. These fourteen tests form part of a test program consisting of eighty single pier tests. Subsequent reports will present test results of the additional sixty-six tests. Each subsequent report will be based on the height to width ratio of the piers.

The test setup was designed to simulate insofar as possible the boundary conditions the piers would experience in a perforated shear wall of a complete building. Each test specimen was a full scale pier 80 inches high and 40 inches wide. Two types of masonry construction were used; a hollow clay brick type, that used an 8 inch wide unit, and a double wythe grouted core clay brick, 10 inch thick wall, that consisted of two wythes 3½ inches thick and a 3 inch grouted core. The variables included in the investigation were the quantity of reinforcement and the type of grouting.

The results are presented in the form of hysteresis envelopes, graphs of stiffness degradation, energy dissipation and shear distortion, and tabulated data on the ultimate strength and hysteresis indicators. A discussion of these test results is presented but no definitive conclusions are offered. These will be included in a final report at the completion of the eighty tests.

ACKNOWLEDGEMENTS

This investigation was jointly sponsored by the National Science Foundation under Grant ENV76-04265 and the Masonry Institute of America, the Western States Clay Products Association and the Concrete Masonry Association of California and Nevada. The authors wish to express their appreciation for technical advice and encouragement received from Mr. Walter Dickey, Mr. John Tawresey, Mr. Donald Wakefield, Mr. Dick Wasson, Mr. James Amrhein, Mr. Stuart Beavers and Mr. Don Prebble. D. A. Sullivan and Co. constructed all the test specimens. Many thanks also are due to Messrs. David Steere, Ivo Van Asten, Robert Robinson, Derald Clearwater, John McNab and Steve Miller of the Earthquake Engineering Research Center for their electronic and machine shop work. The authors also wish to thank the students Bjorn Sveinsson, John Baniesrael and Joyce Pfeiffer for their help in performing the tests and reducing the test data, and Mrs. B. Bolt for reviewing the manuscript. The computing facilities to reduce the data were provided by the Computer Center at the University of California, Berkeley.

The typing was done by Ms. Shirley Edwards and the drafting by Ms. Gail Feazell.

TABLE OF CONTENTS

LIST OF TABLES

LIST OF FIGURES

1. INTRODUCTION

1.1. The Multistory Masonry Building Research Program

A multistory masonry building research program was initiated at the Earthquake Engineering Research Center in September 1972, and has continued for the past six years. After an extensive review of the literature[3,4]* dealing with resistance of masonry to earthquakes, it was concluded that shear walls penetrated by numerous window openings (Fig. 1.1) were the components of multistory masonry buildings most frequently damaged in past earthquakes, and it was decided that an experimental study of the seismic behavior of such components was necessary.

Two structural components can be identified in the shear wall of Fig. 1.1, the piers and the spandrel beams. In order to study the pier behavior, a testing fixture was designed to subject typical full-scale double pier specimens to combined static vertical (gravity) and cyclic lateral (seismic) loads (Fig. 1.2). The results obtained from seventeen such specimens have been reported by Mayes et al.[5]. These results show significant variations in the pier behavior with various test parameters: type of grouting, types of reinforcement, rate of loading, etc. The results are not conclusive and demonstrate the need for more extensive tests to establish definite parametric relationships.

The cost of the double pier tests, both in money and time, precluded carrying out by this procedure the extensive parametric

---

* References are arranged in alphabetical order of the authors' names, and are listed at the end of the text.

variations that are needed, and consequently, a single pier test system was designed which greatly simplified the investigation (Fig. 1.3). A series of eighty single pier tests was programmed, which considers the following test parameters: type of masonry construction, height to width ratio of the piers, type of grouting, and amount and distribution of both vertical and horizontal steel reinforcement. The present report deals with the experimental results of specimens with a height to width ratio of 2.

1.2 Objectives and Scope of the Single Pier Test Program

In determining the strength of masonry piers and panels, the first step is to evaluate the mode of failure. Because most failures in past earthquakes have been characterized by diagonal cracks, many research programs have concentrated on this type of failure mechanism. Test techniques used by Blume[1], Greenley and Cattaneo[2], and others induce the diagonal tension or shear mode of failure. Scrivener[12], Meli[9], Williams[13] and Priestley and Bridgeman[10] recognized that there are two possible modes of failure for cantilever piers. In addition to the shear or diagonal tension mode, they recognized that for certain piers, a flexural failure could occur. This mechanism is characterized by yielding of the tension steel of the wall, followed by a secondary failure at the compressive toe, with associated buckling of the reinforcement once confinement is lost. Meli[9] described the flexural failure as similar to that of an under-reinforced concrete beam; i.e., extensive flexural cracking and strength limited by yielding of the reinforcement,with failure finally due either to crushing of the compressive corner or to rupture of the extreme bars.

Because the double pier tests were the first fixed ended piers

to be tested cyclically, the objective of those tests was to determine the effect of various parameters and compare the results with those already known for cantilever piers. Both the shear and flexural modes of failure were included in that investigation.

One of the main objectives of the single pier test program was to investigate thoroughly the effects of different parameters in the shear mode of failure. It was evident from the double pier test program that the flexural mode of failure in a fixed-ended pier has desirable inelastic characteristics, although these are not as desirable as those obtained by Priestley[11] in cantilever piers. Furthermore, it was recognized that for fixed-ended piers, with height to width ratios commonly found in multistory buildings, the amount of horizontal reinforcement required to force a flexural mode of failure is substantially greater than required by current codes. Therefore, it was decided to investigate the effects of lesser amounts of horizontal reinforcement on the shear mode of failure to determine if desirable inelastic behavior could be obtained.

The fourteen tests reported herein are a part of a total program of eighty single pier tests; a matrix characterizing the first sixty-three tests is shown in Table 1.1. The parameters for the remainder of the tests (seventeen) will be selected after an evaluation of these sixty-three. The test parameters, other than the type of construction and height to width ratio, include the amount of reinforcement and the effect of partial grouting. Hollow concrete block piers having height to width ratio of 2 were not included in the single pier test program because such piers were investigated in the seventeen double pier tests.

This report presents the results for piers with a height to width ratio of 2,of which nine tests were performed on hollow clay brick

specimens (HCBR) and five on double wythe grouted core clay brick specimens (CBRC). Two subsequent reports will present the results obtained from the single pier specimens with height to width ratios of 1 and 0.5. The results on the series of seventeen specimens which will complete the proposed research program will be presented in a separate report.

TABLE 1.1

SINGLE PIER TEST PROGRAM*
(Number of test specimens)

HEIGHT: WIDTH RATIO \ TYPE OF MASONRY	HOLLOW CLAY BRICK (HCBR)	DOUBLE WYTHE GROUTED CORE CLAY BRICK (CBRC)	HOLLOW CONCRETE BLOCK (HCBL)	TOTAL NUMBER
2 : 1	9	5	0	14
1 : 1	13	7	11	31
1 : 2	6	6	6	18

*Last 17 tests to be decided after this phase is completed

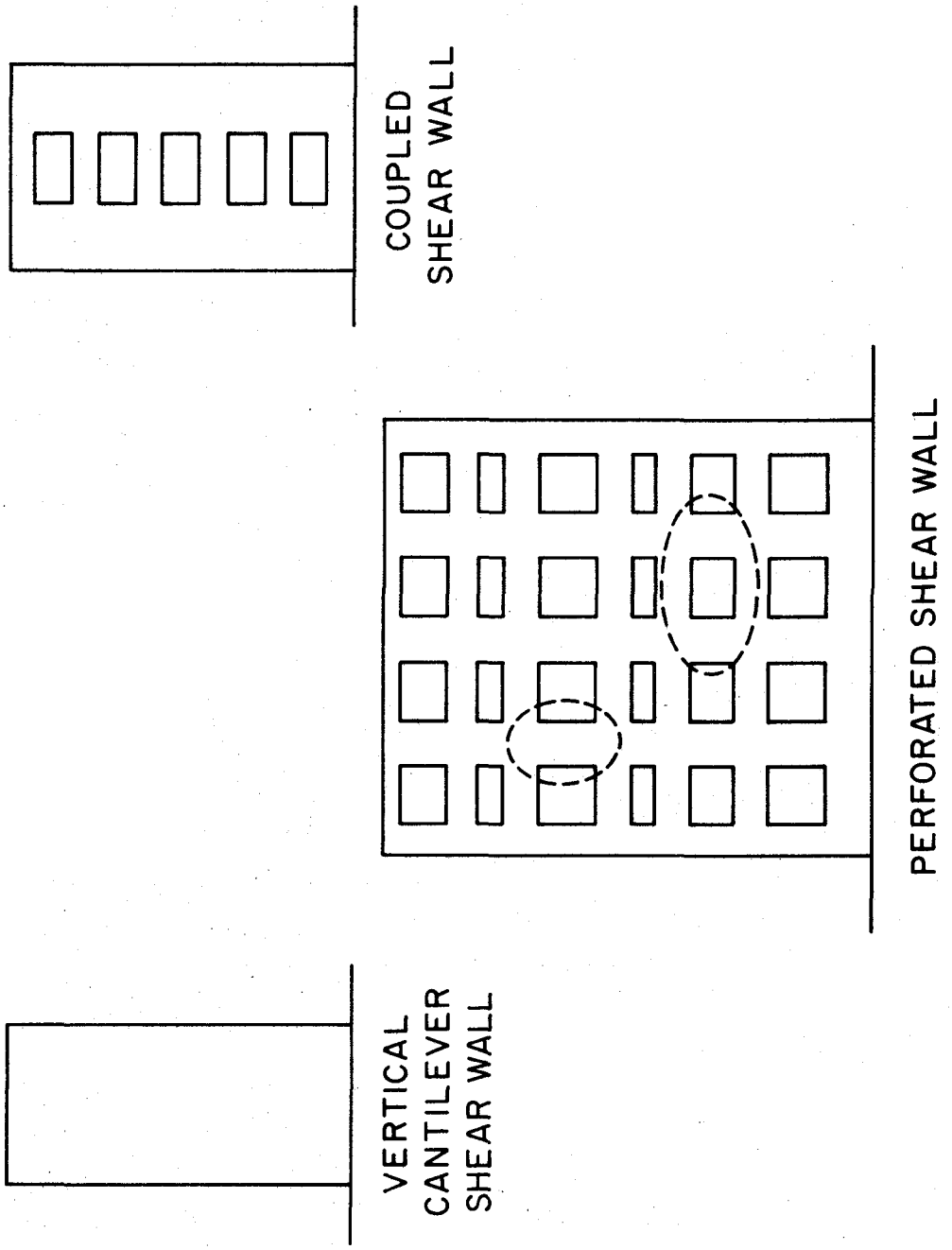

FIG. 1.1 TYPICAL SHEAR WALLS

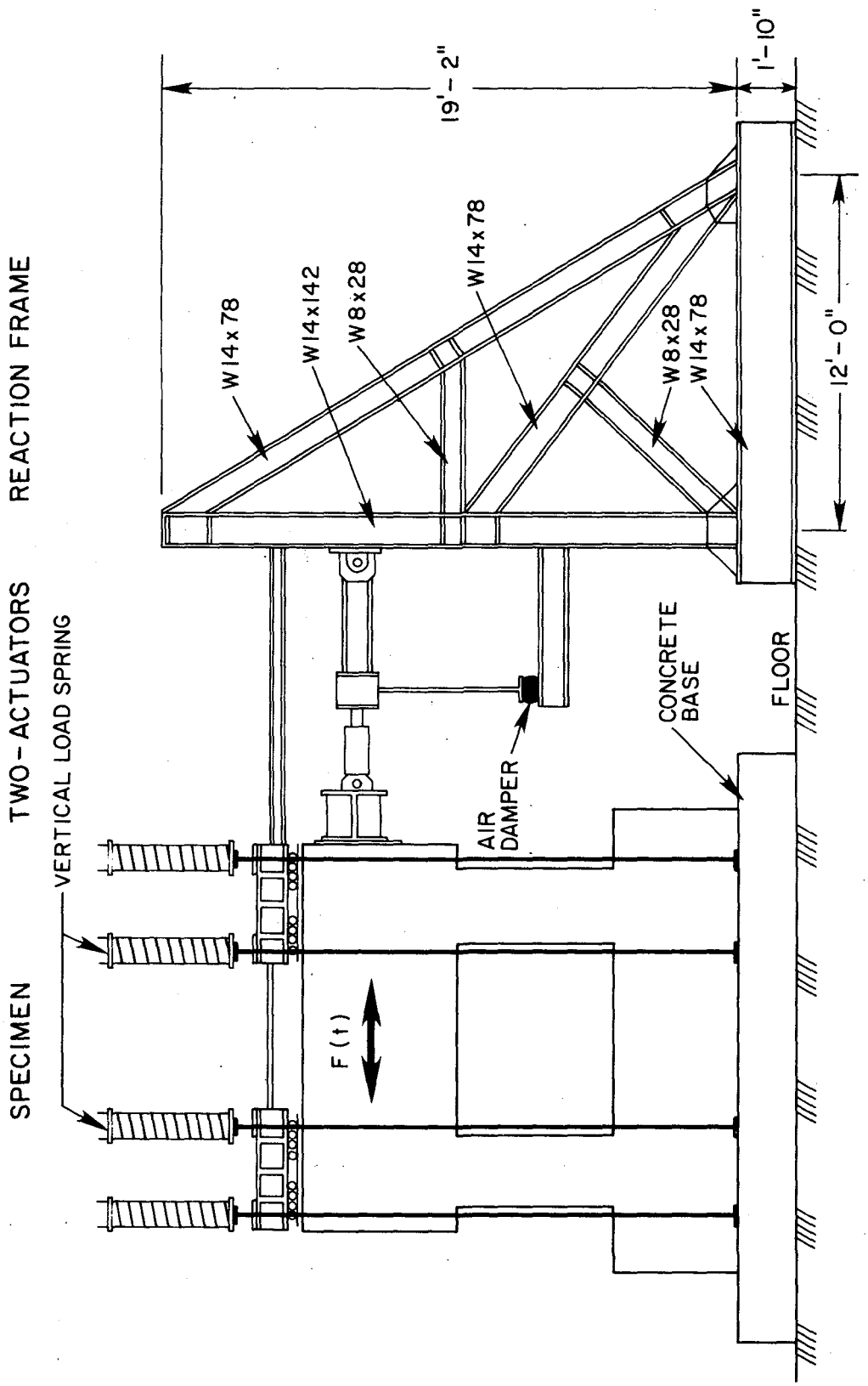

FIG. 1.2 DOUBLE PIER TEST SETUP

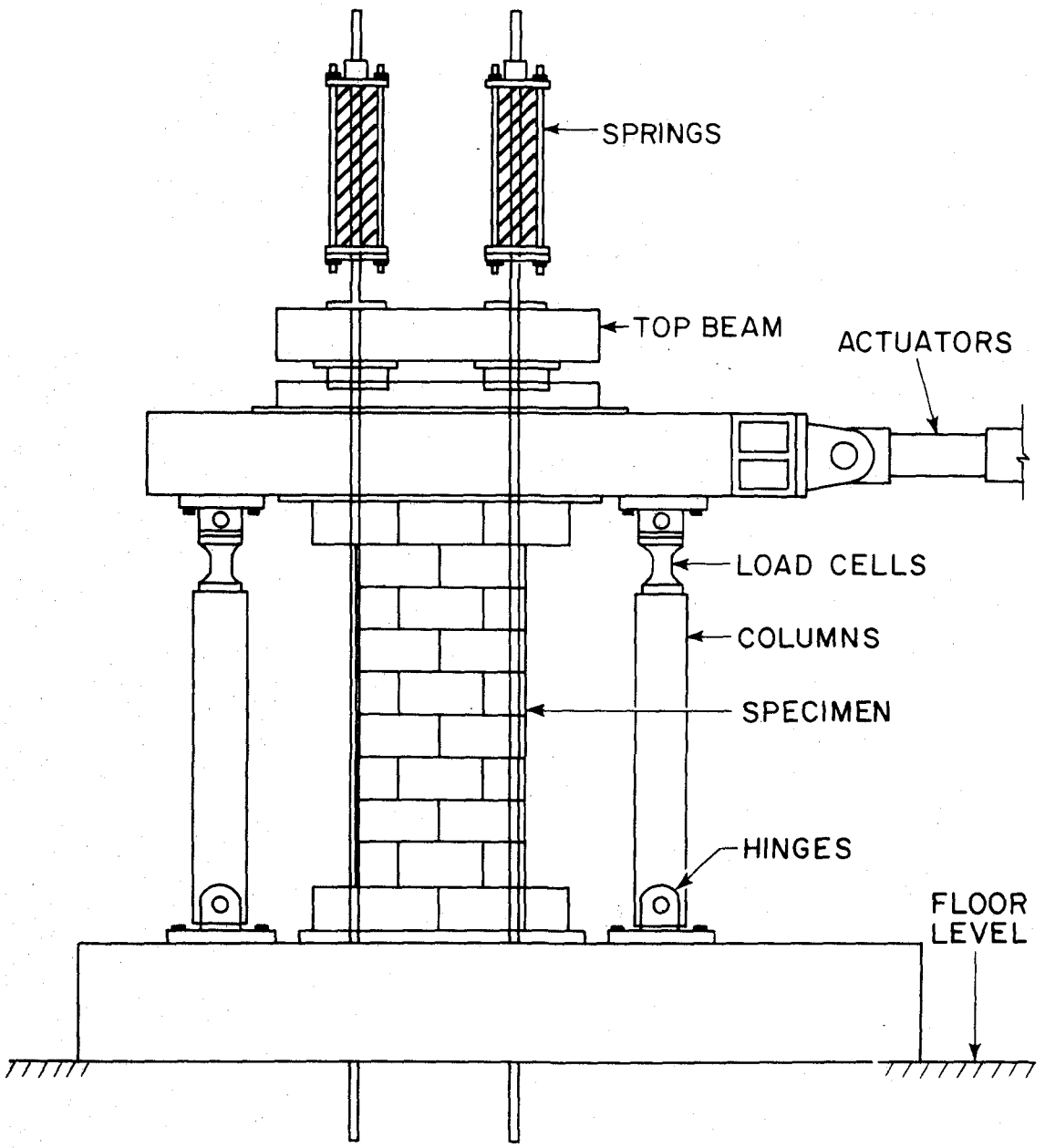

FIG. 1.3 SINGLE PIER TEST SETUP

2. TEST SPECIMENS

2.1 Design and Construction of Specimens

The overall dimensions of the test specimens discussed here are shown in Fig. 2.1. They are the same for all fourteen piers except for the thickness, which is 7-3/8 inches for the hollow clay brick piers (HCBR) and 10 inches for the double wythe grouted core clay brick piers (CBRC).

The HCBR panels were constructed from standard two-core hollow clay bricks, nominally 8 inches wide x 4 inches high x 12 inches long as shown in Fig. 2.3(a). The cored area of each brick is approximately 57.4 square inches and the ratio of net to gross area is 67%.

The CBRC piers were constructed from two wythes of "solid" clay bricks nominally 4 inches wide x 4 inches high x 12 inches long as shown in Fig. 2.3(b). The grouted space between the wythes was 3 inches wide and was filled after the steel reinforcement had been placed in position. The bricks have a core (hollow) area slightly less than 25% of the gross area. The Uniform Building Code definition of a "solid brick" is one with 25% or less coring.

The piers were constructed on 0.75 inch thick steel plates as shown in Fig. 2.2. A similar plate was added on top of the pier after the grout was poured. Both plates had holes to permit anchorage of the vertical steel reinforcement and keys to provide an adequate shear transfer between the masonry pier and the steel plate. The plates also had welded bolts and holes to anchor the pier to the test rig.

Six of the nine HCBR piers were fully grouted. The other three

were partially grouted. Partial grouting consists of grouting the cores containing the vertical reinforcement and the bond beams containing the horizontal reinforcement. All the CBRC piers had the 3 inch core between the wythes fully grouted and have been termed "solid grouted".

The series of tests was planned to determine the effect of the quantity of steel reinforcement and of partial grouting on the strength and deformation properties of the piers, considering combinations of steel and grouting as shown in Table 2.1. Details of the reinforcing bar arrangement are shown in Fig. 2.4(a) for the HCBR piers and in Fig. 2.4(b) for the CBRC piers. The actual position of the vertical reinforcement is indicated in Fig. 2.1. When horizontal reinforcement was used, the bars were evenly distributed over the height of the pier.

The HCBR piers were tested six months after construction. The first of the CBRC piers (No. 5) was tested 42 days, the last (No. 1) 70 days after the grout was poured.

2.2 Material Properties

Table 2.2 shows the mechanical properties of the materials used in the construction of the test specimens. The specimens used to determine the material properties are shown in Fig. 2.3(a) and 2.3(b).

The tests of the single masonry units followed the ASTM C67-73 Specification[8] and were based on five samples for each test.

The joint mortar was specified as standard ASTM Type M (i.e., 1 Cement: 1/4 Lime: 2 1/4 - 3 Sand). The grout was specified as 1 Cement: 3 Sand: 2G, where G refers to 10 mm maximum size local gravel. Because the specimens were not constructed or grouted at the same time, the mortar and grout strength varied according to normal workmanship. A

minimum of four samples of mortar or of both mortar and grout was taken from each batch used during construction.

ASTM A615 Grade 40 steel was specified for both the vertical and horizontal steel reinforcement. Three samples of each bar size were tested to determine the properties listed in Table 2.2.

Six prisms for uniaxial compression tests and three square panels for diagonal tension tests were constructed from the same mortar and grout used in each set of wall panels. Three of the six prisms had a height to thickness ratio of 5. The other three had a height to thickness ratio of 1.5 for the HCBR piers and equal to 2.0 for the CBRC piers. All prism tests were performed at a loading rate of 100,000 lb/min. The compressive strengths are shown in Table 2.2.

The compression test of the prisms having a height to thickness ratio of 5 was also used to determine the modulus of elasticity of the HCBR and the CBRC types of masonry (Fig. 2.5). The axial deformations were measured with mechanical gages attached to both sides of the prism, over a length of 20 inches. The readings were averaged and the modulus of elasticity computed; results are shown in Table 2.3(a) for the HCBR and Table 2.3(b) for the CBRC type of masonry.

The square panels were tested as shown in Fig. 2.6 at a loading rate of 20,000 lb/min. The ultimate load for the square panel tests is also shown in Table 2.2.

The mortar, grout, prism and square panel samples were cured under the same normal atmospheric conditions as the piers; also the prism and square panel tests were performed during the tests of the corresponding piers.

TABLE 2.1

TEST PROGRAM

Pier General Characteristics	Specimen Designation	Test Frequency (cps)	Grouting Full(F) Partial(P) Solid(S)	Reinforcing Steel	
				Vertical	Horizontal
Masonry type: Hollow Clay Brick	HCBR-21-1	0.02	F	No	No
Pier height: H = 80 in	-2	0.02	F	2#8	No
Pier width: D = 42 in	-3	0.02	P	2#8	No
Pier thickness: 7.375 in	-4	0.02	F	2#8	2#5
Gross section area: 310 in^2	-5	0.02	P	2#8	2#5
Bearing load: 19 kip	-6	0.02	F	2#8	3#5
Bearing stress: 61 psi	-7	0.02	P	2#8	3#5
	-8	0.02	F	2#8	4#5
	-9	0.02	F	2#8	5#5
Masonry type: Double Wythe Grouted Core Clay Brick	CBRC-21-1	0.02	S	No	No
	-2	0.02	S	2#8	No
Pier height: H = 80 in	-3	0.02	S	2#8	2#5
Pier width: D = 42 in	-4	0.02	S	2#8	3#5
Pier thickness: 10 in	-5	0.02	S	2#8	5#5
Gross section area: 420 in^2					
Bearing load: 25 kip					
Bearing stress: 60 psi					

TABLE 2.2

MATERIAL PROPERTIES

(Average values. Number in parenthesis indicate the standard deviation as percent of average value)

		HCBR-21	CBRC-21
Masonry unit gross compressive strength (psi)		5816 (6%)	9422 (4%)
Masonry unit net tensile strength (psi)		466 (19%)	303 (24%)
Mortar compressive strength (psi)		4380 (10%)	4438 (10%)
Grout compressive strength (psi)		5175 (17%)	4088 (19%)
Prism (2:1) compressive strength (psi)(*)		4806 (3%)	3384 (5%)
Prism (5:1) compressive strength (psi)(*)		4502 (8%)	3315 (5%)
Ultimate load of square panel (kip)(*)		192 (8%)	197 (9%)
Vertical reinforcement	Yield strength (ksi)	47.3 (1%)	47.3 (1%)
	Ultimate strength (ksi)	81.0 (2%)	81.0 (2%)
	Modulus of elasticity (ksi)	30580	30580
	Yield strain (in/in)	0.0017	0.0017
	Strain hardening strain (in/in)	0.0101	0.0101
Horizontal reinforcement	Yield strength (ksi)	49.7 (3%)	49.7 (3%)
	Ultimate strength (ksi)	75.4 (1%)	75.4 (1%)
	Modulus of elasticity (ksi)	29720	29720
	Yield strain (in/in)	0.00175	0.00175
	Strain hardening strain (in/in)	0.0126	0.0126

(*) Only fully grouted specimens considered

TABLE 2.3(a)

MODULUS OF ELASTICITY MEASUREMENTS FOR HOLLOW CLAY BRICK WALLS
(Area of prism = 85.73 in^2)

LOAD P (kip)	STRESS σ (ksi)	$\Delta\sigma$ (ksi)	STRAIN ε (in/in)	$\Delta\varepsilon$ (in/in)	$E = \frac{\Delta\sigma}{\Delta\varepsilon}$ (ksi)
SPECIMEN 1. Gage length = 19.6 in					E_1 = 2695 ksi
50	0.583	0	2.17×10^{-4}	0	—
100	1.166	0.583	4.08	1.91×10^{-4}	3054
150	1.750	1.166	6.62	4.45	2621
200	2.333	1.750	9.43	7.26	2410
SPECIMEN 2. Gage length = 19.5 in					E_2 = 2362 ksi
50	0.583	0	2.18×10^{-4}	0	—
100	1.166	0.583	4.62	2.44×10^{-4}	2390
150	1.750	1.166	7.18	5.00	2333
SPECIMEN 3. Gage length = 20.1 in					E_3 = 2285 ksi
50	0.583	0	2.11×10^{-4}	0	—
100	1.166	0.583	4.48	2.37×10^{-4}	2461
150	1.750	1.166	7.34	5.23	2230
200	2.333	1.750	10.20	8.09	2163

Average value for HCBR piers: E = 2450 ksi

TABLE 2.3(b)

MODULUS OF ELASTICITY MEASUREMENTS FOR GROUTED CORE BRICK WALLS
(Area of prism = 116.25 in^2)

LOAD P (kip)	STRESS σ (ksi)	$\Delta\sigma$ (ksi)	STRAIN ε (in/in)	$\Delta\varepsilon$ (in/in)	$E = \frac{\Delta\sigma}{\Delta\varepsilon}$ (ksi)
SPECIMEN 1. Gage length = 19.6 in					E_1 = 2248 ksi
50	0.430	0	1.78×10^{-4}	0	
75	0.645	0.215	2.80	1.02×10^{-4}	2108
100	0.860	0.430	3.82	2.04	2108
125	1.075	0.645	5.10	3.32	1943
150	1.290	0.860	5.61	3.83	2246
175	1.505	1.075	5.99	4.21	2554
200	1.720	1.290	6.88	5.10	2530
SPECIMEN 2. Gage length = 20.0 in					E_2 = 1391 ksi
50	0.430	0	2.00×10^{-4}	0	
75	0.645	0.215	3.50	1.50×10^{-4}	1434
100	0.860	0.430	4.88	2.88	1493
125	1.075	0.645	6.00	4.00	1613
150	1.290	0.860	8.63	6.63	1297
175	1.505	1.075	10.50	8.50	1265
200	1.720	1.290	12.38	10.38	1243
SPECIMEN 3. Gage length = 19.1 in					E_3 = 1535 ksi
50	0.430	0	2.24×10^{-4}	0	
75	0.645	0.215	3.68	1.44×10^{-4}	1493
100	0.860	0.430	4.88	2.64	1629
125	1.075	0.645	6.19	3.95	1633
150	1.290	0.860	7.63	5.39	1596
175	1.505	1.075	9.73	7.49	1436
200	1.720	1.290	11.29	9.05	1426

Average value for CBRC piers: E = 1720 ksi

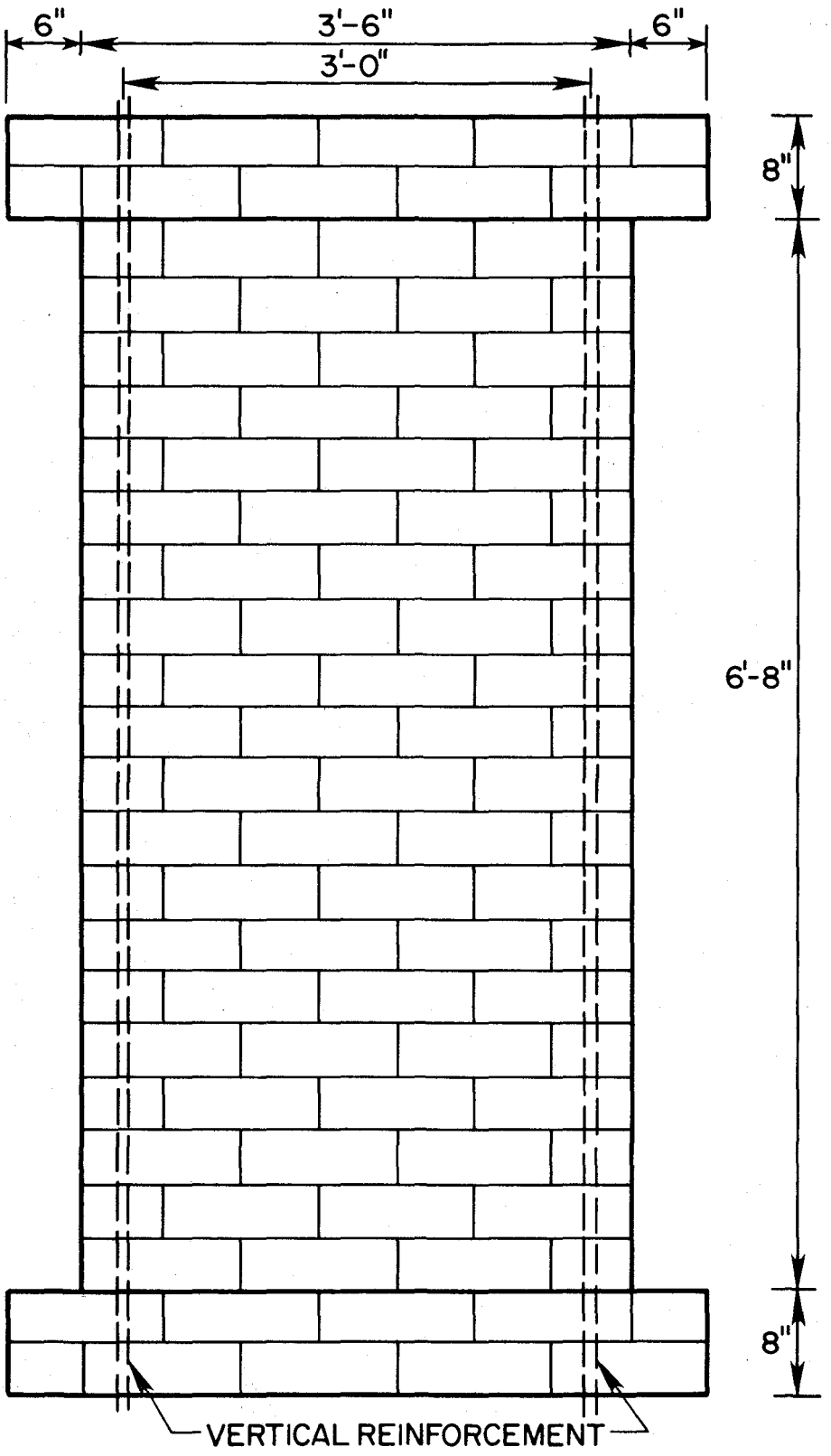

FIG. 2.1 PIER DIMENSIONS

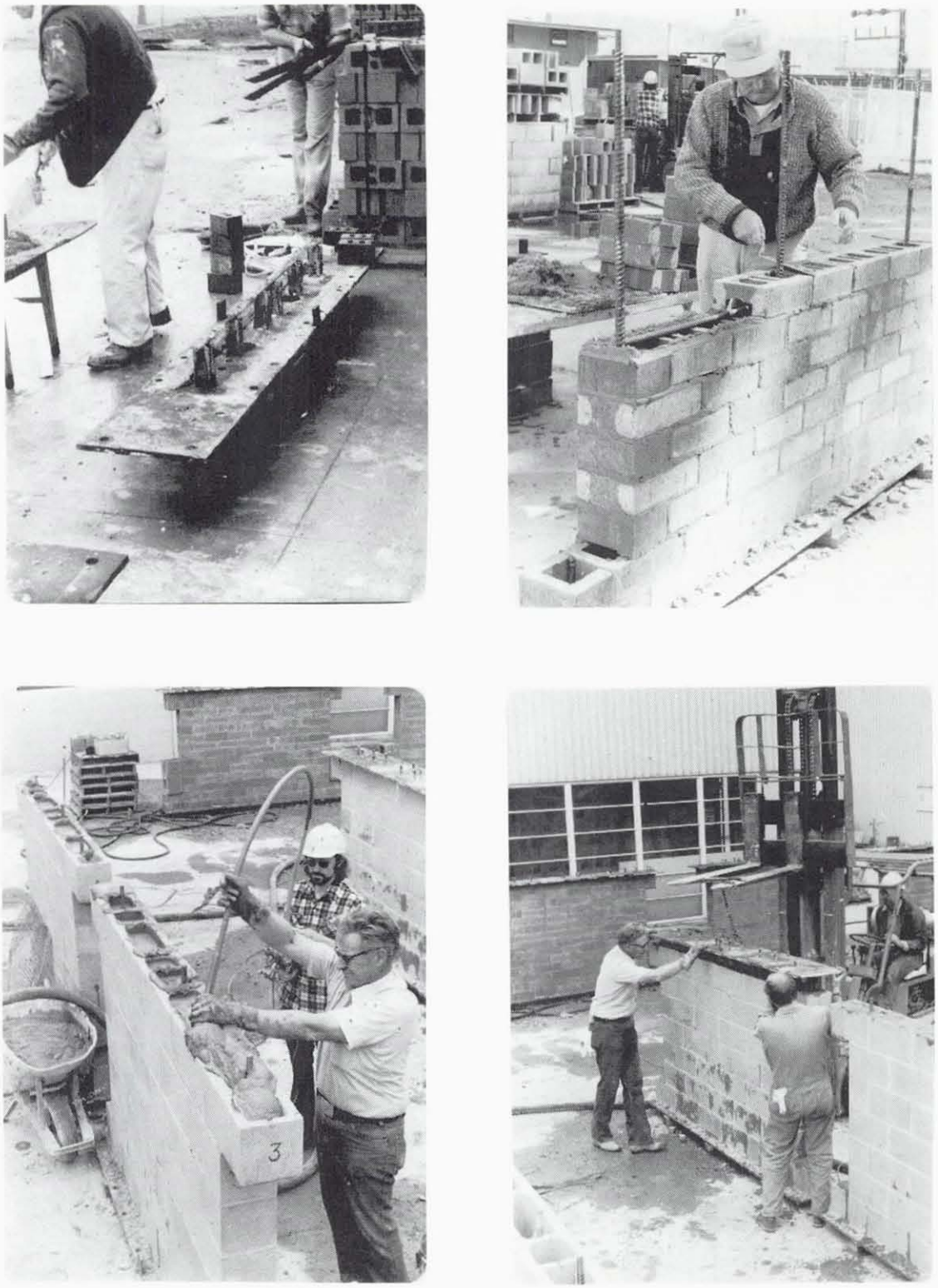

FIG. 2.2 CONSTRUCTION OF TEST SPECIMENS

BASIC MATERIALS

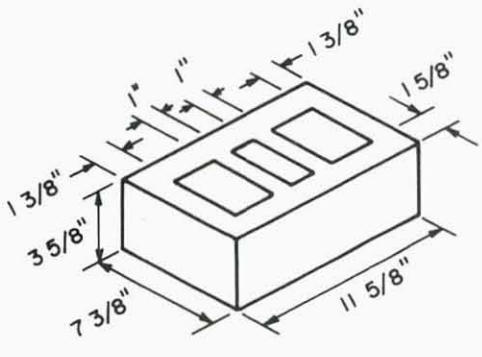

BRICK

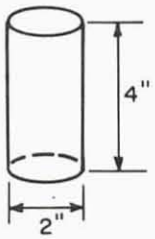

MORTAR

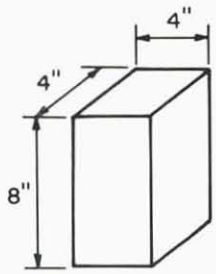

GROUT

MASONRY SUBASSEMBLAGES

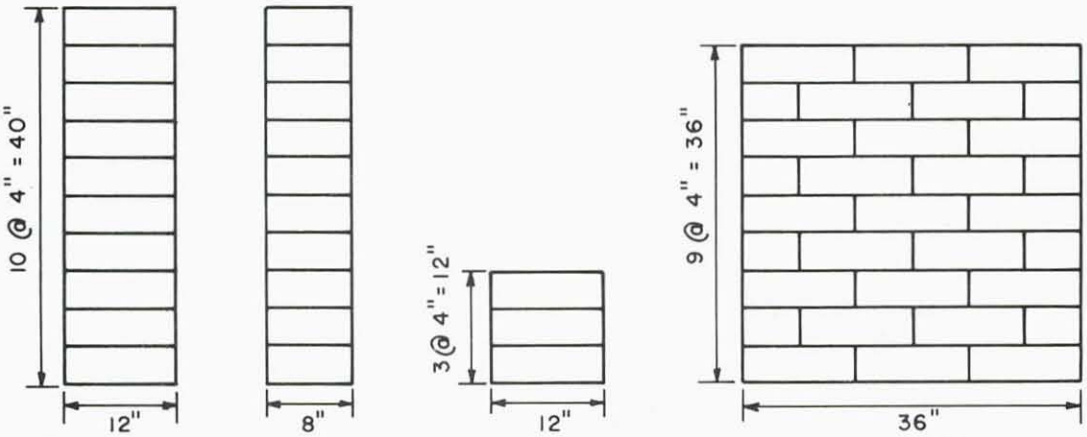

FIG. 2.3(a) SPECIMENS TO DETERMINE MATERIAL PROPERTIES (HCBR)

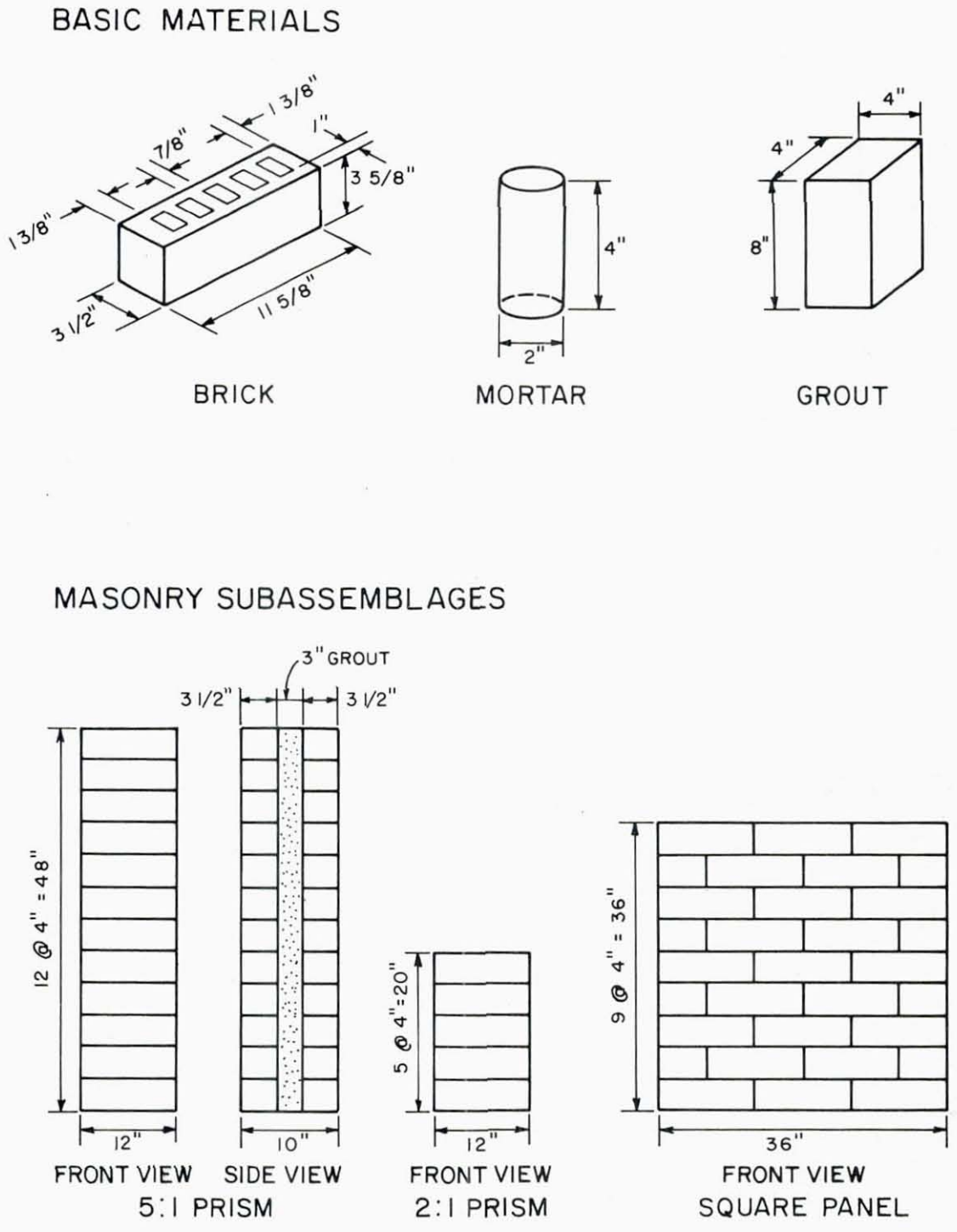

FIG. 2.3(b) SPECIMENS TO DETERMINE MATERIAL PROPERTIES (CBRC)

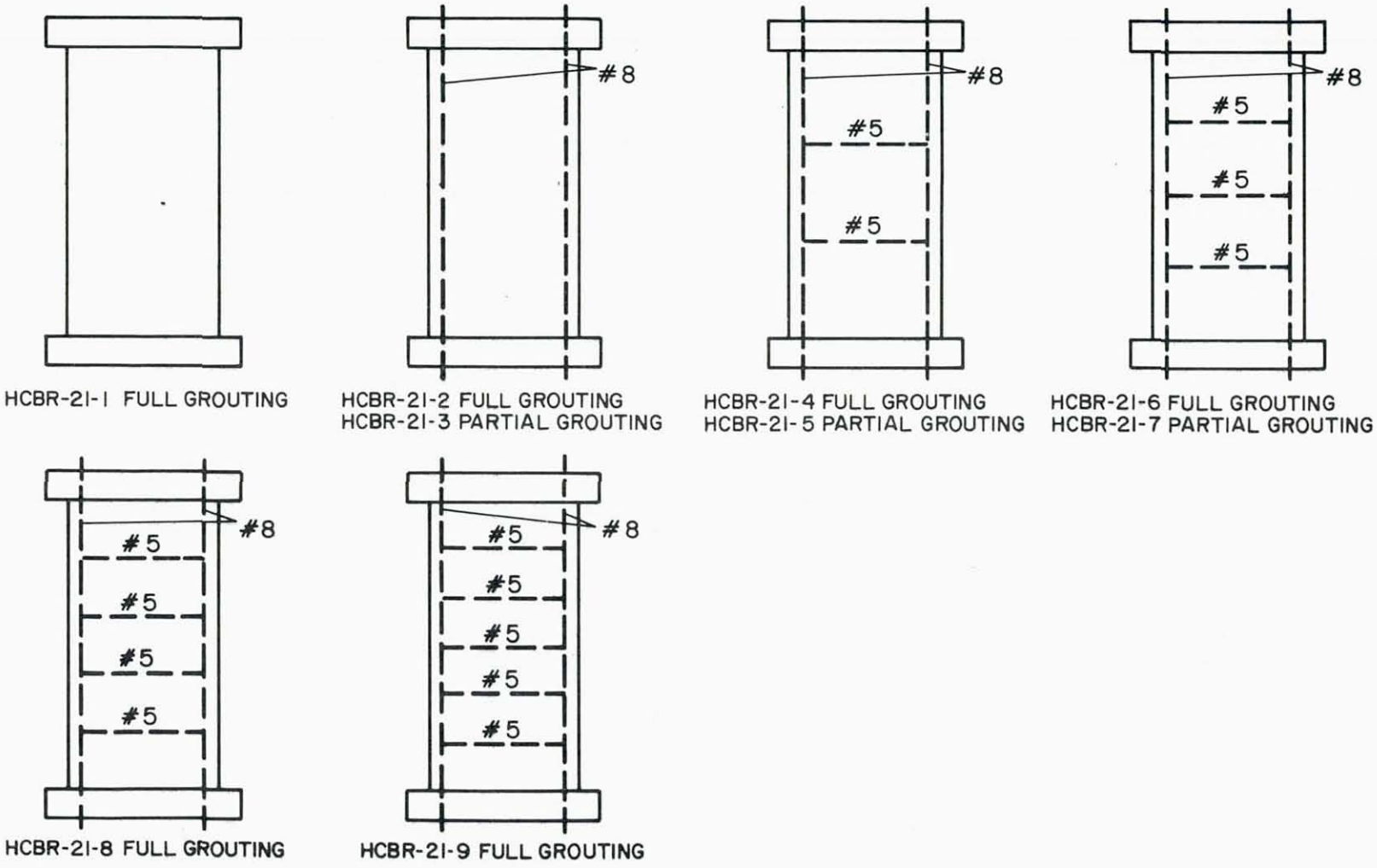

FIG. 2.4(a) REINFORCING STEEL ARRANGEMENTS FOR HOLLOW CLAY BRICK PIERS (HCBR)

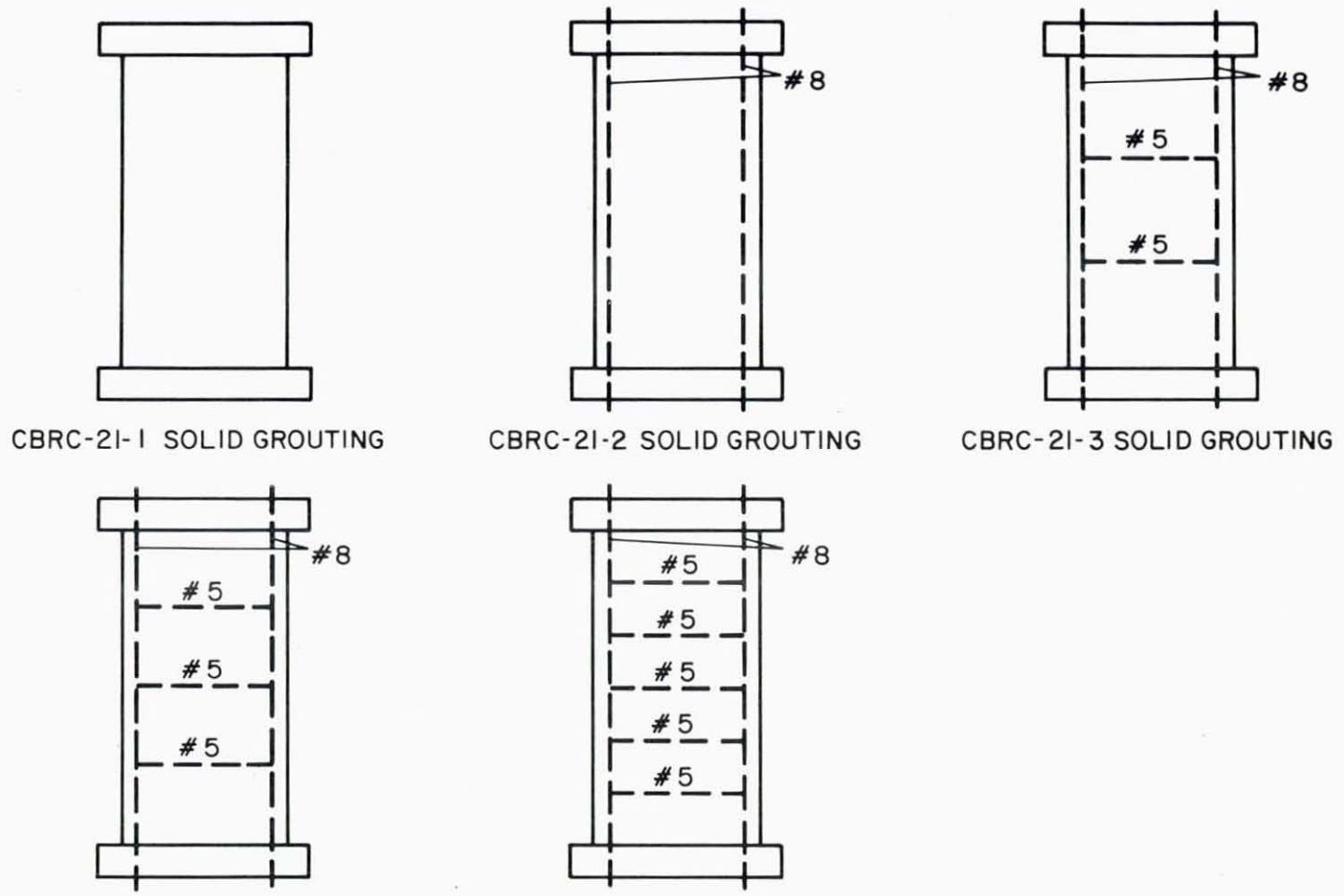

FIG. 2.4(b) REINFORCING STEEL ARRANGEMENTS FOR GROUTED CORE BRICK PIERS (CBRC)

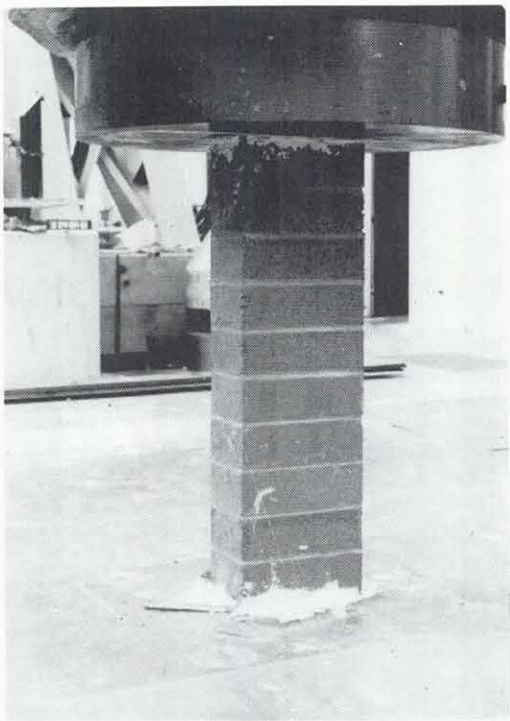

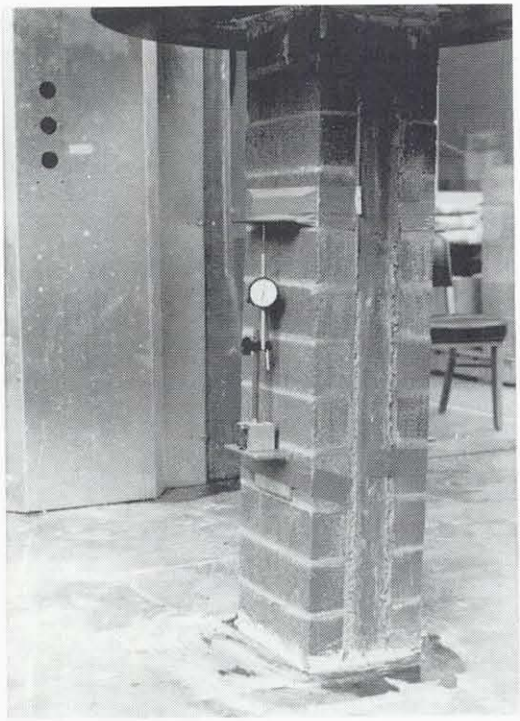

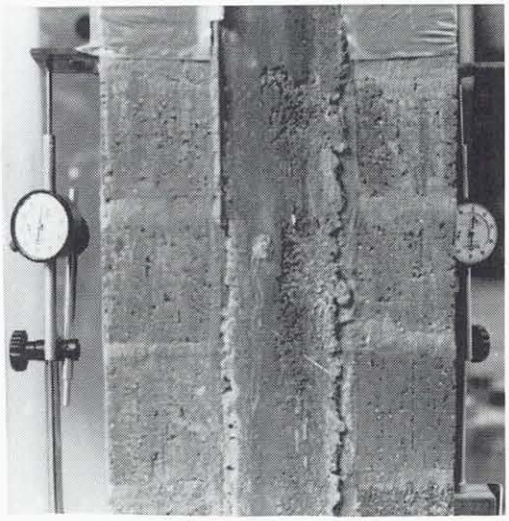

FIG. 2.5 PRISM TEST AND MODULUS OF ELASTICITY MEASUREMENT

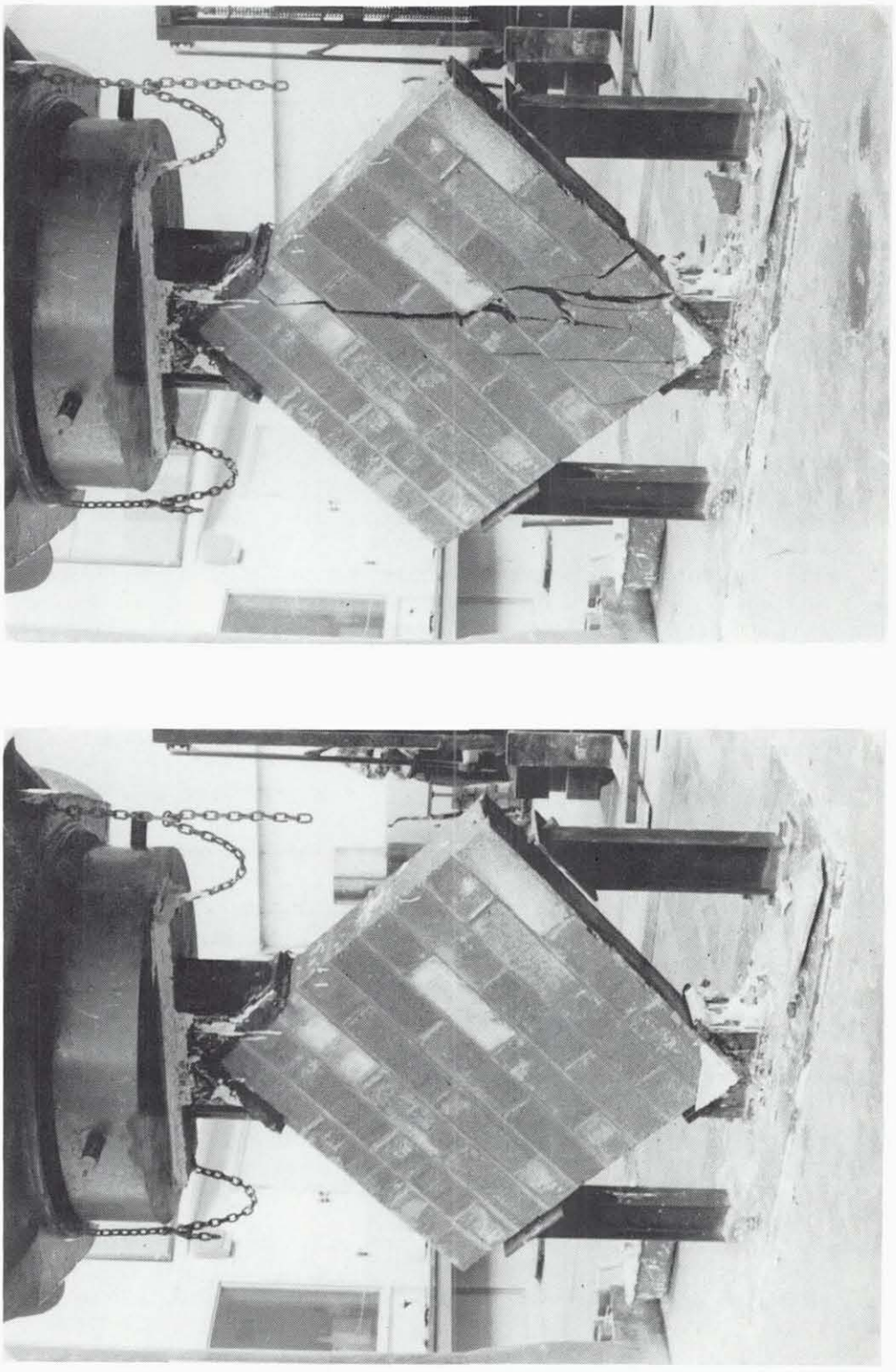

FIG. 2.6 SQUARE PANEL TEST

3. TEST EQUIPMENT AND PROCEDURE

3.1 Test Equipment

Test equipment shown in Figs. 3.1 and 3.2 permits lateral loads to be applied in the plane of the piers in a manner similar to which a floor diaphragm would load the piers during earthquake excitation. It consists of two twenty-feet high, heavily-braced reaction frames supporting a pair of hydraulic actuators which act horizontally; a mechanism capable of applying vertical bearing loads similar to the gravity loads experienced by the piers in an actual structure; a bottom beam composed of a concrete base and a wide flange steel beam which provides anchorage to the test floor and suitable connection holes to the bottom plate of the specimen; and a top beam fabricated from two wide flange, steel beams as shown in Fig. 3.2. The top and bottom beams simulate the action of the spandrel beams in actual masonry construction; they are connected by two steel columns located 10 feet 7 inches apart, which prevent rotation of the top beam and thus provide approximate fixed-fixed end conditions during the test.

The maximum dynamic load which may be developed by each of the horizontal actuators is 75 kips, using an hydraulic pressure of 3000 psi. The maximum stroke is ± 6 inches, the maximum piston velocity is 26 in/sec and the flow capacity of the servovalves is 200 gpm. Either displacement or load can be controlled with these actuators. Their operational capabilities are limited by the above mentioned force capacity, and also by a frequency limitation of about 5 Hz. The actuator control consoles are shown in Fig. 3.5.

A vertical load up to 160 kips can be applied to the pier through the springs and rollers shown in Fig. 3.2. The Thomson Dual Roundway

Bearings connecting the springs to the top of the panel allow the panel to move freely with minimal friction force. The coefficient of friction of bearings is purported to be 0.007.

An additional vertical, compressive load results from the characteristics of this test setup. As significant lateral displacements are imposed on the top beam by the hydraulic actuators, the constraint provided by the side columns forces the top beam to move in a circular arc. The vertical component of this motion is opposed by the axial stiffness of the pier, resulting in a compressive load being applied to the pier. The significance of this additional, cyclic varying compressive load on the test results is discussed in Chapter 5.

Each pier was constructed on a 0.75 inch thick steel plate and had a similar plate on top, as discussed in Section 2.1. This allowed the piers to be moved into place before each test and bolted to the bottom and top steel beams. Prior to the bolting process, hydrostone was placed between the surfaces of the plates and beam flanges as well as between the top plate and the top brick course of the pier.

3.2 Loading Sequence

Each pier was subjected to a series of displacement controlled, in-plane shear loads. The full sequence of loading consisted of sets of three sinusoidal cycles of loading at a specified actuator displacement amplitude. The specified amplitude was gradually increased; the full loading sequence is given in Table 3.1. After each stage, (one set of three sinusoidal displacements at the same amplitude), the walls were visually inspected and the crack pattern identified and photographed. The sinusoidal cycles were applied at a frequency of 0.02 cycles per second throughout the test program.

The test of each pier had a duration of 2½ to 3 hours. The test was usually terminated when the shear strength of the pier had dropped below one third of the maximum shear strength. At this stage the pier was generally not capable of supporting significant vertical loads. All of the tests were carried out under a constant primary bearing stress of 60 psi. Additional cyclic vertical compressive loads were developed during the test, as indicated in Section 3.1, and discussed further in the following chapters.

Partially grouted piers were subjected to maximum input displacements of 0.60 inch to 0.70 inch. Fully grouted pier tests failed at input displacements ranging from 1.00 inch to 2.00 inches.

Because of the flexibility of the reaction frame and other load transferring devices, the lateral displacement actually experienced by the pier was always less than the actuator input displacement, this difference being smaller towards the end of the test when the pier stiffness had attained its lowest values. There was also a slight difference between the maximum loads developed during the push and pull half cycles due to the different type of stress placed on the bolting system and to the different pier stiffness associated with non-symmetric crack patterns.

3.3 Instrumentation

The total horizontal load applied by the hydraulic actuators, as well as the vertical forces developed by the side columns, were measured using pre-calibrated load cells. Each pier was instrumented as indicated in Fig. 3.3.

DCDT's (direct current differential transformers) H_1, H_2, H_3 and H_4 were attached to an external reference frame and were intended to

measure the lateral deformation of the pier during each sequence of loading. The difference between H_1 and H_4 was used to indicate the relative lateral deflection of each pier. DCDT's D_1, D_2, D_3, and D_4 measured the changes in distance between points along the diagonals of the pier and were used to indicate the shear distortion of the pier as defined in Fig. 3.4. DCDT's V_1 and V_2 were also attached to the external reference frame and measured the rotation at the top of the pier. This provided a measurement of how well the side columns prevented the rotation of the top section of the pier.

Finally, strain gages were attached by epoxy glue to the vertical reinforcing bars at the top and bottom sections of the pier, in order to measure the steel strain at the sections that were expected to crack first during a test.

3.4 Data Acquisition and Data Processing

Two different data acquisition systems were used during the test program. The main one consisted of a high speed scanner able to handle up to 25 channels of information, and the corresponding tape recording system (Fig. 3.5). All the data were acquired and stored on tape after being scanned at a rate of 1 point per second per channel. (No higher rate was necessary because of the low frequency used to run the test). Three computer programs were used to read the original tape data, to input the calibration values and geometrical data of each pier and to reduce the data to their final presentation in computer plots.

The second data acquisition system was used to monitor the progress of the test and to act as a back-up system in case of any failure in the main system. It consisted of a direct writing oscillograph (visicorder) and was used only to record the most important

data; namely, forces at the actuators and side columns, actuator stroke and lateral displacement of the pier. This second data acquisition system proved to be extremely useful in detecting occasional malfunctions of the actuators or the instruments attached to the piers and provided excellent visualization of the behavior of the piers as the test progressed.

TABLE 3.1

LOADING SEQUENCE

STAGE*	INPUT DISPLACEMENT AMPLITUDE (in)	STAGE*	INPUT DISPLACEMENT AMPLITUDE (in)
1	0.02	14	0.60
2	0.04	15	0.70
3	0.06	16	0.80
4	0.08	17	0.90
		18	1.00
5	0.12	19	1.10
6	0.16	20	1.20
7	0.20	21	1.30
		22	1.40
8	0.25	23	1.50
9	0.30	24	1.60
10	0.35	25	1.70
11	0.40	26	1.80
12	0.45	27	1.90
13	0.50	28	2.00

*Each stage consists of three sinusoidal cycles at the amplitude shown

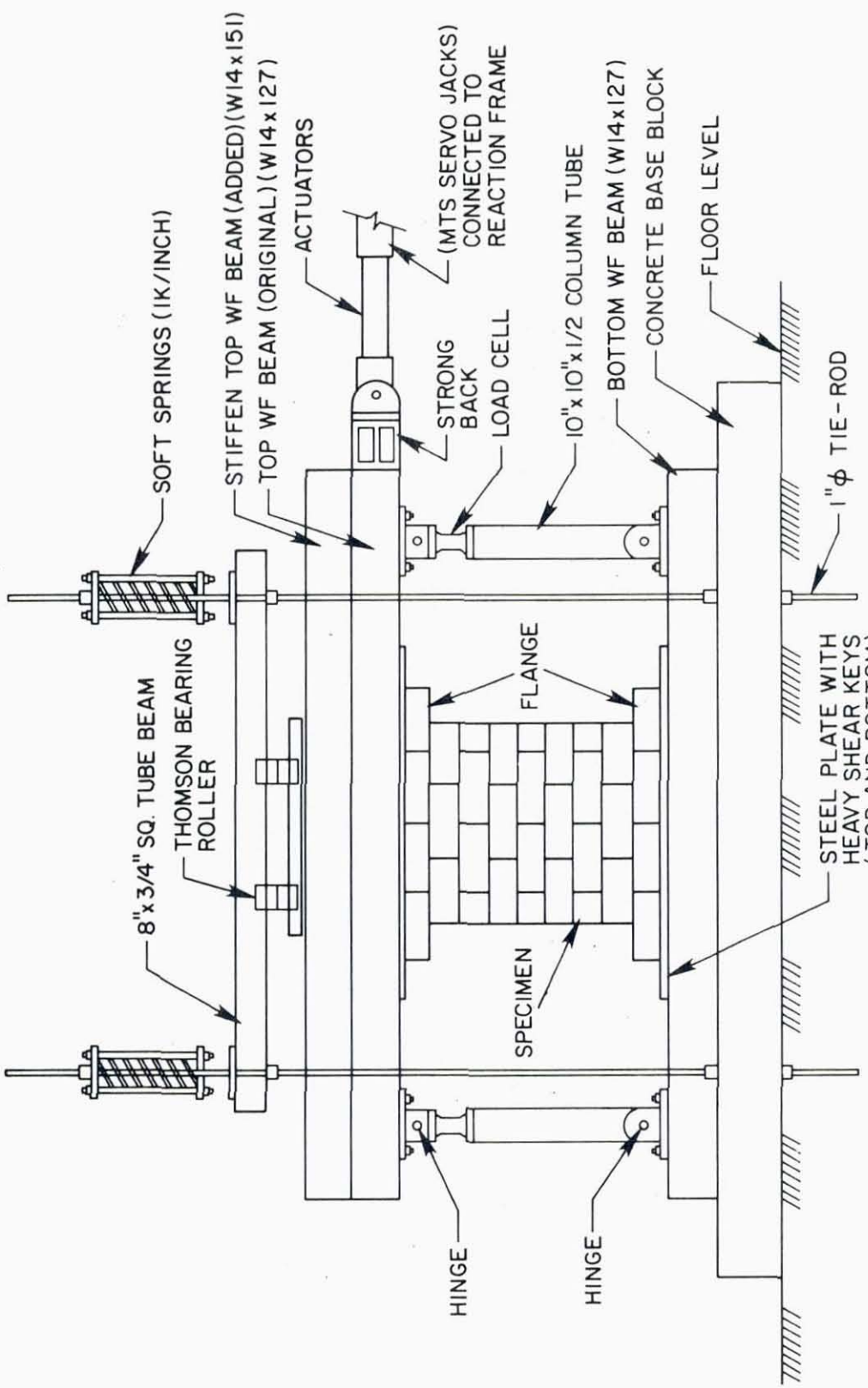

FIG. 3.1 SCHEMATIC ILLUSTRATION OF SINGLE PIER TEST

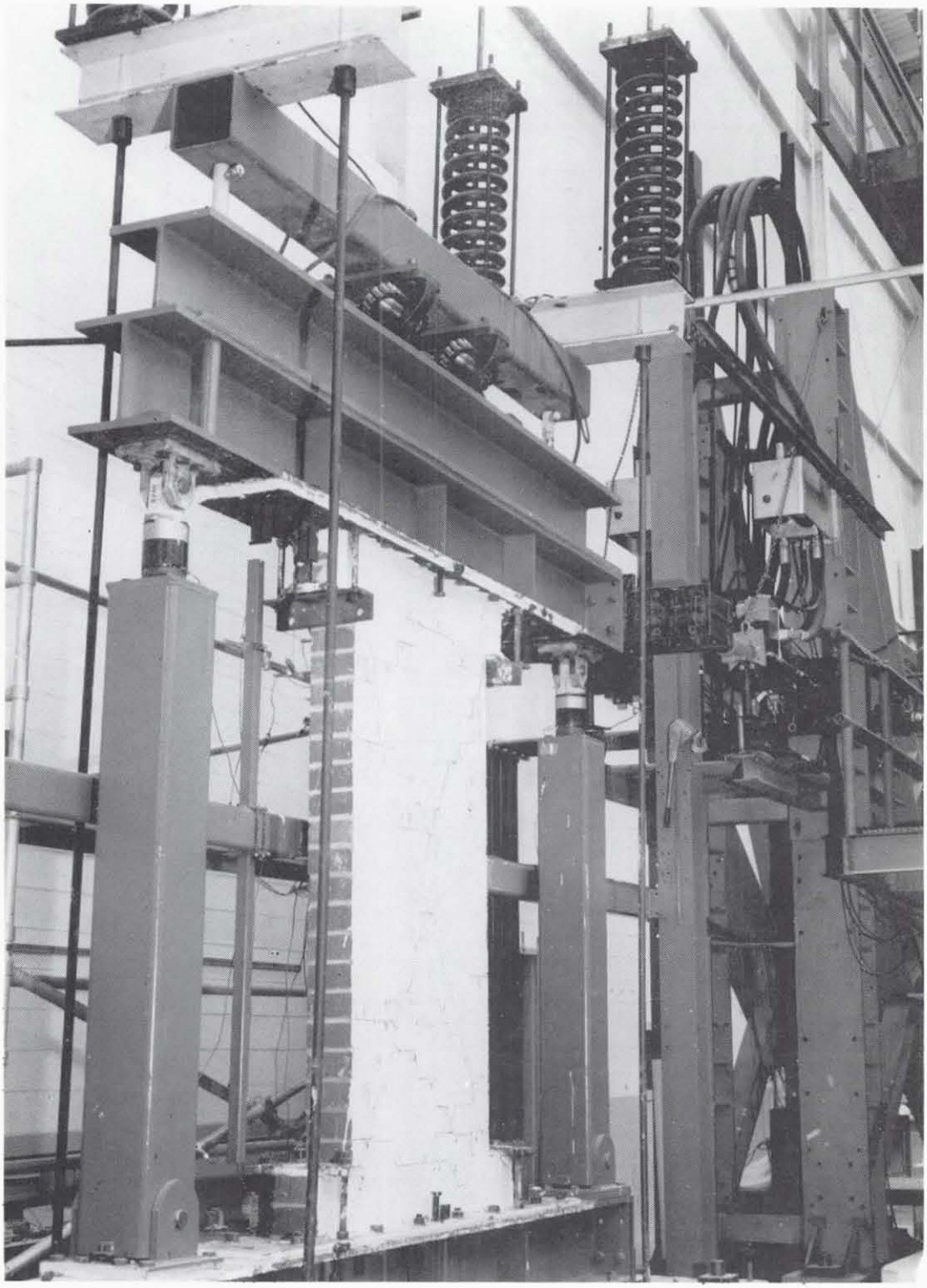

FIG. 3.2 OVERVIEW OF SINGLE PIER TEST

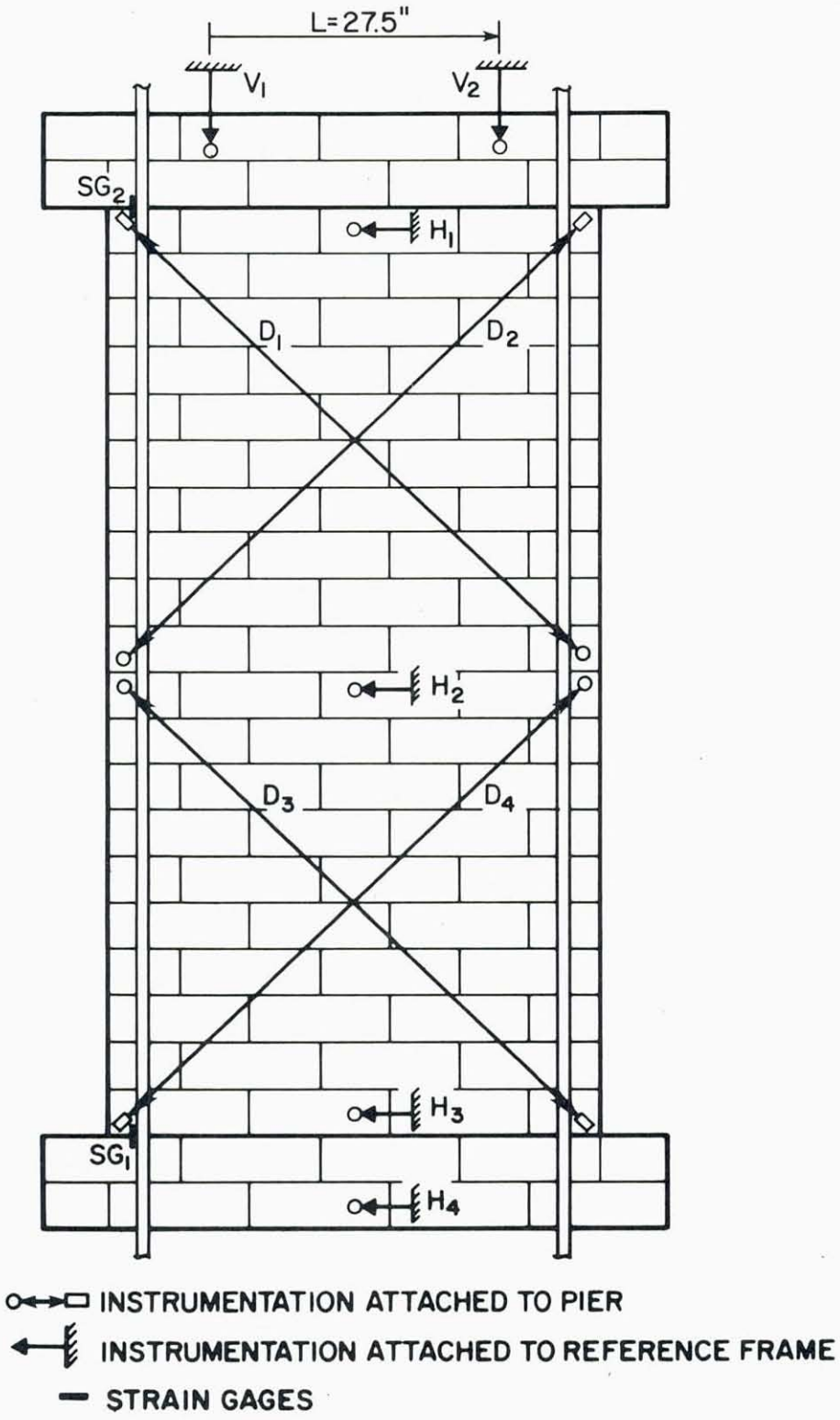

FIG. 3.3 PIER INSTRUMENTATION

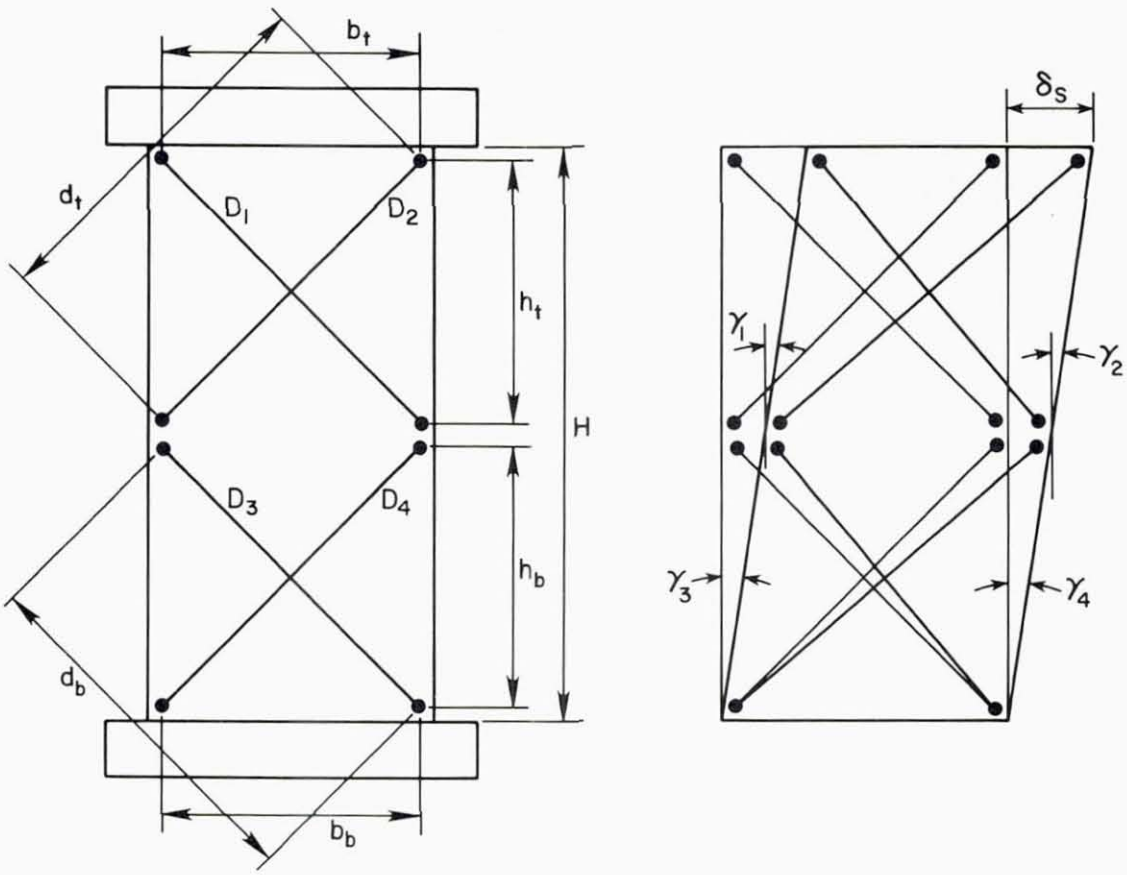

d_t , b_t , h_t = AVERAGE TOP PIER DIMENSIONS

d_b , b_b , h_b = AVERAGE BOTTOM PIER DIMENSIONS

Δ_i = LENGTH CHANGE IN DIAGONAL D_i

γ_i = SHEAR ROTATION

$\gamma_{AVG.}$ = AVERAGE SHEAR ROTATION

δ_s = AVERAGE SHEAR DISTORTION

$$\gamma_i = |\Delta_i| \cdot \frac{d_t}{b_t \cdot h_t} \qquad i = 1,2$$

$$\gamma_j = |\Delta_j| \cdot \frac{d_b}{b_b \cdot h_b} \qquad j = 3,4$$

$$\gamma_{AVG.} = \frac{1}{4} \sum_{i=1}^{4} \gamma_i$$

$$\delta_s = \gamma_{AVG.} \cdot H$$

FIG. 3.4 MEASUREMENT OF AVERAGE SHEAR DISTORTION

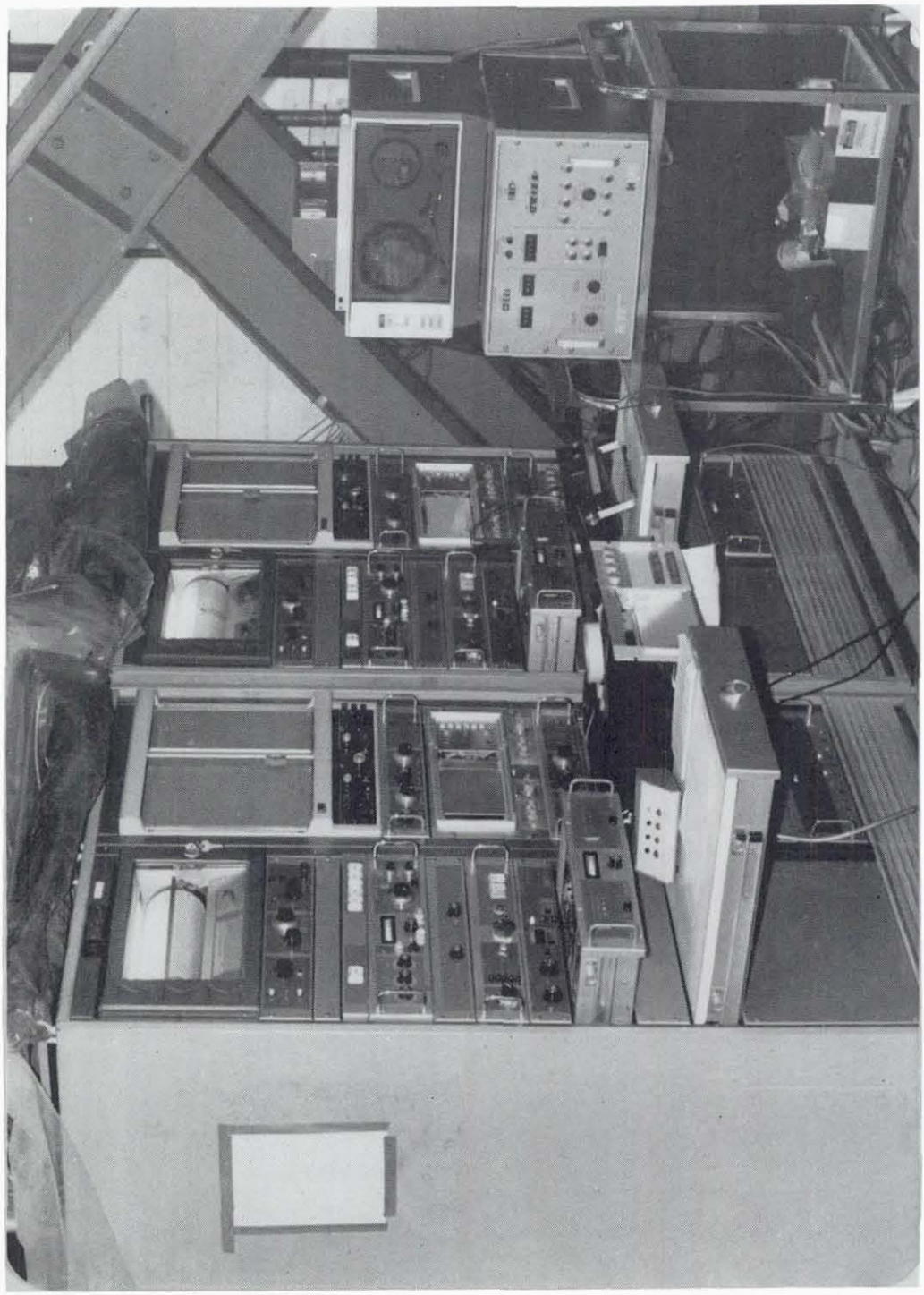

FIG. 3.5 TEST CONTROL CONSOLES AND DATA ACQUISITION SYSTEM

4. TEST RESULTS

4.1 Introduction

The experimental results of the fourteen piers having a height to width ratio of 2 are presented in the form of hysteresis loops, hysteresis envelopes, stiffness degradation properties, energy dissipation characteristics, and relative shear distortion. In addition, a sequence of photographs of the successive crack patterns is given for each test. An explanation of how each of the graphs was obtained and the meaning of the terms used above is included in Section 4.3. The complete presentation of the figures and photographs has been arranged by test numbers and is included in Appendix A. In order to indicate the loading stage at which major diagonal cracking occurred, a black dot has been placed at the appropriate location on all of the figures and photographs in Appendix A.

In addition, data on the ultimate strength and hysteresis indicators for each test are listed in Table 4.1. A discussion of the modes of failure observed follows in Section 4.2 and a discussion of the test results is presented in Chapter 5.

4.2 Modes of Failure

Most of the piers (HCBR-21-2, 4, 6, 8 and 9) displayed a combined shear and flexural [6] mode of failure (Fig. 4.1a). This is characterized by early flexural cracks at the toes of the pier (horizontal cracks) and later augmented with diagonal cracks that extend through only a partial zone on the pier. As the load increased the vertical steel began to yield and the corners of the pier developed high compressive stresses. The additional compressive load induced by

the test setup with the increase in lateral deflection allowed the critical moment sections (top and bottom of the piers) to increase their flexural moment capacities, thus enabling the horizontal load to increase while the vertical reinforcement substained further yield deformation and the compressive toe showed evidence of crushing. This process continued until the shear strength of the pier was attained and full diagonal cracks developed. The diagonal tension or shear failure generally coincided with the ultimate strength of the pier and was followed by a strength degradation characterized by the opening of diagonal cracks and the inability of the walls to maintain a serviceable condition.

The partially grouted piers (HCBR-21-3, 5 and 7) showed a similar behavior to that described above, the only difference being a lower shear load capacity than that of the fully grouted piers. As a consequence of this fact, the vertical reinforcement showed only a mild yield deformation (pier No. 5) or no yielding at all (piers No. 3 and 7) at the time the ultimate shear strength was attained.

The solid grouted core clay brick piers (CBRC-21-2, 3, 4 and 5) followed the same type of failure as the fully grouted hollow clay brick walls, showing a more drastic strength degradation after the shear failure, characterized by a split between the grouted core and the brick wythe, as shown in Fig. 4.1b.

Two of the specimens (HCBR-21-1 and CBRC-21-1) had no steel reinforcement at all. HCBR-21-1 showed a mode of failure similar to the fully grouted hollow clay brick piers. However, it is clear that the additional vertical load imposed by the columns had a significant effect in that it prevented sliding and rotation of the top and bottom of the

pier, thus permitting the horizontal load to increase until a shear failure was produced. Photographs in Fig. A.1 (Appendix A) show that until stage 16 the flexural type of cracks was confined to the top and bottom courses of the pier with no diagonal cracks at all. Pier CBRC-21-1 showed a similar behavior except that in this case crushing at the toes of the pier became so severe that the shear strength was not attained. This mode of failure is illustrated in Fig. 4.1c and has been termed as a flexural mode of failure, although there is no vertical reinforcement and the compressive failure of the toes was not due to substantial yielding of the vertical steel in tension.

4.3 Load-Displacement Characteristics

As mentioned above, Table 4.1 summarizes the strength and hysteresis characteristics of the piers and Appendix A presents the test results for each of the specimens. In order to indicate the loading stage at which major diagonal cracking occurred, a black dot has been placed at the appropriate location on all figures and photographs in Appendix A.

The details of the derivation of each of the figures in Appendix A are discussed in the following sections.

a) Hysteresis Loops. (Shear Stress vs. Lateral Deflection Diagram).

This graph was obtained by plotting the gross shear stress against the relative lateral displacement of the pier for the duration of the test. The gross shear stress is computed by dividing the measured horizontal force by the gross cross section area of the pier, (the thickness multiplied by the width), as indicated in Table 2.1 (310 in^2 for the HCBR piers and 420 in^2 for the CBRC piers). The relative lateral displacement is computed from the difference between the lateral deflections at the top and

bottom of the pier (H_1 - H_4 as defined in Fig. 3.3), for the CBRC piers; in the case of the HCBR piers, only the displacement at the top of the pier is considered because of problems with the measurement of H_4. The hysteresis loops are not smooth lines because of the electronic noise associated with the ± 2.0 inch DCDT used to record the displacement at the top of the pier (H_1). This problem was solved for future tests by using a filter that eliminates the electronic noise.

b) Hysteresis Envelopes

This plot was obtained from the hysteresis loops by averaging the absolute values of the three extreme positive and the three extreme negative forces (or gross shear stresses) and the corresponding absolute values of the relative lateral displacement, for each stage of the test at a given input displacement. One point on the hysteresis envelope was obtained for each stage of 3 cycles of loading. The average lateral displacement obtained in the hysteresis envelope is always less than the input displacement, as explained in Section 3.2.

The black dot indicated on this graph generally corresponds to the stage at which the diagonal crack occurred, as observed in the corresponding photographs. This shear crack usually developed during the first of the three cycles and coincided with the maximum strength of the pier. Nevertheless, the black dot is almost always below and following the peak of the curve. This is due to the fact that the load usually drops in the cycles following the one where the shear crack occurs and the average maximum load computed for this stage is smaller than the average value for the previous stage.

The maximum strength obtained from the hysteresis envelope is indicated in Table 4.1 under "average ultimate shear force or stress". The "peak ultimate shear force or stress" values that appear in Table 4.1 were obtained from the maximum force (stress) developed in any one cycle of loading. The average value is always less than the peak value, varying from 85% to 95% of the peak value. The compressive load at ultimate indicated in Table 4.1 corresponds to the maximum axial compressive load developed during each of the tests. This maximum value always occurred at the same time as the peak ultimate shear force, and is computed from the readings of the load cells located in the vertical columns plus the bearing load applied prior to each test (Table 2.1).

The last two columns of Table 4.1 correspond to hysteresis indicators obtained from the hysteresis envelopes and defined in Fig. 4.2. The level of 0.70 P_u used to define these indicators, where P_u is the maximum strength indicated by the hysteresis envelope, was arbitrarily chosen. Indicator h_1 tells how much the pier has deviated from its initial, theoretical stiffness, and indicator d_2 gives an indication of the deformation capability of the pier. The initial theoretical stiffness of the pier was computed assuming that the piers were fixed against rotation at both the top and bottom. The moment of inertia was calculated using the gross, uncracked section, neglecting the effect of steel reinforcement; the modulus of elasticity was taken from the measured values (Tables 2.3a and 2.3b) and the Poisson's ratio was assumed to be 0.15. Further discussion on the correlation of the theoretical stiffness and the measured stiffness is presented in Chapter 5.

c) Stiffness Degradation

A cyclic definition of the stiffness, as indicated in Fig. 4.3, was used to measure the stiffness of the piers throughout each test. The three cyclic stiffness values obtained from each stage of loading were averaged and plotted against the average gross shear stress and the relative lateral displacement.

d) Energy Dissipation

The energy dissipated per cycle of loading was expressed in terms of a dimensionless ratio EDT. EDT is defined as the ratio of the energy dissipated to the total stored strain energy per cycle and is diagrammatically shown in Fig. 4.3. The three EDT values obtained for each stage of loading were averaged and plotted against the average lateral displacement.

e) Shear Distortion

The values of the shear distortion δ_s were calculated as indicated in Fig. 3.4. The absolute values of δ_s corresponding to the three extreme positive and three extreme negative forces were averaged for each stage of the test, and plotted against the respective average relative lateral displacement, (total deformation of the pier), obtained from the hysteresis envelope. The plot depicts how much of the total deformation of the pier is due to shear distortion as defined in Fig. 3.4. Since the instruments used to measure the diagonal deformations were usually removed three or four stages before the end of the tests, the number of stages used to plot this graph is usually smaller than the number used for the previous graphs.

TABLE 4.1

PIER CHARACTERISTICS AND TEST RESULTS

(Gross cross section of wall: HCBR piers = 310 in^2, CBRC piers = 420 in^2
Net cross section area (bedded plus grouted cells area) for HCBR piers = 171 in^2)

Specimen	Test Frequency (cps)	Grouting Full(F) Partial(P) Solid(S)	Vert. reinf. steel		Horizontal reinforcing steel				Ratio of Total Area of Steel to Gross Area of Wall $p_v + p_h$	Average Ultimate Shear Force (kip)	Average* Ultimate Shear Stress (psi)	Peak Ultimate Shear Force (kip)	Peak* Ultimate Shear Stress (psi)	Compressive Load at Ultimate (kip)	Bearing* Stress at Ultimate (psi)	Hysteresis Indicators	
			No. of Bars	$p_v = \frac{A_{vs}}{A_g}$	No. of Bars	Yield Strength (ksi)	$p_h = \frac{A_{hs}}{A_g}$	$A_{hs}\ f_{hy}$ (kip)								h_1	d_2 (in)
HCBR-21-1	0.02	F	No	—	No	—	—	—	—	75.4	244	82.6	267	179.5	580	11.8	0.91
-2	0.02	F	2#8	0.0051	No	—	—	—	0.0051	63.7	206	73.7	238	113.9	368	6.7	0.61
-3	0.02	P	2#8	0.0051	No	—	—	—	0.0051	27.1	159(88)	31.0	181(100)	33.0	193(107)	4.2	0.38
-4	0.02	F	2#8	0.0051	2#5	49.7	0.0020	30.8	0.0071	84.6	273	95.4	308	128.6	415	7.6	0.79
-5	0.02	P	2#8	0.0051	2#5	49.7	0.0020	30.8	0.0071	47.6	279(154)	51.8	303(167)	53.6	314(173)	4.9	0.40
-6	0.02	F	2#8	0.0051	3#5	49.7	0.0030	46.2	0.0081	98.2	317	106.3	343	152.4	492	7.5	0.90
-7	0.02	P	2#8	0.0051	3#5	49.7	0.0030	46.2	0.0081	47.5	278(153)	51.9	304(168)	52.3	306(169)	4.4	0.30
-8	0.02	F	2#8	0.0051	4#5	49.7	0.0040	61.6	0.0091	99.3	321	107.2	346	150.2	485	6.4	1.02
-9	0.02	F	2#8	0.0051	5#5	49.7	0.0050	77.0	0.0101	95.1	307	107.9	348	147.5	476	6.3	0.93
CBRC-21-1	0.02	S	No	—	No	—	—	—	—	92.7	221	100.3	239	221.7	528	9.9	1.38
-2	0.02	S	2#8	0.0038	No	—	—	—	0.0038	114.2	272	123.8	295	200.5	477	6.0	0.91
-3	0.02	S	2#8	0.0038	2#5	49.7	0.0015	30.8	0.0052	106.0	252	110.8	264	192.5	458	6.8	1.11
-4	0.02	S	2#8	0.0038	3#5	49.7	0.0022	46.2	0.0060	104.2	248	112.3	267	175.2	417	5.7	0.76
-5	0.02	S	2#8	0.0038	5#5	49.7	0.0037	77.0	0.0075	105.0	250	110.0	262	158.5	377	5.5	0.68

*Partially grouted pier stresses computed using net areas. Values in parenthesis indicate gross area stresses.

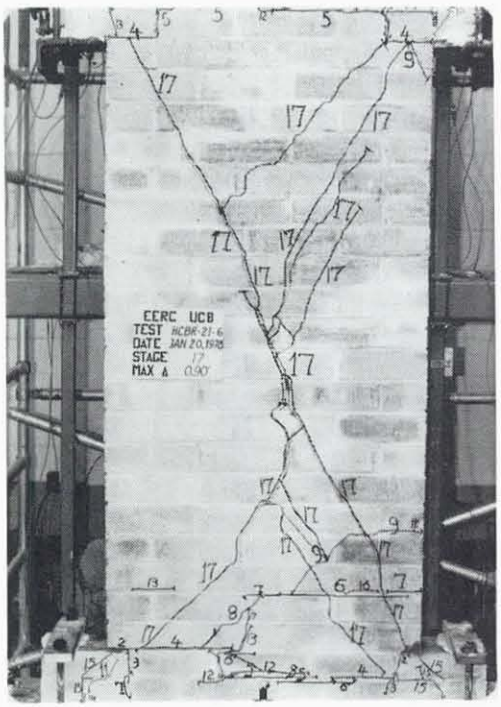

(a) COMBINED SHEAR AND FLEXURAL YIELDING

(b) CORE SPLIT IN GROUTED CORE BRICK WALLS

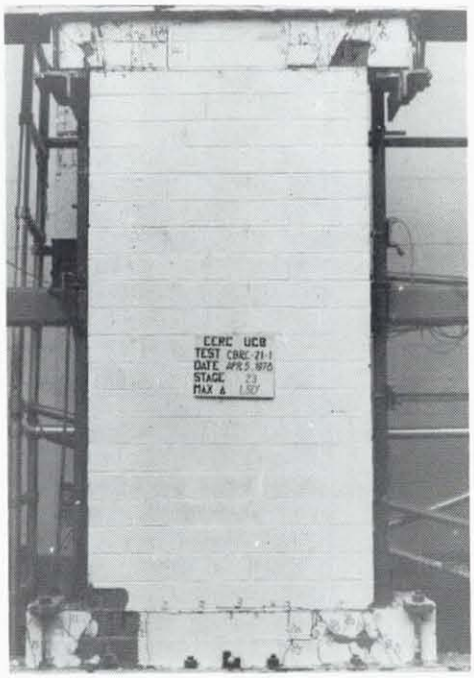

(c) FLEXURAL

FIG. 4.1 MODES OF FAILURE

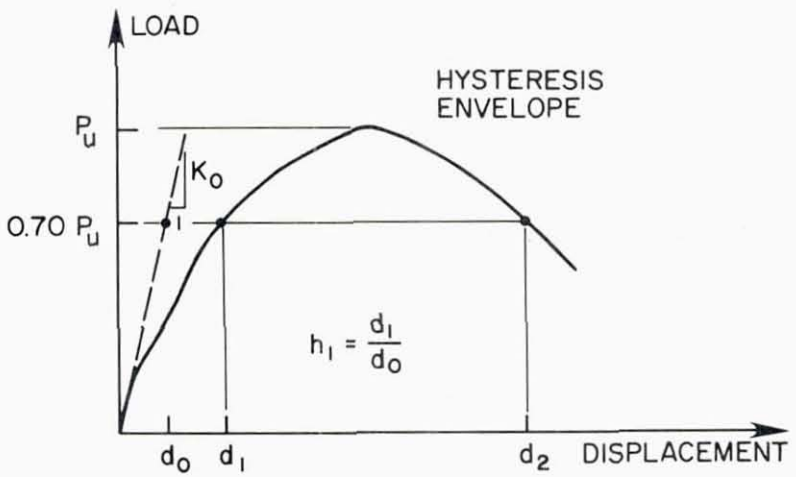

DEFINITION OF HYSTERESIS INDICATORS h_1 AND d_2

COMPUTATION OF INITIAL STIFFNESS K_o

$$K_o^{-1} = \frac{L^3}{12EI} + 1.2 \frac{L}{AG}$$

L = height of pier

E = modulus of elasticity

G = $\frac{E}{2(1+\nu)}$ shear modulus

D = width of pier

t = thickness of pier

SPECIMEN	L (in)	D (in)	t (in)	I (in^4)	A (in^2)	E (Ksi)	ν	K_o (kip/in)
HCRB-21 Full grouting	80	42	7.375	45533	309.75	2450	0.15	1485
HCBR-21 (*) Partial grouting	80	42	7.375	33864	170.84	2450	0.15	960
CERC-21 Solid grouting	80	42	10.0	61740	420.0	1720	0.15	1414

(*) Bedded plus grouted cell area considered

FIG. 4.2 DEFINITION OF HYSTERESIS INDICATORS AND COMPUTATION OF INITIAL STIFFNESS

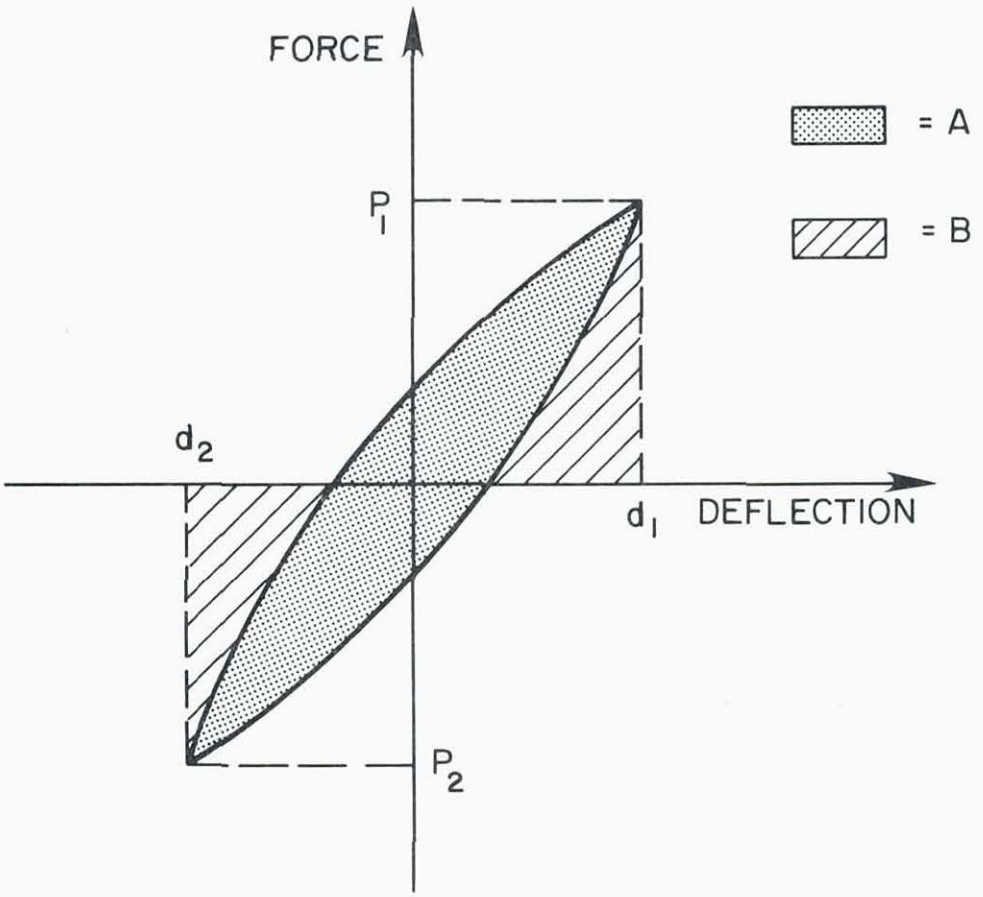

ENERGY DISSIPATION RATIO:

$$EDT = \frac{\text{DISSIPATED ENERGY}}{\text{TOTAL STORED ENERGY}} = \frac{A}{A+B}$$

PIER STIFFNESS:

$$K = \frac{|P_1 - P_2|}{|d_1 - d_2|}$$

P_1 , P_2 , d_1 , d_2 MUST BE TAKEN WITH THEIR OWN SIGN

FIG. 4.3 DEFINITIONS OF ENERGY DISSIPATION RATIO AND PIER STIFFNESS

5. DISCUSSION OF TEST RESULTS

5.1 Introduction

The test results presented in Appendix A and Table 4.1 are discussed in this chapter with reference to the two parameters that were varied during these fourteen tests, namely, the amount of horizontal reinforcement and the type of grouting. Other parameters, such as the initial bearing stress and the cyclic frequency, which were varied in the first seventeen double pier tests[6], were held constant during these fourteen tests. It is also important to note that the results presented herein were obtained from a particular loading sequence. The choice of this loading sequence has been discussed previously[6]. Other types of load sequences are used in some of the additional sixty-six tests that complete the single pier test program.

In considering the results of these fourteen tests on 2 to 1 piers it is important to realize that conclusions which appear valid for these tests may not hold for tests on piers with other height to width ratios. The complexity of the problem requires the completion of the test program (eighty tests) before valid conclusions concerning an adequate design of masonry structural elements can be made.

Finally, it is important to recall that all of the fourteen piers except CBRC-21-1 showed a shear mode of failure combined with flexural yielding of the vertical reinforcement. The ultimate strength always occurred when diagonal cracks developed in both directions of horizontal loading over the full height of the pier.

5.2 Ultimate Strength

5.2.1 Effect of Horizontal Reinforcement

In the hollow clay brick tests (HCBR-21) no increase in the ultimate shear strength of the fully grouted piers was observed when the amount of horizontal reinforcement was increased over three No. 5 steel bars, (a reinforcement ratio of 0.0030). Piers with three, four or five No. 5 bars exhibited an average ultimate shear stress of the order of 315 psi (Table 4.1). The ultimate strength decreased from this value by 13% and 35% as the amount of horizontal reinforcement was reduced to two No. 5 bars (reinforcement ratio of 0.0020) and to none, respectively. This increase in the ultimate shear strength with increasing amounts of horizontal reinforcement (up to a certain point) was not observed in the double wythe, grouted core clay brick piers (CBRC-21). In this case, the piers attained an average ultimate shear stress of the order of 250 psi (Table 4.1), independent of the amount of horizontal reinforcement.

5.2.2 Effect of Partial Grouting

The ultimate shear stress of partially grouted piers, computed using net areas, was of the order of 90% of the stress of comparable fully grouted piers (Table 4.1). It should be noted that the partially grouted piers required much less horizontal load to develop the ultimate shear strength, and as a result practically no yielding of the vertical reinforcement occurred. Correspondingly, the amount of compressive load developed at ultimate was considerably smaller than that for the tests of the fully grouted piers.

5.3 Inelastic Behavior

The hysteresis envelopes (average maximum force-deflection curves) are used as a frame of reference to discuss the inelastic behavior of the piers. The question as to what can be considered a desirable hysteresis envelope has been discussed in reference [6] pp. 68-70 in qualitative terms. It is appropriate to recall that the usefulness of the hysteresis envelopes is that they provide visual comparisons of ductility and ultimate strength; however, they give no indication of the energy dissipated per cycle, and consideration of this parameter in conjunction with the ultimate strength, the deformation capacity and a comparison of crack patterns at equal displacements is necessary to evaluate completely the inelastic characteristics of the pier behavior.

The problem of making mathematical models to predict the hysteretic behavior revealed in the data has recently been explored. Such a model includes not only the hysteresis loops themselves, but also the hysteresis envelope.

In order to quantify the deformation capabilities of the piers, hysteresis indicators, defined in Section 4.3, are listed in the last two columns of Table 4.1.

5.3.1 Effect of Horizontal Reinforcement

Figures 5.1 and 5.2 show the changes in the hysteresis envelopes as the amount of horizontal reinforcement varies. The observations of Section 5.2 with respect to ultimate strength also are evident in these figures. In addition the form of the hysteresis envelopes of the HCBR piers improves as the amount of horizontal reinforcement increases from none to three No. 5 bars. However, there is no

significant difference in the hysteresis envelopes of the piers as the horizontal reinforcement increases from three to four to five No. 5 reinforcing bars (Fig. 5.1). Hysteresis indicator h_1 has a constant value around 7.0 and d_2 increases from 0.61 inch for no horizontal reinforcement to 0.95 inch for three, four or five No. 5 steel bars. In the case of the CBRC piers, there is no significant difference in the hysteresis envelopes as the amount of horizontal reinforcement increases from none to five No. 5 horizontal reinforcing bars (Fig. 5.2). Hysteresis indicator h_1 has a constant value around 6.0 and d_2 shows a decrease (from 1.0 inch to 0.68 inch) as the amount of horizontal reinforcement is increased (from none to five No. 5 steel bars). Therefore, the use of increasing amounts of horizontal reinforcement has a slight detrimental effect on the deformation capabilities of the CBRC piers.

A heavy dot has been drawn on all figures at the loading stage where the major diagonal crack first developed. It can be observed that all the CBRC piers, as well as the HCBR piers with horizontal reinforcement less than three No. 5 bars, have a sharp degradation of strength following the formation of major diagonal cracking. As the horizontal reinforcement of the HCBR piers is increased to three No. 5 bars or more, the strength degradation is less pronounced after the formation of the major diagonal cracks.

The piers with no vertical or horizontal reinforcement (HCBR-21-1 and CBR-21-1) have not been included in the above discussion and their characteristics are not compared with others. It was clear to the investigators that the behavior of the nonreinforced piers was significantly influenced by the presence of the additional compressive

axial load imposed by the columns and discussed in Section 4.2. Accordingly, these tests will be repeated in a later sequence where the test setup will be modified to exclude this increase in compressive load.

5.3.2 Effect of Partial Grouting

Figure 5.3 shows the comparison of hysteresis envelopes of fully and partially grouted HCBR piers based on gross shear stress. Figure 5.4 shows the same comparison using the net shear stress (net area based on bedded plus grouted cell area). Although the effect of partial grouting was not significant as far as ultimate strength was concerned, it definitely reduced the deformational capability of the piers; the hysteresis envelopes of the fully grouted piers have a much more desirable shape. The hysteresis indicator d_2 of the partially grouted piers dropped to between 0.30 inch and 0.40 inch. The post cracking behavior of the partially grouted piers displayed more brittle characteristics compared with that of the corresponding fully grouted piers.

5.4 Stiffness Degradation

It is apparent from the test results that the piers suffer substantial stiffness degradation when subjected to gradually increasing lateral displacements. Table 5.1 summarizes this effect and shows two types of results. The first is a comparison between the theoretical initial stiffness and the maximum stiffness measured during the early stages of the test. The theoretical initial stiffness has been computed in Fig. 4.2 and the assumptions used are indicated in Section 4.3(b). The measured value is always smaller than the theoretical value and it ranges from 32% to 74% of the theoretical value for the

HCBR fully grouted piers, from 43% to 75% for the HCBR partially grouted piers, and from 37% to 79% for the CBRC piers. These large differences in the two values are attributed to the flexibility of the boundary conditions at small lateral displacements as discussed in Section 5.8. Unlike the double pier test results[7], the assumed fixed-fixed rotation conditions at the top and bottom of the pier do not appear to be achieved physically for small displacements and hence the discrepancy in the calculated and measured values.

The second set of results presented in Table 5.1 is a comparison of the measured stiffnesses of all piers at applied shear stresses of 50 psi and 100 psi, and the percentage decreases in stiffness at these stress levels with respect to the maximum initial measured value. The applied stress level of 50 psi generally corresponds to the shear stress at which the first visible cracks occur (usually flexural cracks). Because the maximum initial stiffness developed at a shear stress close to 50 psi for some of the tests, the percentage of stiffness degradation is more uniform for the 100 psi level than for the 50 psi level.

5.4.1 Effect of Horizontal Reinforcement

Figures 5.5 and 5.6 present the stiffness degradation curves for different amounts of horizontal reinforcement for HCBR and CBRC piers, respectively. It can be seen from the figures that there appears to be no relationship between the amount of horizontal reinforcement and the rate at which the stiffness degrades. Specimens 4 and 6 show a lower stiffness degradation with respect to the initial measured stiffness. However, these results are attributed to the particularly flexible boundary conditions during the early stages of the test, which produced very low initial measured stiffness values (Table 5.1).

5.4.2 Effect of Partial Grouting

Figure 5.7 shows a comparison of the stiffness degradation curves for fully and partially grouted HCBR piers based on gross areas. Figure 5.8 is similar but uses the net area to compute the shear stress of the partially grouted piers. The trend of these results for both types of grouting is similar, and so it appears that degradation is independent of the type of grouting. However, it must be noted that these results were obtained under displacement increments that gradually increase. Later tests will determine if the type of degradation observed is similar for both grouting conditions under a more random type of loading sequence.

5.5 Energy Dissipation

The effect of horizontal reinforcement on the EDT ratio is shown in Fig. 5.9 for the HCBR piers and in Fig. 5.10 for the CBRC piers. The effect of partial grouting is shown in Fig. 5.11. It can be concluded from these graphs that the energy dissipation capacity of the piers appears to be independent of the amount of horizontal reinforcement and the type of grouting. For all piers the EDT ratio increases linearly as a function of the imposed displacement until a major crack forms. At this point there is a significant increase in the EDT ratio as further increases in lateral displacement occur. As with stiffness degradation, investigation of the EDT ratio under a more random load sequence is important before analytical models based on the results are formulated.

5.6 Effect of Compressive Load on Inelastic Behavior

The additional compressive load imposed by the columns during the tests has been discussed briefly in Sections 3.1 and 4.2. The

magnitude of the load appears to be directly proportional to the axial stiffness of the pier and to the square of the lateral displacement, and inversely proportional to the height of the vertical columns that restrain the top beam from rotation. The presence of this compressive axial load is generally detected as soon as an applied actuator amplitude displacement of 0.10 inch is achieved and reaches maximum values close to 150 kip (484 psi) in the HCBR piers and 200 kip (476 psi) in the CBRC piers, (See Table 4.1). Specimens HCBR-21-1 and CBRC-21-1 sustained larger lateral deformations at their maximum lateral loads and consequently developed compressive stresses larger than 500 psi. On the other hand, partially grouted piers have a lower deformation capability at their ultimate load and therefore develop lower compressive loads than the fully grouted specimens. The additional imposed compressive load began to decrease immediately after the maximum shear strength was attained coincident with the occurrence of major diagonal cracking. This decrease is attributed to the reduction in the axial stiffness of the specimens.

Although this increasing compressive load is not uncommon in multistory buildings subjected to the overturning effects of earthquake excitation, it forces the piers to fail in the shear mode even though they exhibit a flexural type of behavior as explained below; this may affect the desirability of the hysteresis envelopes (see [6], pp. 68-70). Desirable inelastic behavior can generally be characterized in two ways. It is desirable for the pier to sustain a sizable horizontal load for large amplitude of deflection and also for the pier to absorb and dissipate as much energy as possible before this horizontal load drops off. Both of these properties are reflected in the hysteresis envelope derived for a particular pier.

If the horizontal load, together with a moderate vertical load, imposes more demands on the pier in flexure than in shear, the vertical reinforcing on the tension side can be made to yield allowing a large horizontal displacement at the top before failure occurs due to crushing of the compressive corner or to rupture of the bars in tension. In this case the hysteresis envelope would show a yield plateau extending to a large displacement thus displaying desirable characteristics.

When a significant increase in vertical load accompanies an increase in displacement, the resisting flexural moment can continue to increase without any sizable increase in the extreme tensile stresses. Thus both the top displacement and the resisting horizontal force continue to increase without the vertical tension reinforcing displaying much, if any, increase in yield strain. But as the horizontal and vertical forces increase they build up a stress field in the pier in which diagonal tension reaches the tensile strength capacity of the masonry so that large diagonal cracks appear which are associated with shear failure. This is a brittle failure and occurs at top horizontal displacements which are much smaller than would accompany a ductile tension failure.

Since the growth in vertical load during a test caused the piers to display shear failures, it is interesting to speculate how the piers would behave (reflected through their hysteresis envelopes) if these additional vertical loads were absent. In what follows a theory to predict this behavior is developed.

In quantitative terms the effect of the compressive load is illustrated in Fig. 5.12, where the figure depicts a free-body diagram

at the bottom section of the pier. By taking moments about 0 (the toe of the pier), and neglecting the moment of the compressive force at the toe, an equation can be developed for the increase in lateral force capacity ΔP above that required to yield the vertical reinforcement. This is expressed in terms of the increment in axial compressive force, ΔN, and the associated increment in moment, ΔM, developed by applied loads of the external steel columns.

Table 5.2 presents a comparison of the computed and measured ΔP for specimen HCBR-21-9. To perform the computation a specific point in one load cycle was chosen: the point at which the maximum lateral force in the pull direction developed as indicated in Fig. 5.12. The stage at which the tension vertical reinforcement commenced to yield was determined from the strain gage readings for the vertical reinforcement (SG_1 in Fig. 3.3). The incremental computed values of the lateral force, ΔP, are indicated in the second to last column. The last column indicates the incremental values $(\Delta P)_0$ actually measured from the actuator load cells. The values of ΔP and $(\Delta P)_0$ are significantly close until stage 19, where the tension steel reinforcement ceased to yield and major diagonal cracking occurred.

The same computations shown in Table 5.2 for specimen HCBR-21-9 were performed for all of the tests where the vertical reinforcement yielded in tension. The results are shown in Fig. 5.13(a) for HCBR piers and Fig. 5.13(b) for CBRC piers. Because the peak values in each stage were considered for this analysis, the hysteresis envelope obtained from peak values has been used for comparison, (the hysteresis envelopes obtained from average values are also shown as reference). The computed ΔP values have been subtracted from the hysteresis envelope to produce a theoretical hysteresis envelope that would have

been obtained if no additional axial compressive force was present. It is apparent from the curves in Fig. 5.13 that a flexural type of failure with a yield plateau would have developed. Future tests, with a modified test setup to remove this axial force effect, will be performed to validate this analytical result. Hysteresis envelopes to be obtained from future tests will not be exactly the same as the curves presented in Fig. 5.13, due to the following assumptions made in the above analysis:

a) The onset of yielding in the vertical reinforcement is delayed by the presence of the compressive axial force, and should occur at an earlier stage when this axial force is removed. In fact, if the yield stress of the vertical steel is used to compute the yielding moment at the top and bottom sections of the pier and no effect of additional compressive force is considered, the lateral load at which yielding would begin is 47 kip for HCBR piers and 50 kip for the CBRC piers. The yield point shown in Figs. 5.13(a) and 5.13(b) ranges from 56 kip to 72 kip.

b) The hysteresis envelope computed after removal of the axial force effect has been based on the assumption that the lateral displacement does not change when ΔP is subtracted from the shear force P; this may not be true.

c) The analytical curves can only be derived from the hysteresis envelopes (peak values) while the vertical steel is yielding in tension. Besides, it is assumed that the deformation capacity cannot be larger than the capacity shown for the shear mode of failure. The deformation capacity of a pier failing in the flexural mode, with no additional axial force present, may be larger than the capacity shown by the analytical curves.

d) The strain hardening effect in the steel reinforcement under tension has not been taken into account in this analysis.

The test setup is being modified so that the vertical load is controlled during a test; and therefore, the additional vertical load is eliminated. This setup will enable tests to be carried out to verify the preceding theory.

5.7 Correlation Between Square Panel and Pier Critical Tensile Strength

This analysis is presented in Table 5.3 and is discussed in more detail in reference [7]. The purpose of this investigation is to evaluate an alternative and more appropriate test procedure for determining the code allowable shear strength of masonry walls. Currently, the code allowable shear strength is based on the compressive strength of a masonry prism.

The square panel critical tensile strength has been determined from a study made by Blume[1], who proposed the expression shown in Table 5.3. The ultimate load P was taken as the average value obtained from three square panel tests for each type of pier, as indicated in Table 2.2.

The critical tensile strength of the piers has been computed at the neutral axis of the pier sections, following the simple beam theory for a section under combined flexure, shear and axial force. A parabolic distribution of shear stresses over the cross section has been assumed. The piers developed their shear cracks at the same time that the ultimate shear strength was attained. Therefore the peak shear force, and the corresponding compressive load from Table 4.1, have been used to evaluate the pier critical tensile strength.

The square panels were all fully grouted; for this reason the correlation only considers fully grouted HCBR piers and all the CBRC piers.

The correlation obtained is considered to be reasonable. This type of analysis will continue to be performed throughout the pier test program. Future results will permit a better assessment of this test method in predicting the shear strength of masonry walls.

5.8 Other Test Results

The last graph in the test results is a comparison between the lateral displacement of the piers and the percentage of this displacement that can be attributed to shear distortion as defined in Fig. 3.4. These results reflect the amount of diagonal cracking present at each stage of the test. In accordance with the absence of diagonal cracking in specimens HCBR-21-1 and CBRC-21-1 the figures for these piers show only a small amount of shear distortion (as can be observed from the photographs). It is interesting that in the initial stiffness computed in Fig. 4.2, the flexural and shear components of the deformation are in the ratio of 1.3:1 for fully or solid grouted piers and 1:1 for the partially grouted HCBR piers.

Also it is appropriate to report on how well the test rig reproduced the fixed end condition at the top of the pier. There are two measures of the rotation of the top section; one is an absolute measure through the instruments placed at the top of the pier, (DCDT'S V_1 and V_2 in Fig. 3.3), and the other is the computation of the location of the inflection point from the forces acting on the pier. The results of these measurements and computations show that at the very early stages of the test the absolute rotation of the top spandrel

beam reached 60% of the value that could be expected from a cantilever type of test. As a result the initial calculated pier stiffness (Section 5.4) was substantially underestimated. However, after the first four or five loading stages, the position of the inflection point was confined to the 10% of the pier immediately above the mid-height. This indicates a reasonably good reproduction of fixed end conditions against rotation at the top of the pier.

TABLE 5.1

EFFECT OF SHEAR STRESS, STEEL REINFORCEMENT AND TYPE OF GROUTING ON STIFFNESS DEGRADATION
(Net areas used for partially grouted piers)

Specimen	Grouting Full(F) Partial(P) Solid(S)	Vertical Steel Reinforcement	Horizontal Steel Reinforcement	Theoretical Initial Stiffness (kip/in)	Measured Maximum Initial Stiffness (kip/in)	Stiffness at 50 psi		Stiffness at 100 psi	
						Measured (kip/in)	Percentage Decrease (%)	Measured (kip/in)	Percentage Decrease (%)
HCBR-21-1	F	No	No	1485	545	490	10	140	74
-2	F	2#8	No	1485	908	605	33	265	71
-3	P	2#8	No	960	483	*	*	262	46
-4	F	2#8	2#5	1485	468	444	5	265	44
-5	P	2#8	2#5	960	410	*	*	357	13
-6	F	2#8	3#5	1485	500	424	15	241	52
-7	P	2#8	3#5	960	718	577	20	377	48
-8	F	2#8	4#5	1485	992	516	48	324	67
-9	F	2#8	5#5	1485	1094	545	50	328	70
CBRC-21-1	S	No	No	1414	1122	173	85	150	87
-2	S	2#8	No	1414	973	492	49	399	59
-3	S	2#8	2#5	1414	537	365	32	382	48
-4	S	2#8	3#5	1414	525	370	30	371	29
-5	S	2#8	5#5	1414	640	505	21	349	46

*Maximum initial stiffness obtained after 50 psi.

TABLE 5.2

COMPUTATION EXAMPLE (HCBR-21-9) TO DETERMINE THE INFLUENCE OF AXIAL FORCE ON THE PIER LATERAL STRENGTH

(Definition of terms as given in Fig. 5.12)

$\Delta P = (\Delta P)_N + (\Delta P)_M$: increase in strength due to axial compressive force increase

$(\Delta P)_O$: increase in strength measured during the test (third column values).

STAGE	MAX. DISPL. (in)	MEASURED FROM TEST (at P_{max})			COMPUTED USING V_D AND V_F					$(\Delta P)_O$ (kip)	
		P(kip)	V_D(kip)	V_F(kip)	$(V_D+V_F)\frac{21}{97}$	$(V_D-V_F)\frac{63.5}{97}$	$(\Delta P)_N$(kip)	$(\Delta P)_M$(kip)	$\Delta P=(\Delta P)_N+(\Delta P)_M$(kip)		
9(Yield pt)	0.30	60.1	44.6	- 5.2	8.5	32.6	0	0	0	0	
10	0.35	67.0	52.9	- 3.4	10.7	36.9	2.2	4.3	6.5	6.9	
11	0.40	72.9	60.4	- 1.0	12.9	40.2	4.4	7.6	12.0	12.8	
12	0.45	78.4	67.4	+ 1.4	14.9	43.2	6.4	10.6	17.0	18.3	
13	0.50	83.3	73.5	+ 3.2	16.6	46.0	8.1	13.4	21.5	23.2	
14	0.60	92.4	88.2	+ 9.9	21.2	51.3	12.7	18.7	31.4	32.3	
15	0.70	101.0	99.2	+14.6	24.6	55.4	16.1	22.8	38.9	40.9	
16	0.80	107.9	109.4	+19.1	27.8	59.1	19.3	26.5	45.8	47.8	
17	0.90	105.1	111.0	+23.9	29.2	57.0	20.7	24.4	45.1	45.0	
18	1.00	99.6	110.2	+29.8	30.3	52.6	21.8	20.0	41.8	39.5	
19	1.10	82.9	94.6	+29.3	26.8	42.7	18.3	10.1	28.4	22.8	(*)
20	1.20	20.2	24.7	+ 7.9							

(*) The difference between the last two columns indicates that the vertical reinforcement is not yielding any more.

TABLE 5.3

CORRELATION BETWEEN SQUARE PANEL AND PIER CRITICAL TENSILE STRENGTH

Specimen	SQUARE PANEL (1)				PIER (2)						$\frac{\sigma^o_{tcr}}{\sigma_{tcr}}$
	Ultimate Load P(kip)	Side Area $A(in^2)$	$\tau = \frac{P}{\sqrt{2}A}$ (psi)	Blume's Formula $\sigma^o_{tcr}=0.734\tau$ (psi)	Ultimate Shear Force P(kip)	Compressive Load at Ultimate N(kip)	Cross Section $A(in^2)$	Ultimate Shear Stress $\frac{P}{A}$ (psi)	Bearing Stress at Ultimate $\frac{N}{A}$ (psi)	Critical Strength σ_{tcr} (psi)	
HCBR-21-1	192.0	265.5	511.4	375.3	82.6	179.5	310	266.6	579.6	204.1	1.84
-2					73.7	113.9	310	237.9	367.8	217.5	1.73
-4					95.4	128.6	310	307.9	415.2	298.8	1.26
-6					106.3	152.4	310	343.3	492.1	324.7	1.16
-8					107.2	150.2	310	346.2	485.0	330.6	1.14
-9					107.9	147.5	310	348.3	476.1	336.1	1.12
CBRC-21-1	196.7	360	386.3	283.5	100.3	221.7	420	Did not fail in shear			
-2					123.8	200.5	420	294.8	477.4	263.8	1.07
-3					110.8	192.5	420	263.8	458.3	228.1	1.24
-4					112.3	175.2	420	267.4	417.1	243.5	1.16
-5					110.0	158.5	420	261.9	377.4	247.1	1.15

(1) Square Panel Critical Tensile Strength

Blume's formula: $\sigma^o_{tcr} = -0.582\,\frac{P}{A} - \frac{\sigma_c}{2} + \frac{1}{2}\sqrt{4.849\left(\frac{P}{A}\right)^2 + \sigma_c^2}$

If edge pressure $\sigma_c = 0$, $\tau = 0.734\,\frac{P}{\sqrt{2}A}$

(2) Pier Critical Tensile Strength

Assuming a parabolic distribution of shear stress

$\sigma_{tcr} = -\frac{\sigma_c}{2} + \sqrt{(1.5\tau)^2 + \left(\frac{\sigma_c}{2}\right)^2}$

$\sigma_c = \frac{N}{A}$: applied compressive stress

$\tau = \frac{P}{A}$: average shear stress

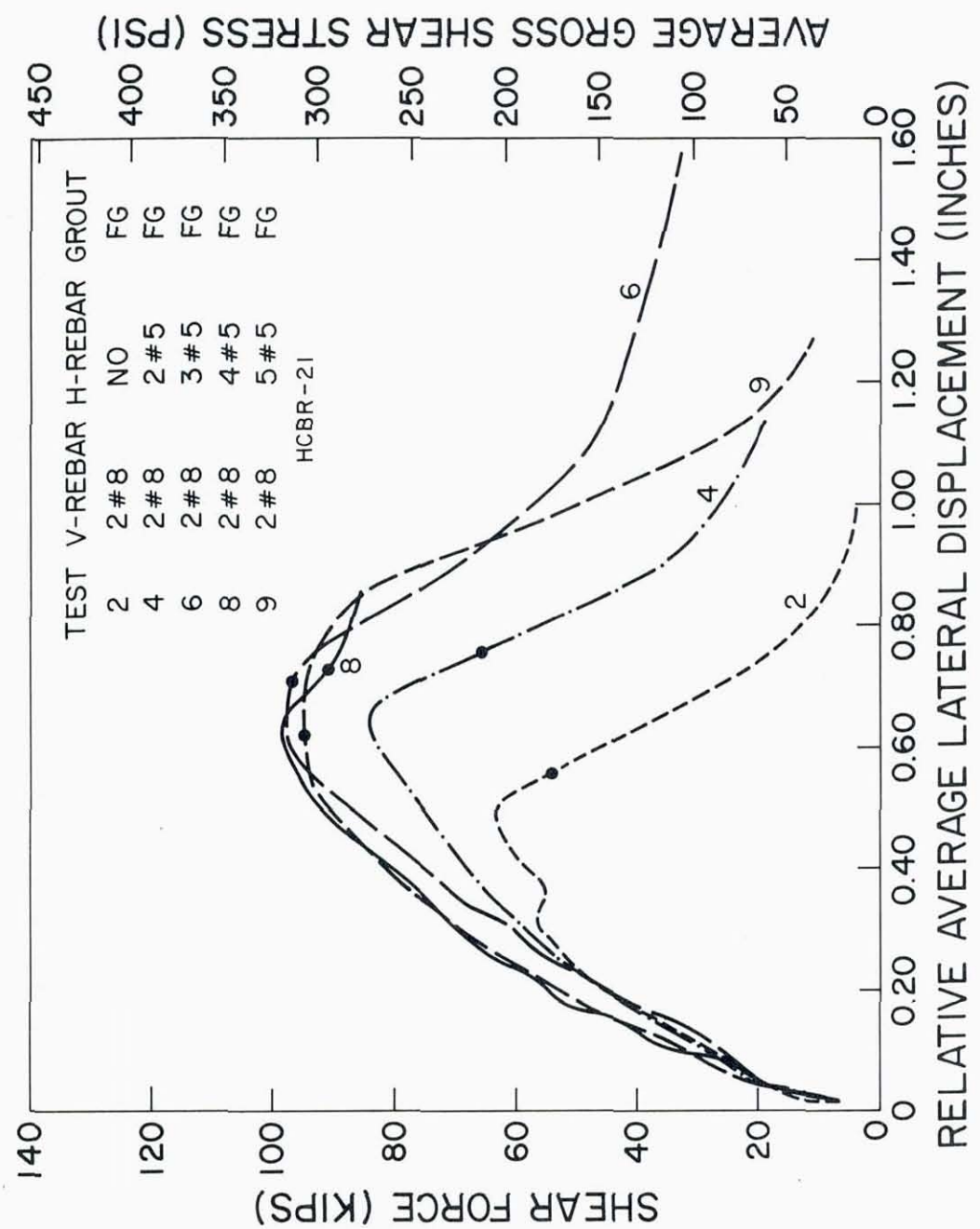

FIG. 5.1 EFFECT OF HORIZONTAL REINFORCEMENT ON HYSTERESIS ENVELOPE (HCBR)

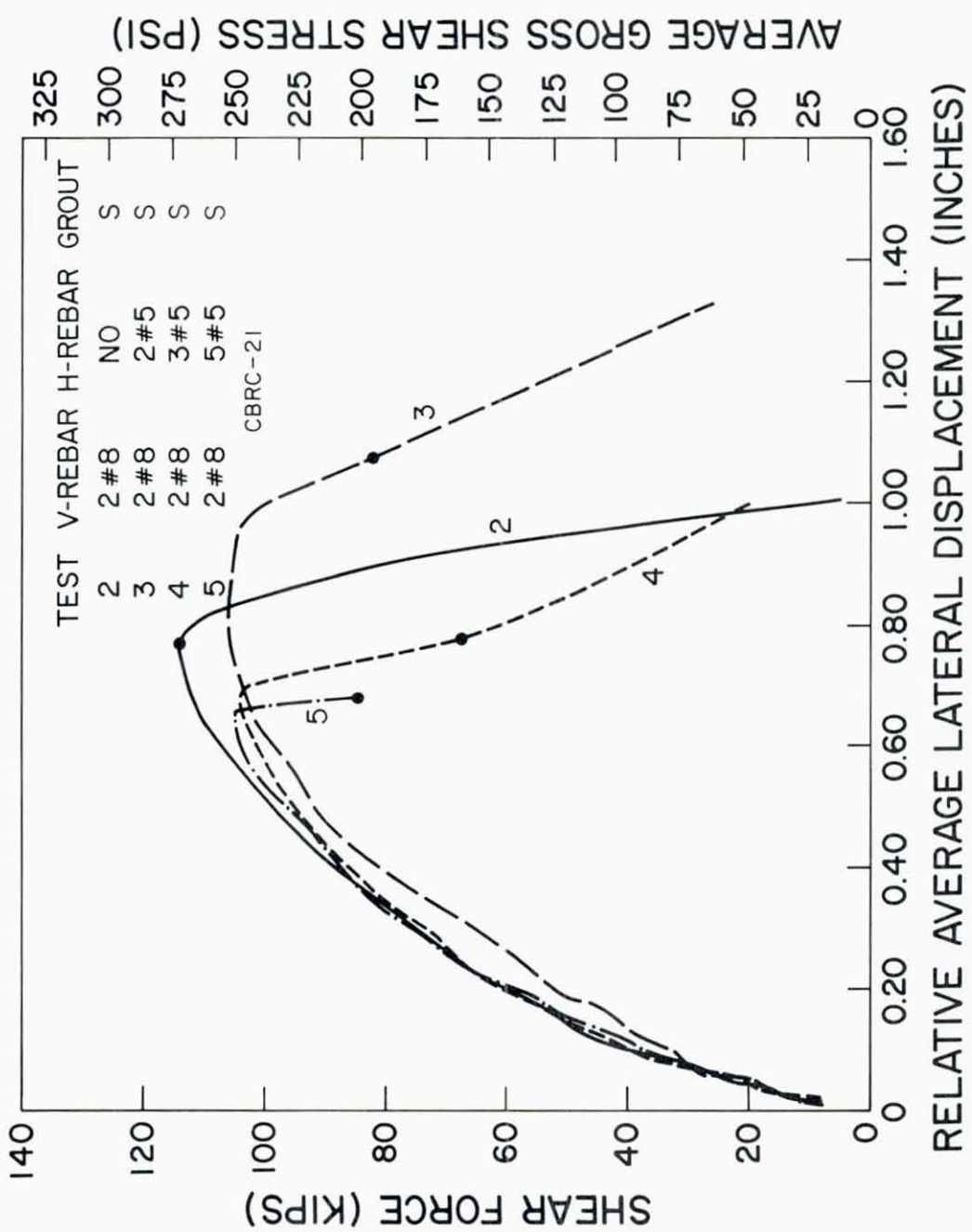

FIG. 5.2 EFFECT OF HORIZONTAL REINFORCEMENT ON HYSTERESIS ENVELOPE (CBRC)

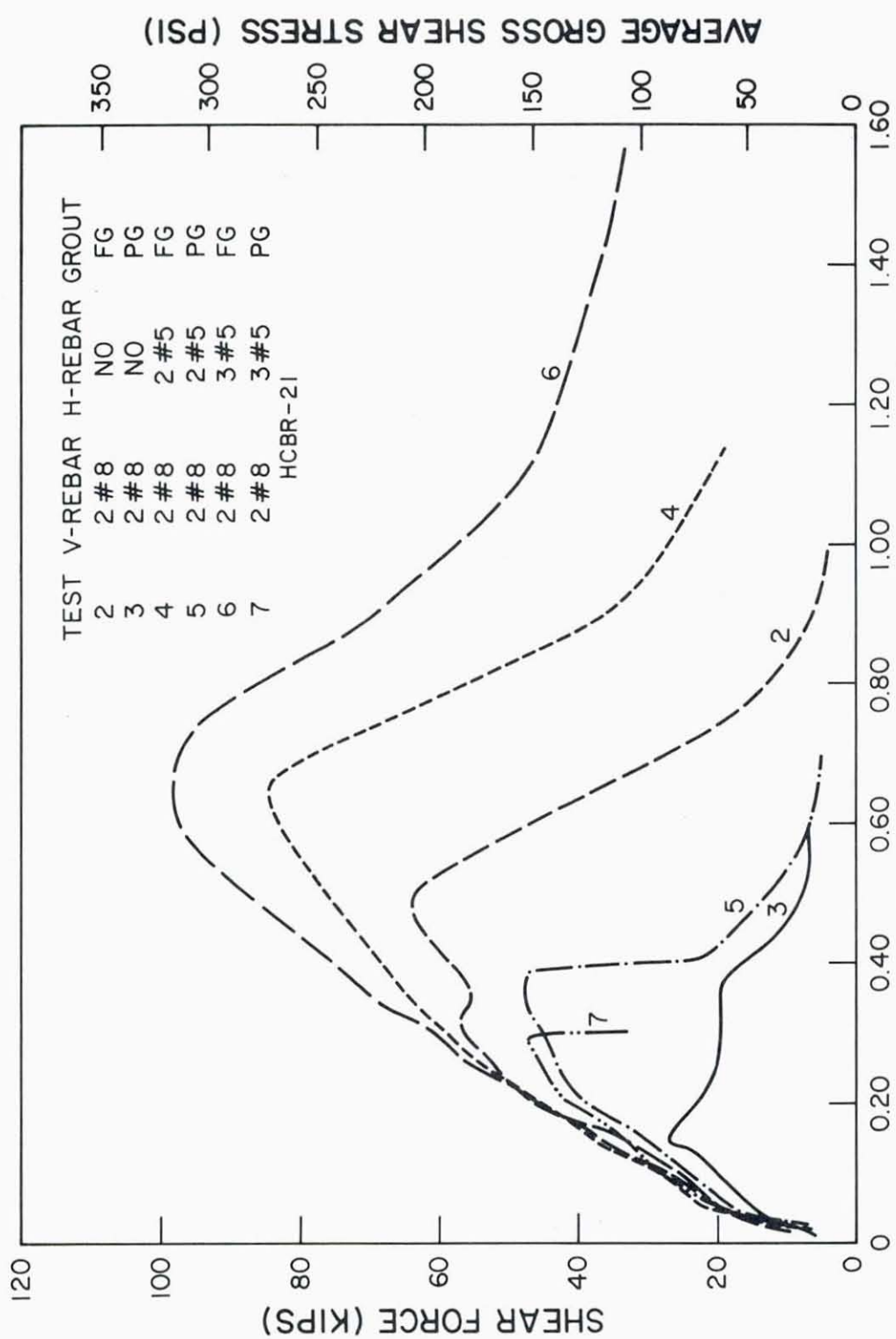

FIG. 5.3 EFFECT OF PARTIAL GROUTING ON HYSTERESIS ENVELOPE (HCBR GROSS AREA)

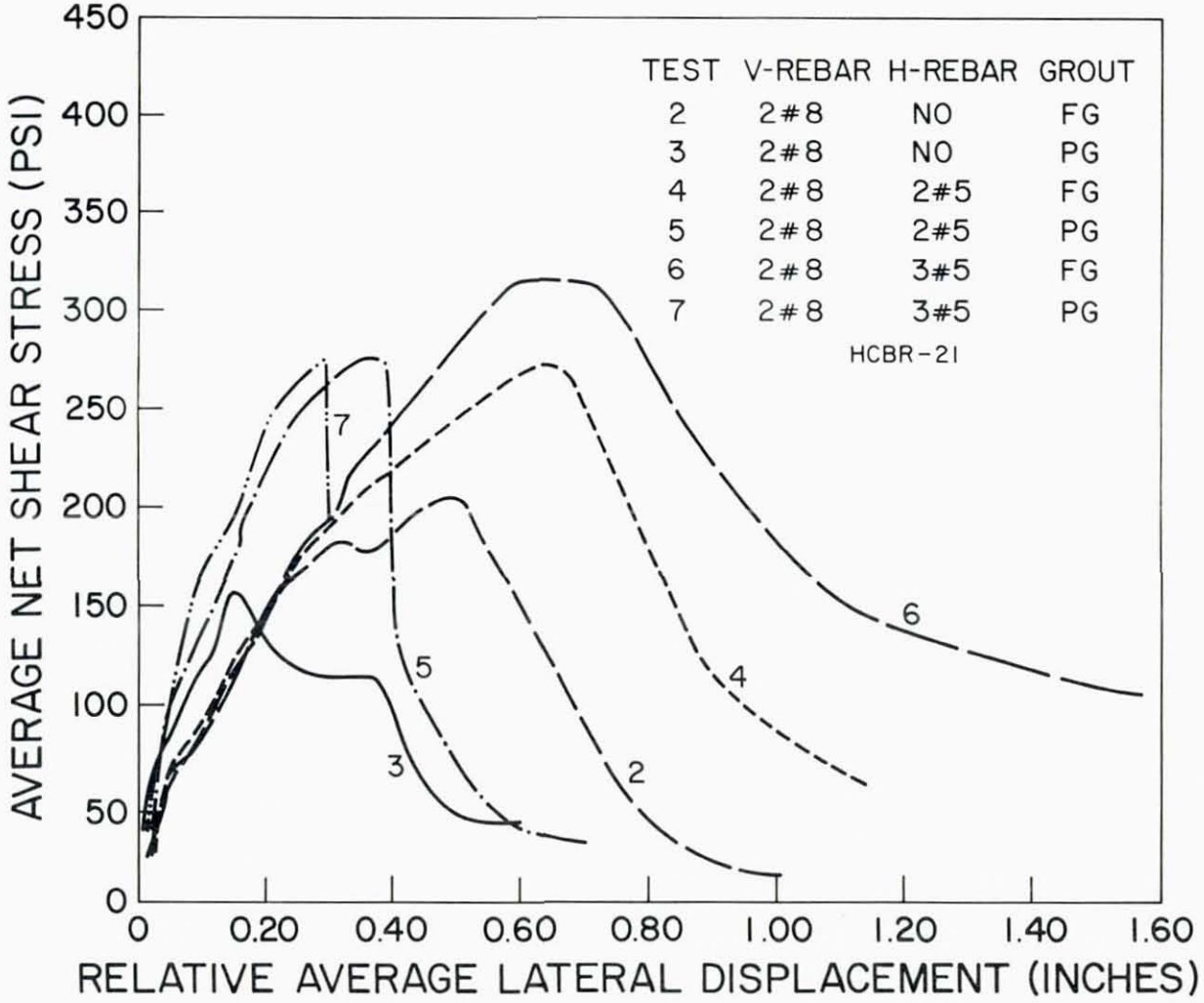

FIG. 5.4 EFFECT OF PARTIAL GROUTING ON HYSTERESIS ENVELOPE (HCBR NET AREA)

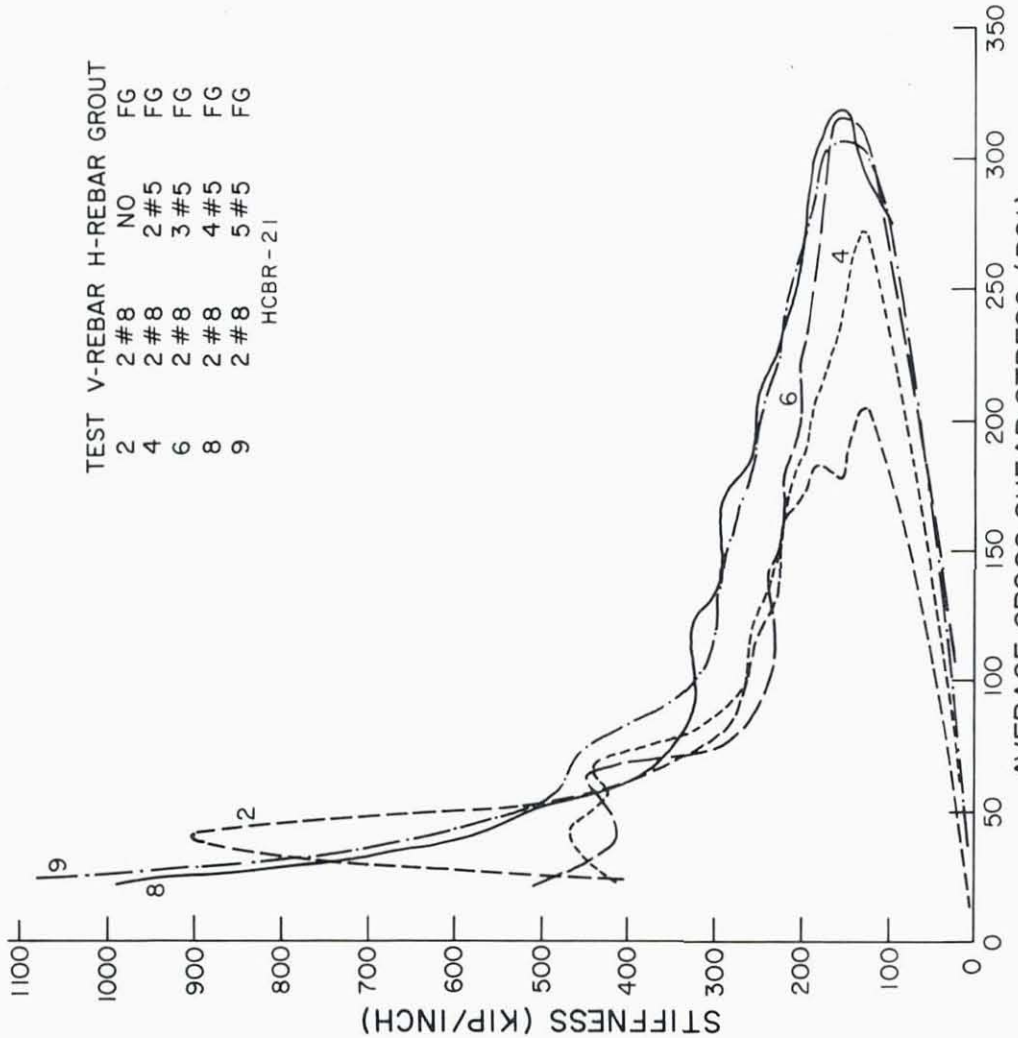

FIG. 5.5 EFFECT OF HORIZONTAL REINFORCEMENT ON STIFFNESS DEGRADATION (HCBR)

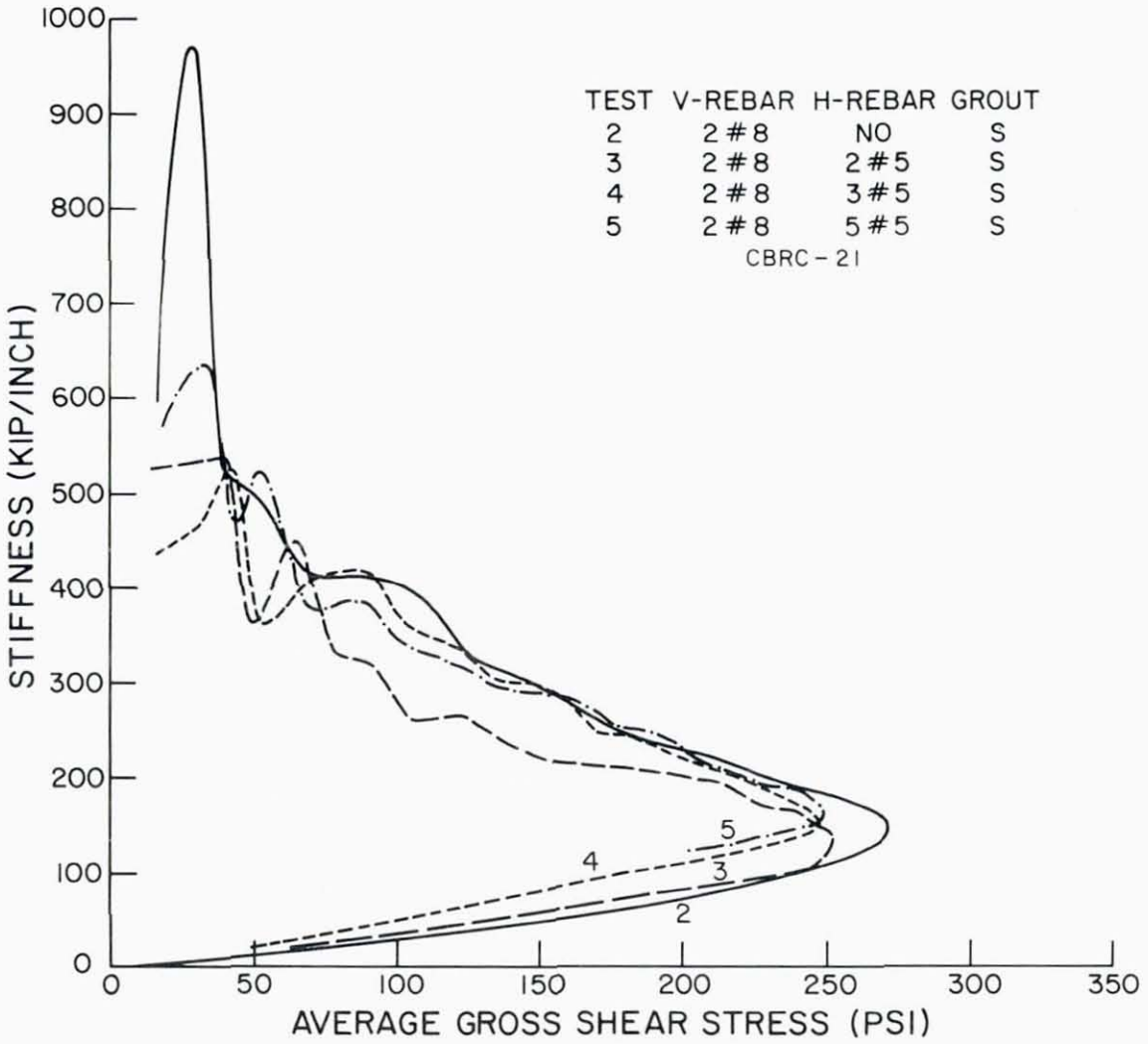

FIG. 5.6 EFFECT OF HORIZONTAL REINFORCEMENT ON STIFFNESS DEGRADATION (CBRC)

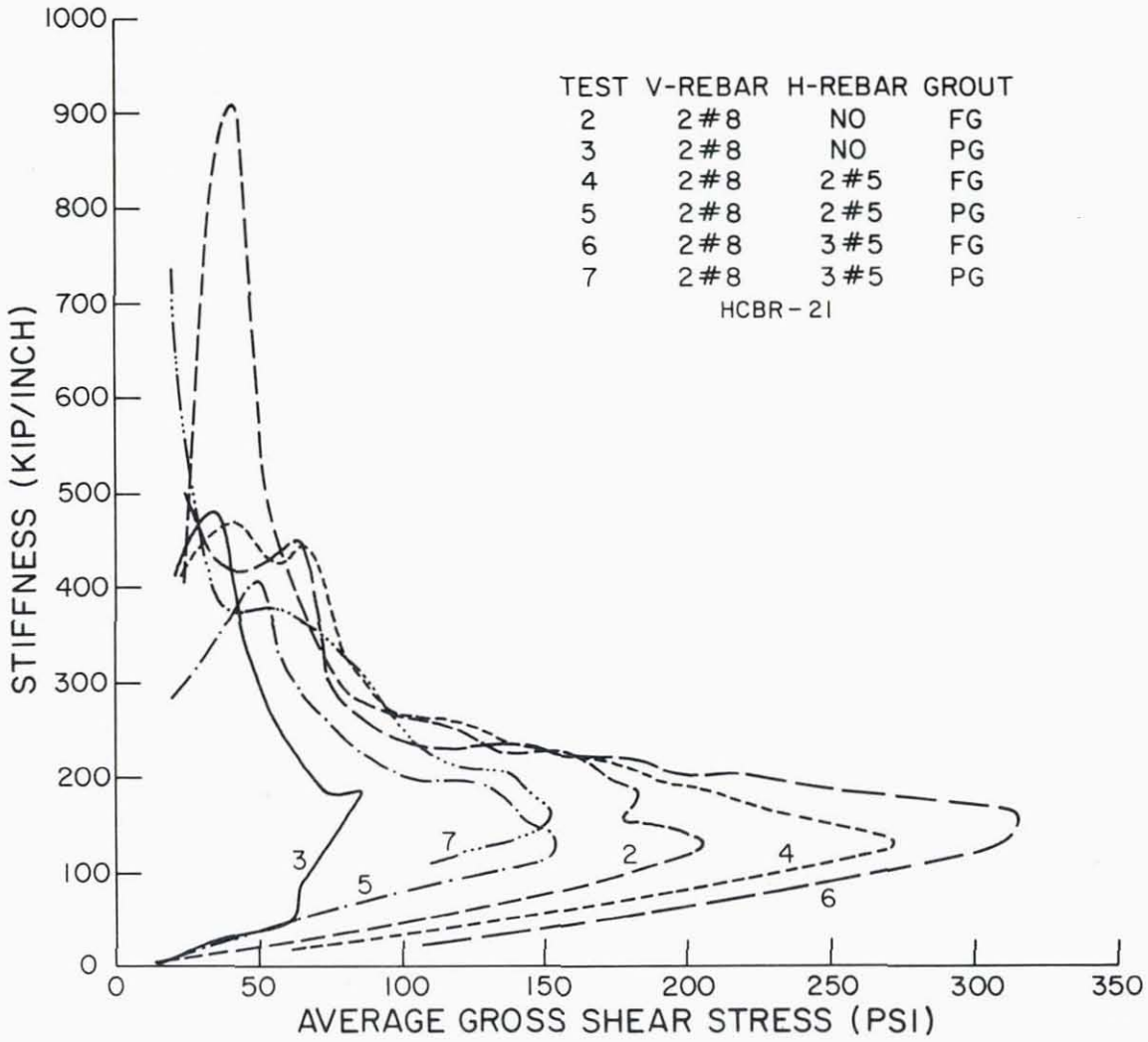

FIG. 5.7 EFFECT OF PARTIAL GROUTING ON STIFFNESS DEGRADATION (HCBR GROSS AREA)

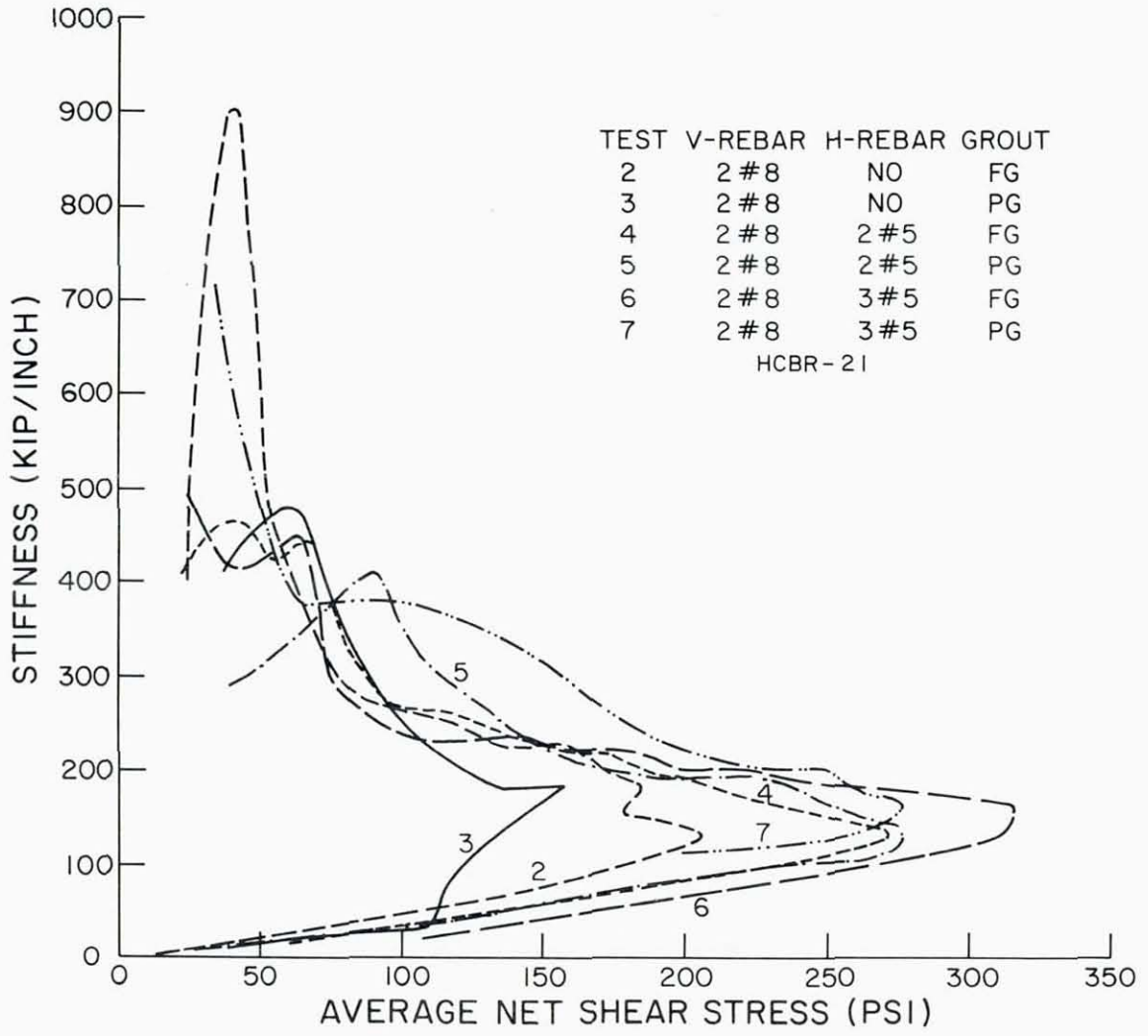

FIG. 5.8 EFFECT OF PARTIAL GROUTING ON STIFFNESS DEGRADATION (HCBR NET AREA)

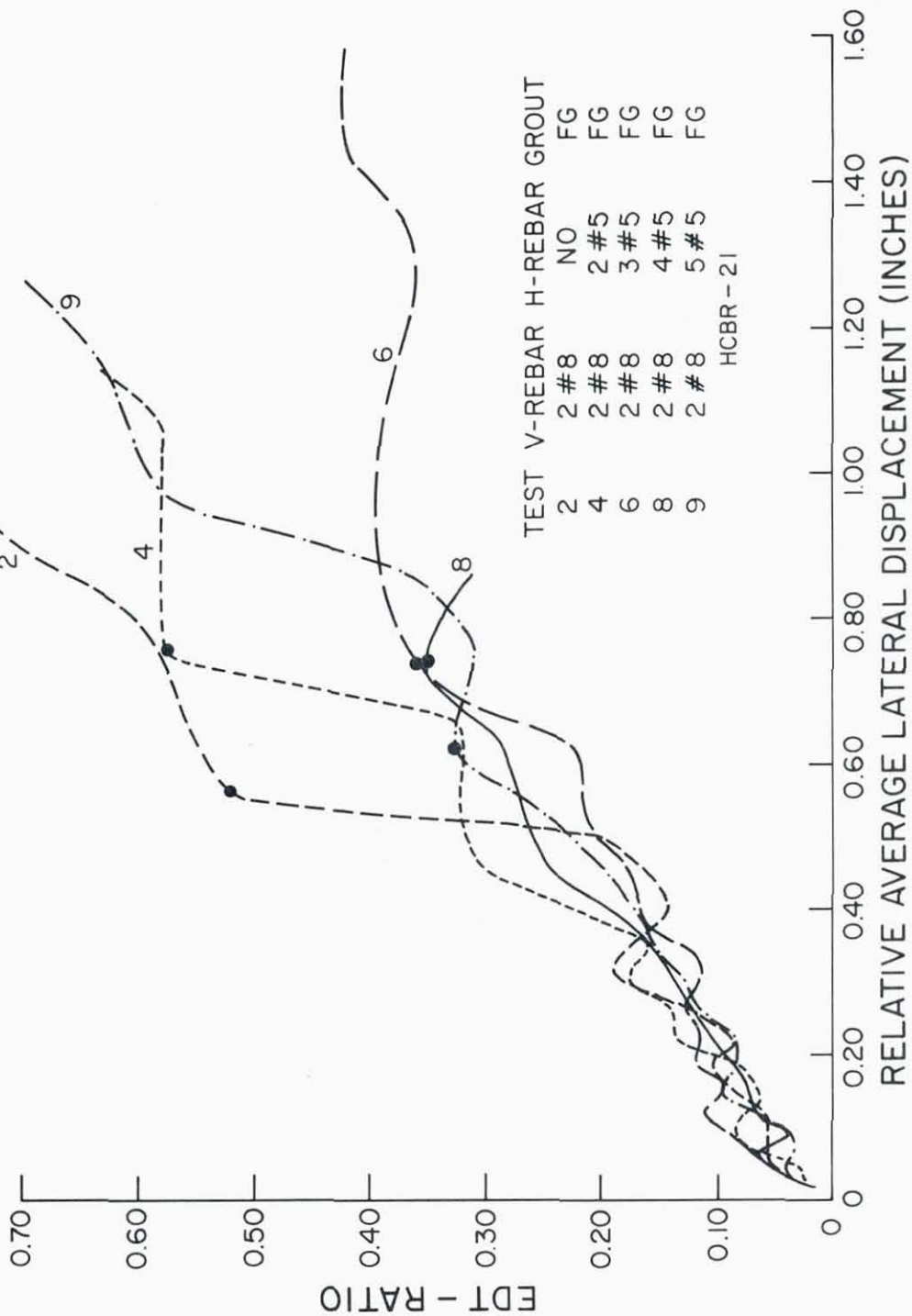

FIG. 5.9 EFFECT OF HORIZONTAL REINFORCEMENT ON ENERGY DISSIPATION (HCBR)

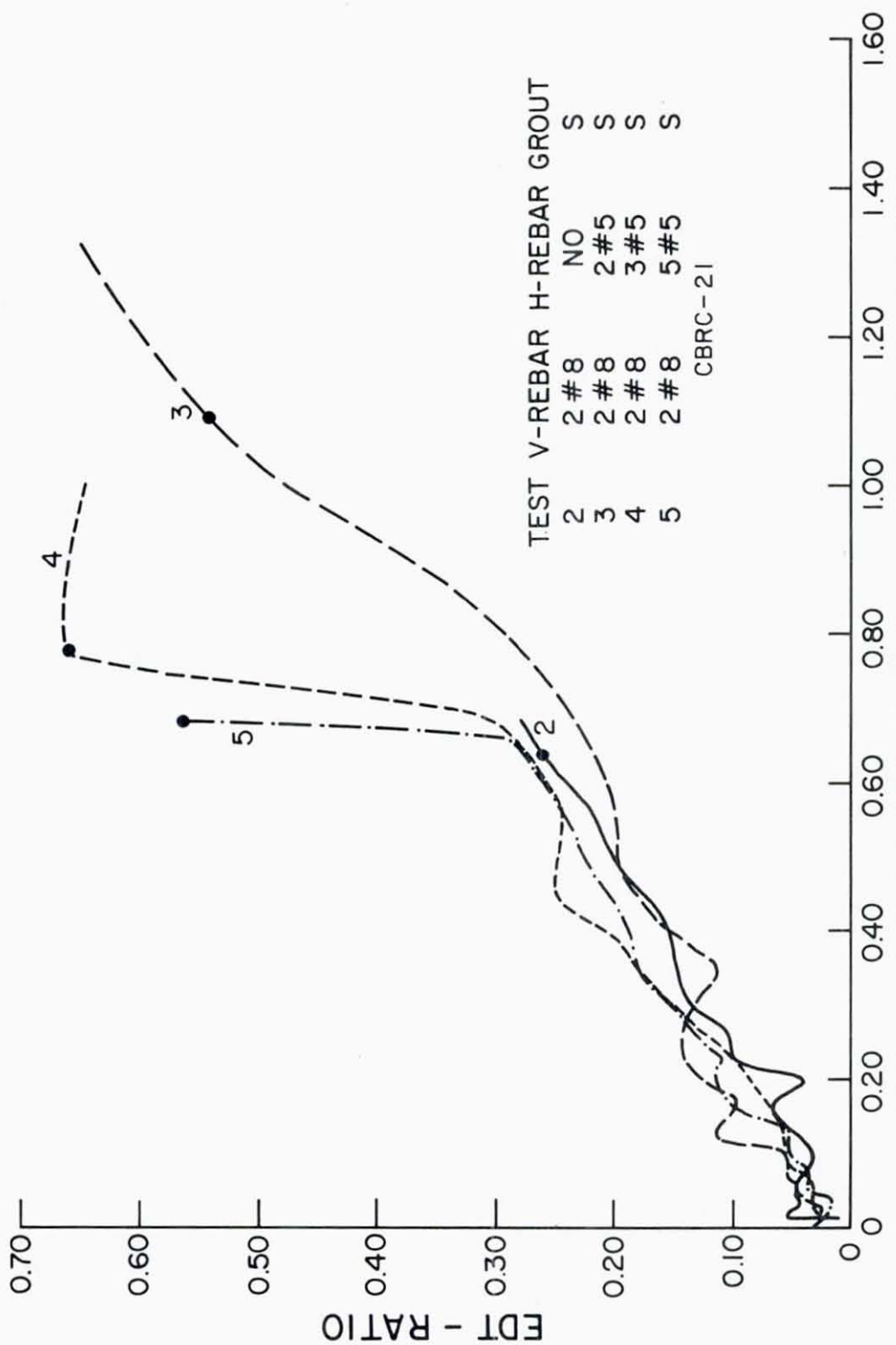

FIG. 5.10 EFFECT OF HORIZONTAL REINFORCEMENT ON ENERGY DISSIPATION (CBRC)

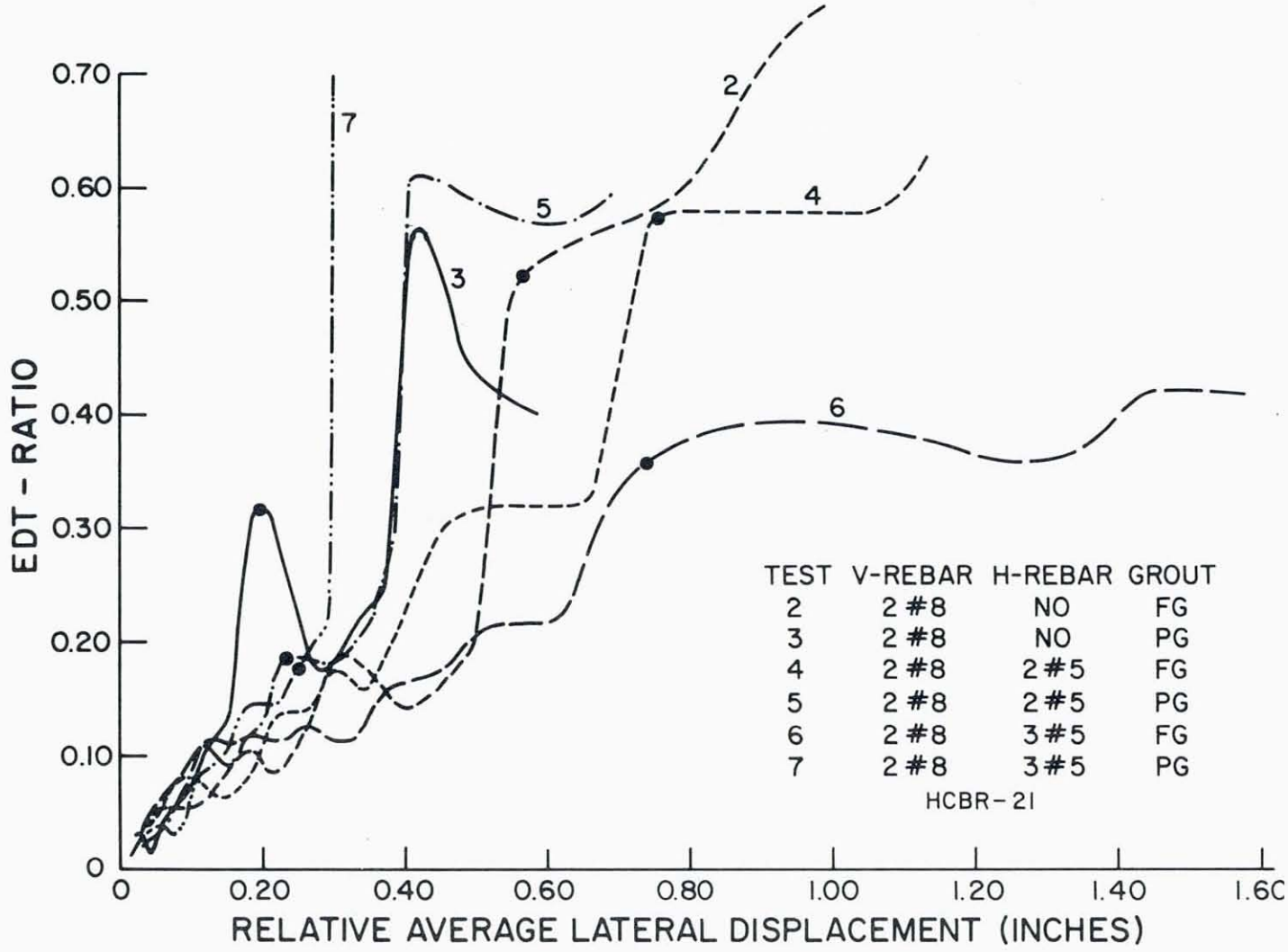

FIG. 5.11 EFFECT OF PARTIAL GROUTING ON ENERGY DISSIPATION (HCBR)

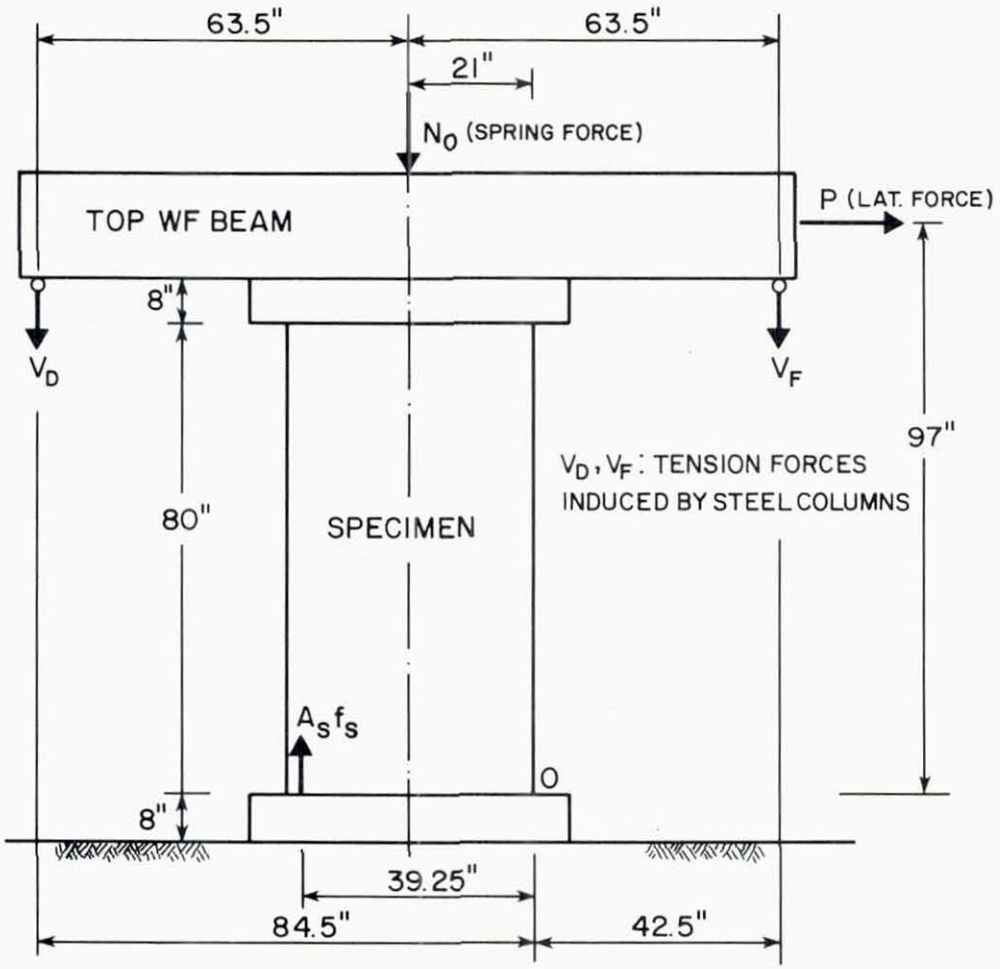

AXIAL COMPRESSIVE FORCE = $N_O + V_D + V_F$

GENERAL MOMENT EQUATION ABOUT O (center of compressive force) :

$$P \times 97 - (N_O + V_D + V_F) \times 21 - (V_D - V_F) \times 63.5 = A_s f_s \times 39.25$$

AT INITIATION OF YIELDING :

$$P_Y \times 97 - (N_O + V_{DY} + V_{FY}) \times 21 - (V_{DY} - V_{FY}) \times 63.5 = A_s f_Y \times 39.25$$

FOR ANY SUBSEQUENT STAGE WHERE THE STEEL CONTINUES YIELDING ($f_s = f_Y$) :

$$\underbrace{(P-P_Y)}_{\Delta P} \times 97 - \underbrace{(V_D + V_F - V_{DY} - V_{FY})}_{\Delta N} \times 21 - \underbrace{(V_D - V_F - V_{DY} + V_{FY})}_{\Delta M} \times 63.5 = 0$$

$$\Delta P = \underbrace{\Delta N \frac{21}{97}}_{(\Delta P)_N} + \underbrace{\Delta M \frac{1}{97}}_{(\Delta P)_M}$$

FIG. 5.12 INFLUENCE OF AXIAL FORCE ON PIER LATERAL STRENGTH

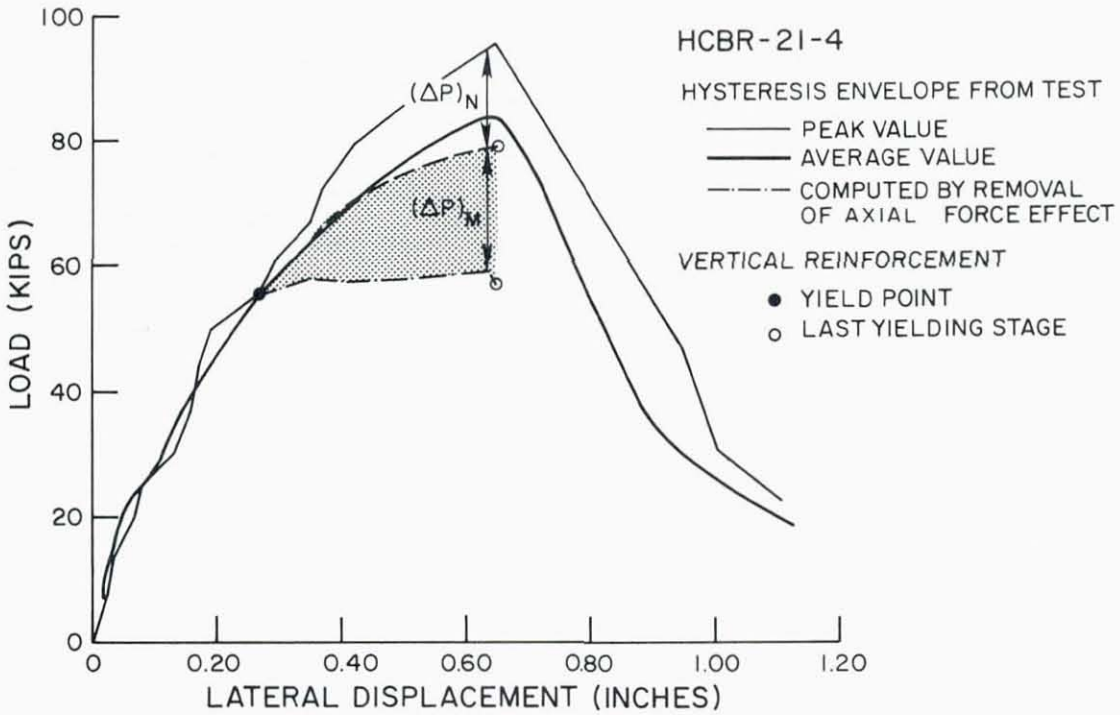

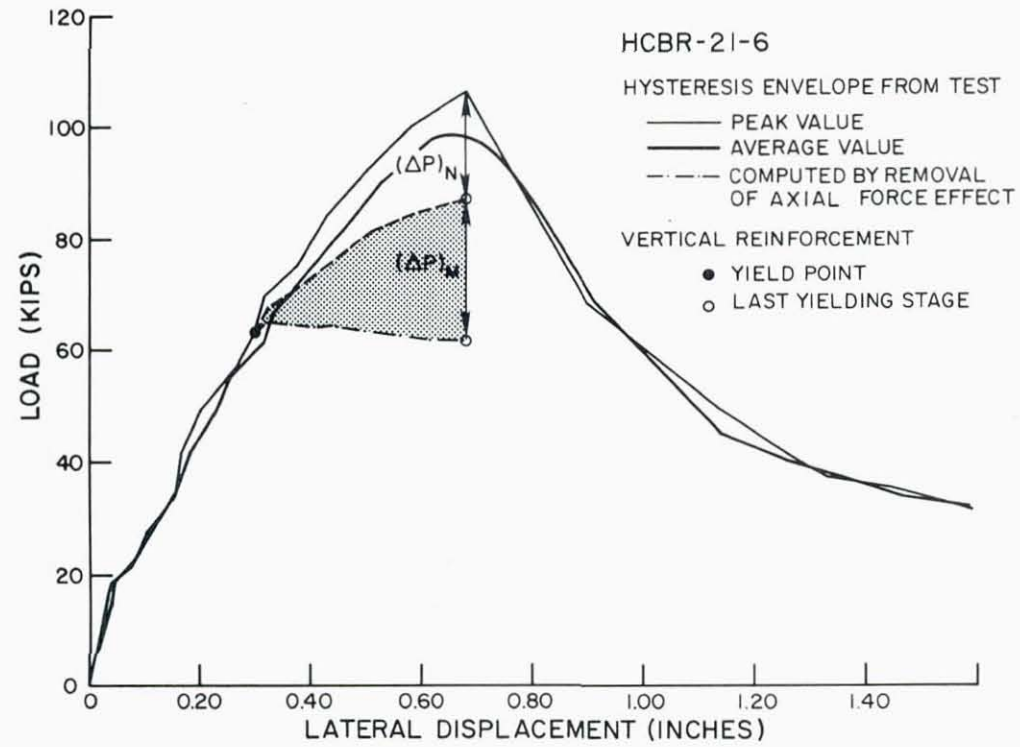

FIG. 5.13(a) INFLUENCE OF AXIAL FORCE ON PIER BEHAVIOR (HCBR)

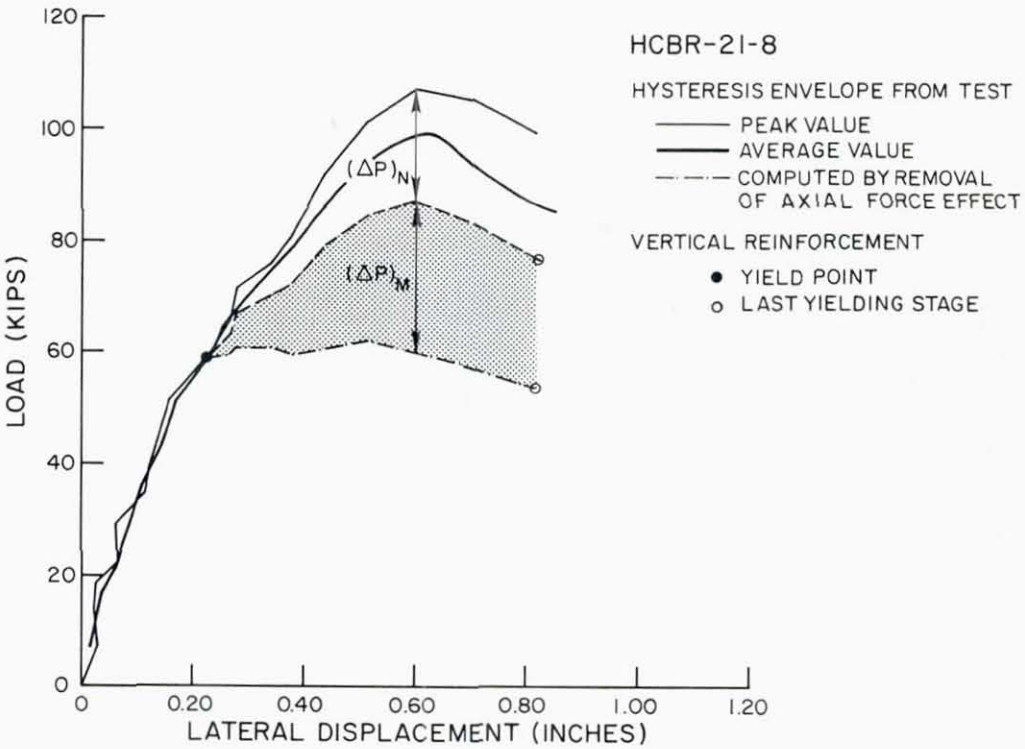

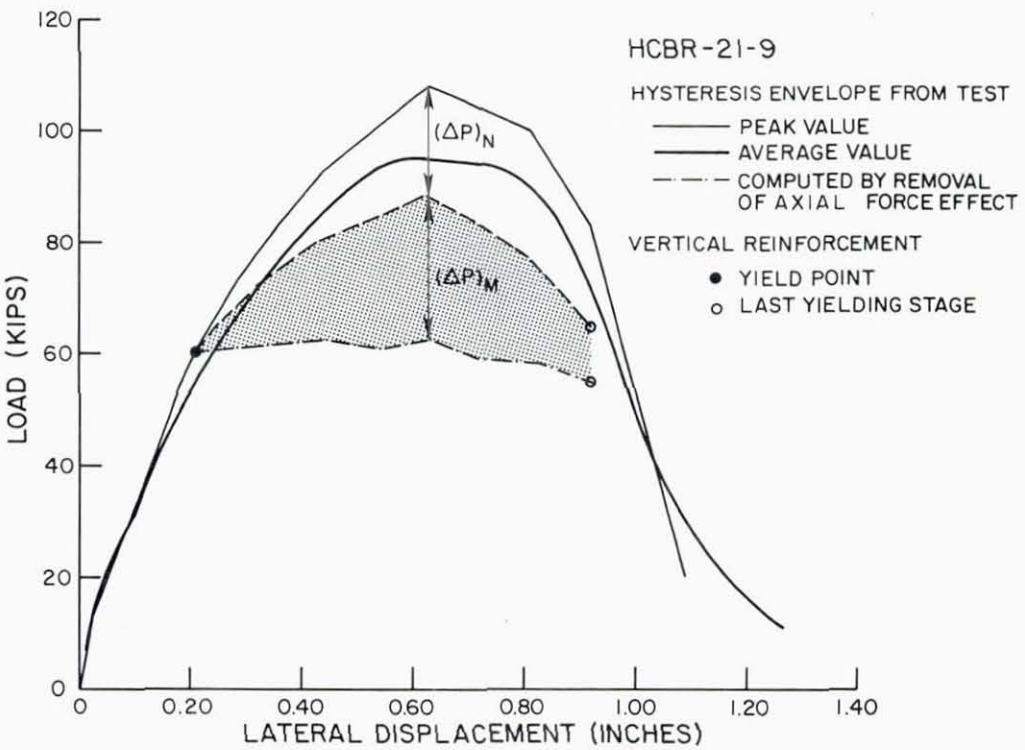

FIG. 5.13(a) CONTINUED

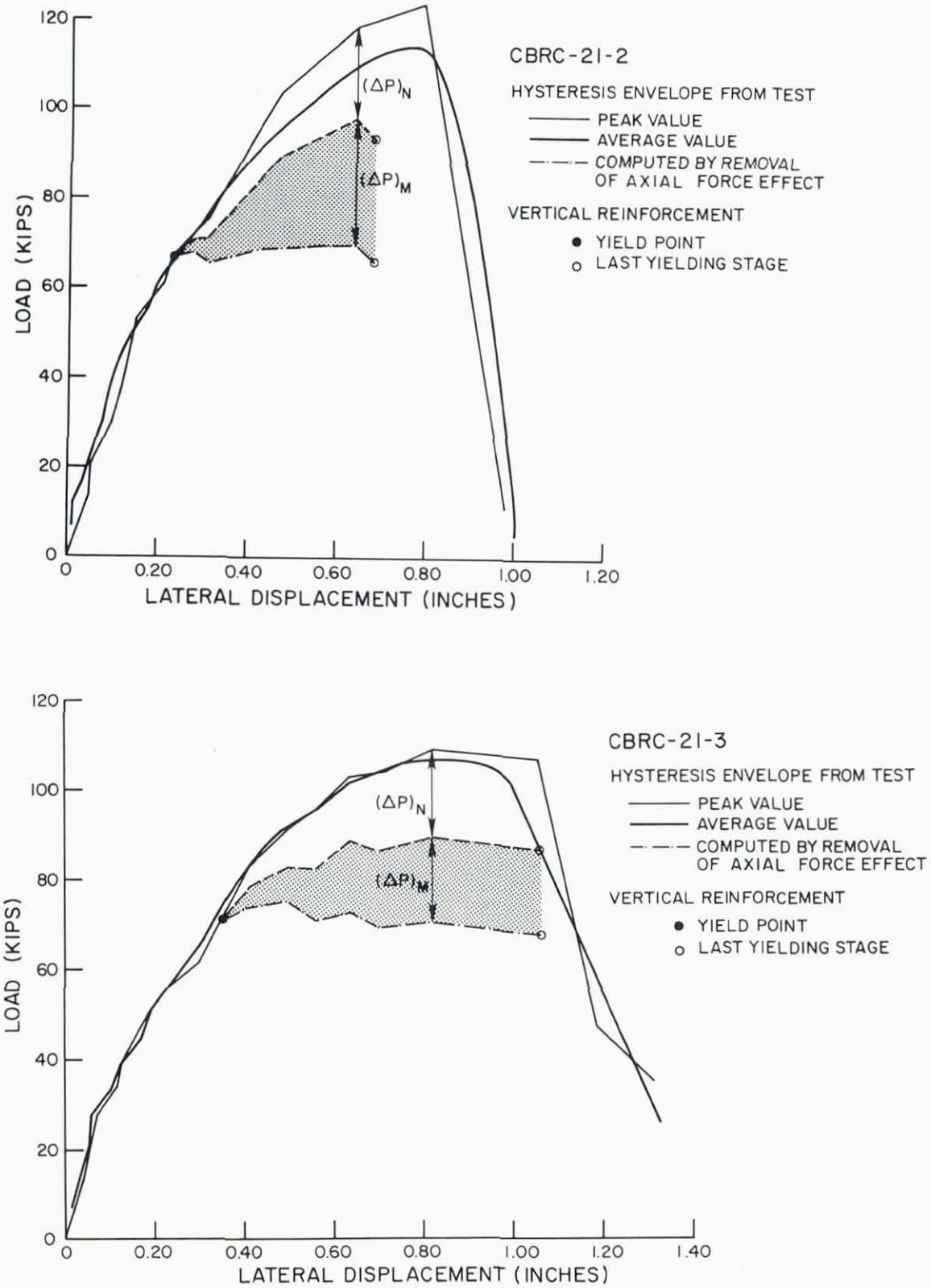

FIG. 5.13(b) INFLUENCE OF AXIAL FORCE ON PIER BEHAVIOR (CBRC)

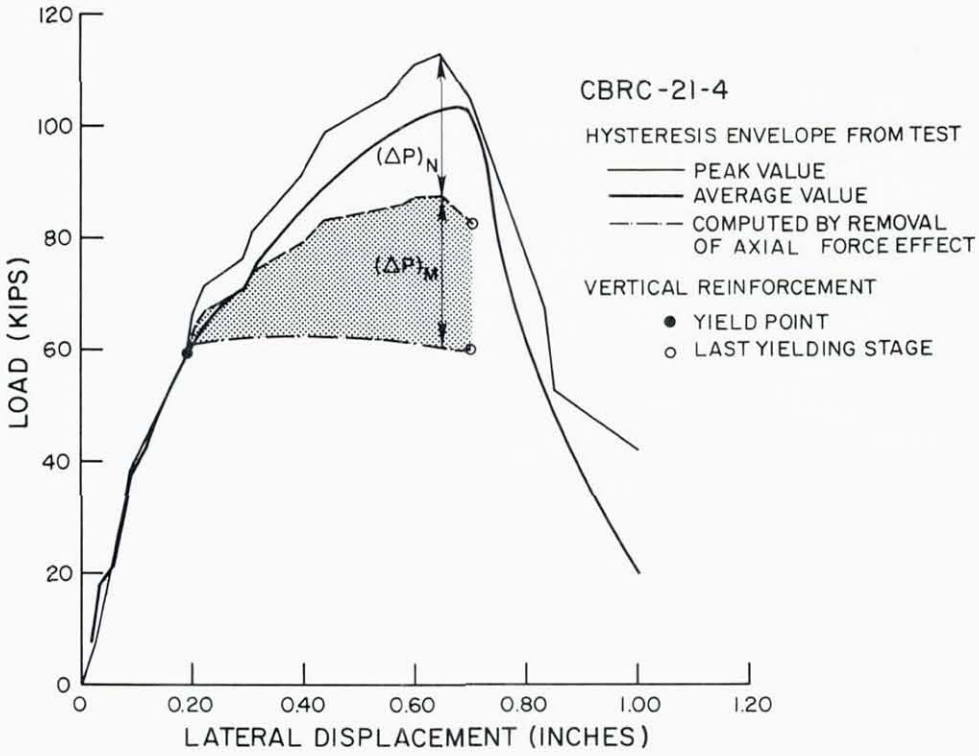

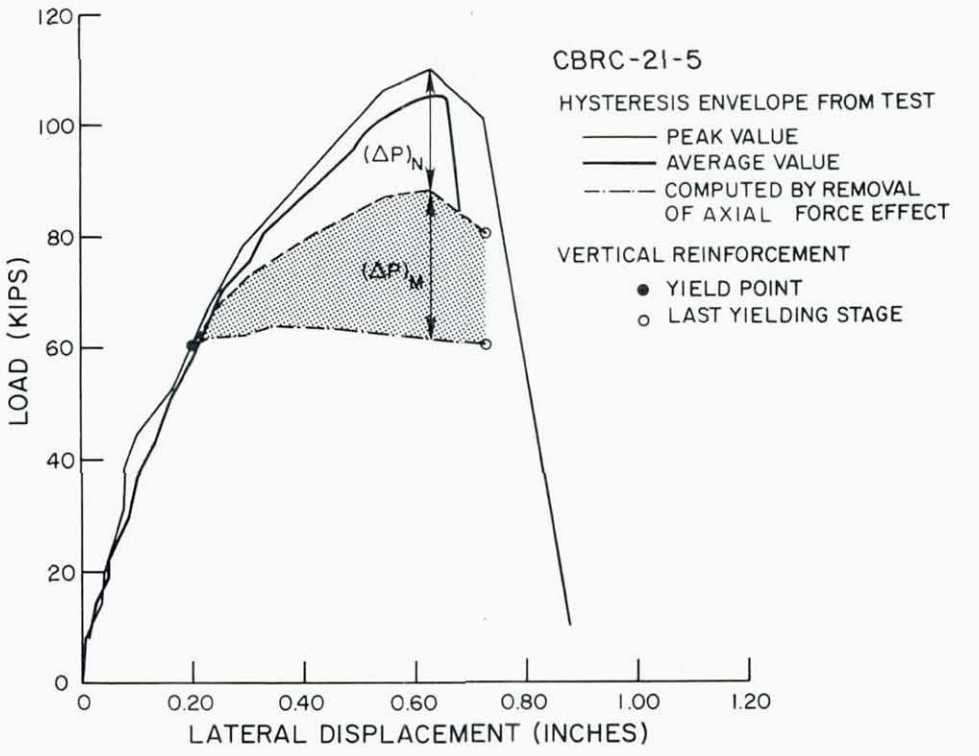

FIG. 5.13(b) CONTINUED

REFERENCES

1. Blume, J.A., and Prolux, J., "Shear in Grouted Brick Masonry Wall Elements," Report to Western States Clay Products from J.A. Blume and Associates, 1968.

2. Greenley, D.G., and Cattaneo, L.E., "The Effect of Edge Load on the Racking Strength of Clay Masonry," Proceedings, Second International Brick Masonry Conference, Stoke-on-Trent, 1970.

3. Mayes, R.L., and Clough, R.W., "A Literature Survey--Compressive, Tensile, Bond and Shear Strength of Masonry," EERC Report No. 75-15, University of California, Berkeley, 1975.

4. Mayes, R.L., and Clough, R.W., "State-of-the-Art in Seismic Strength of Masonry--An Evaluation and Review," EERC Report No. 75-21, University of California, Berkeley, 1975.

5. Mayes, R.L., Omote, Y., Chen, S.W., and Clough, R.W., "Expected Performance of Uniform Building Code Designed Masonry Structures," EERC Report No. 76-7, University of California, Berkeley, 1976.

6. Mayes, R.L., Omote, Y., and Clough, R.W., "Cyclic Shear Tests of Masonry Piers, Volume I--Test Results," EERC Report No. 76-8, University of California, Berkeley, 1976.

7. Mayes, R.L., Omote, Y., and Clough, R.W., "Cyclic Shear Tests on Masonry Piers, Volume II - Analysis of Test Results," Report No. EERC 76-16, 1976.

8. 1977 Masonry Codes and Specifications, Published by the Masonry Industry Advancement Committee, California, 1977.

9. Meli, R., "Behaviour of Masonry Walls under Lateral Loads," Proceedings of the Fifth World Conference on Earthquake Engineering, Rome, 1973.

10. Priestley, M.J.N., and Bridgeman, D.O., "Seismic Resistance of Brick Masonry Walls," Bulletin of the New Zealand National Society for Earthquake Engineering, Vol. 7, No. 4, 1974.

11. Priestley, M.J.N., "Seismic Resistance of Reinforced Concrete Masonry Shear Walls with High Steel Percentages," Bulletin of the New Zealand National Society for Earthquake Engineering, Vol. 10, No. 1, 1977.

12. Scrivener, J.C., "Concrete Masonry Wall Panel Tests with Predominant Flexural Effects," New Zealand Concrete Construction, 1966.

13. Williams, D.W., "Seismic Behaviour of Reinforced Masonry Shear Walls," Ph.D. Thesis, University of Canterbury, Christchurch, New Zealand, 1971.

APPENDIX A

CATALOG OF TEST RESULTS

The experimental results are arranged in three pages for each test, containing six photographs of the successive crack patterns and six graphs obtained from the data collected during the test. These graphs include the hysteresis loops, the hysteresis envelope, stiffness degradation, energy dissipation and amount of shear distortion as compared with total deformation.

In order to show the relation between the photographs of the crack patterns and the diagrams showing the results, a black dot has been drawn on the graphs and by the corresponding picture of the crack pattern.

The details on how each of the diagrams was obtained are presented in Chapter 4.

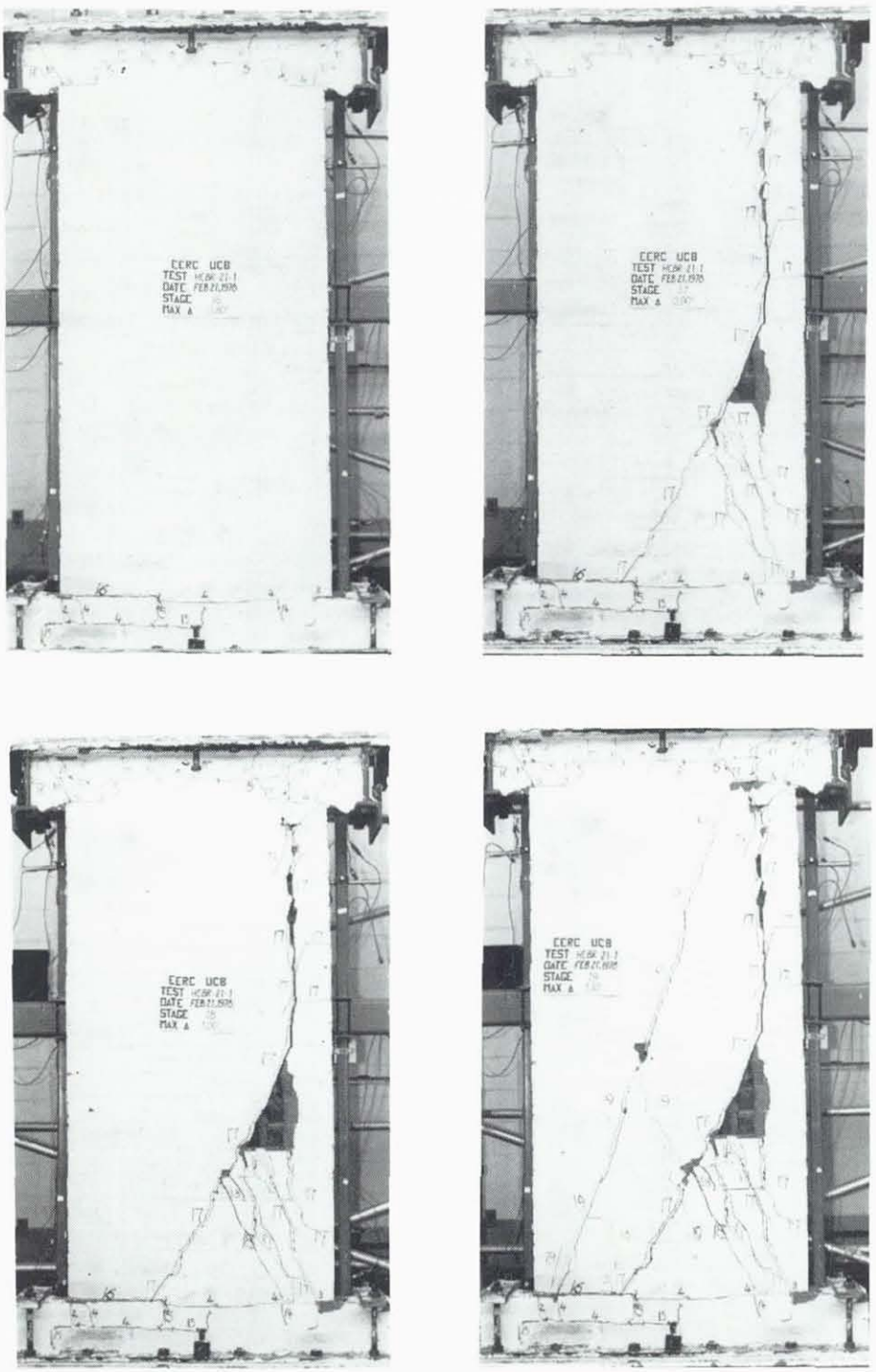

FIG. A.1 SUCCESSIVE CRACK FORMATION
AND EXPERIMENTAL RESULTS
TEST HCBR-21-1

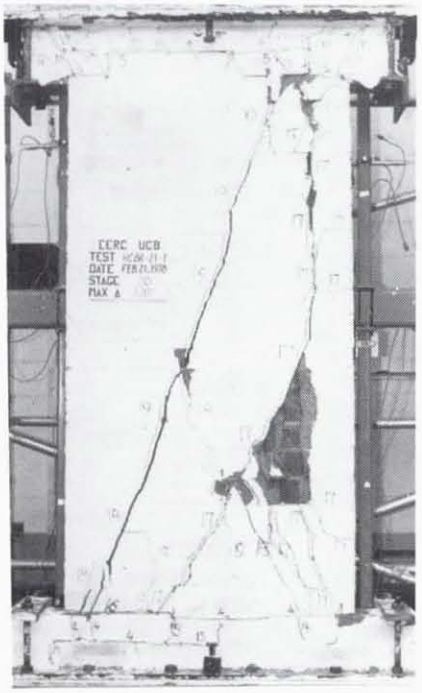

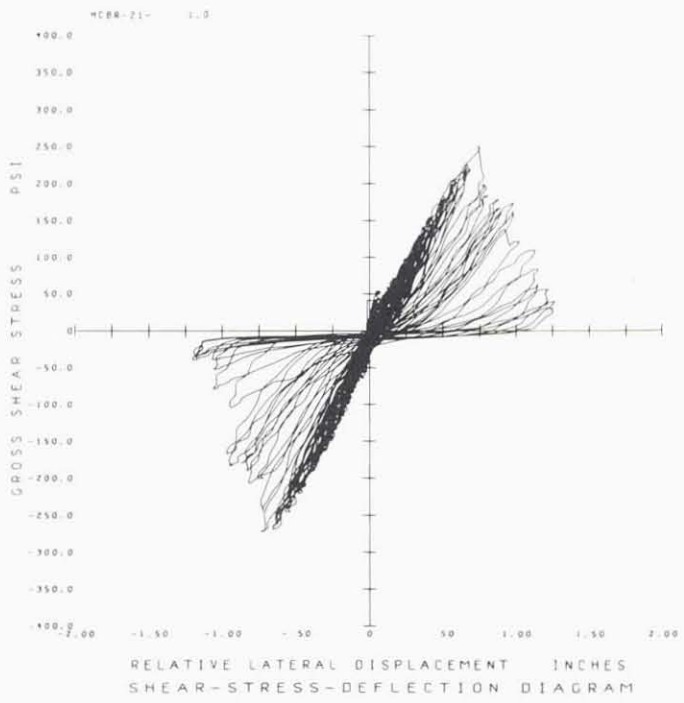

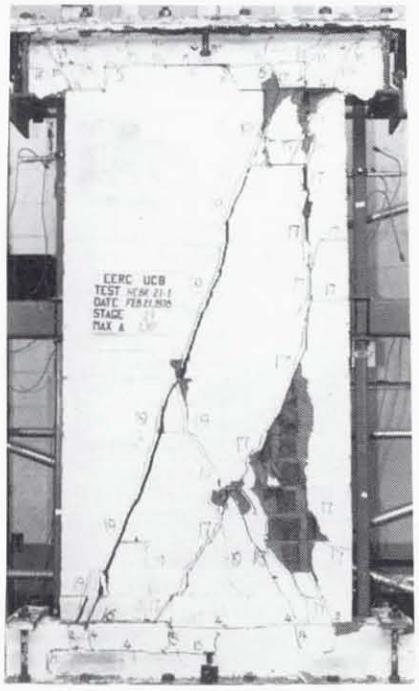

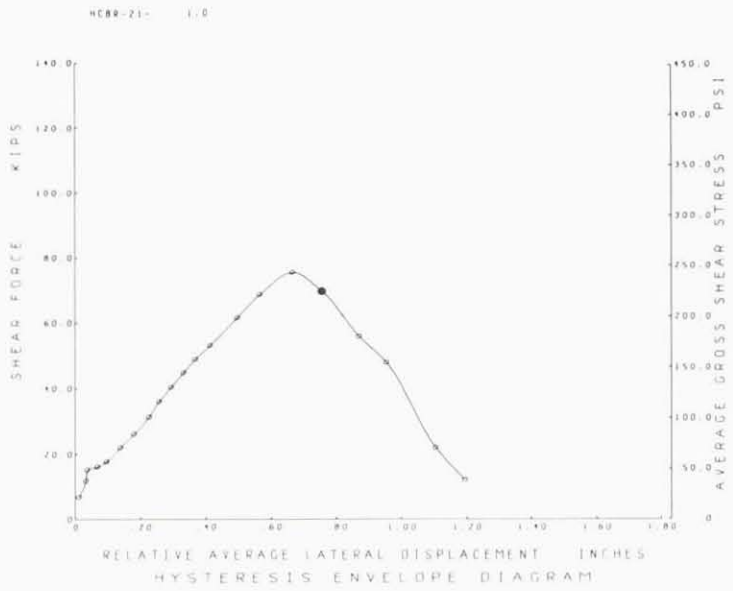

FIG. A.1 CONTINUE HCBR-21-1

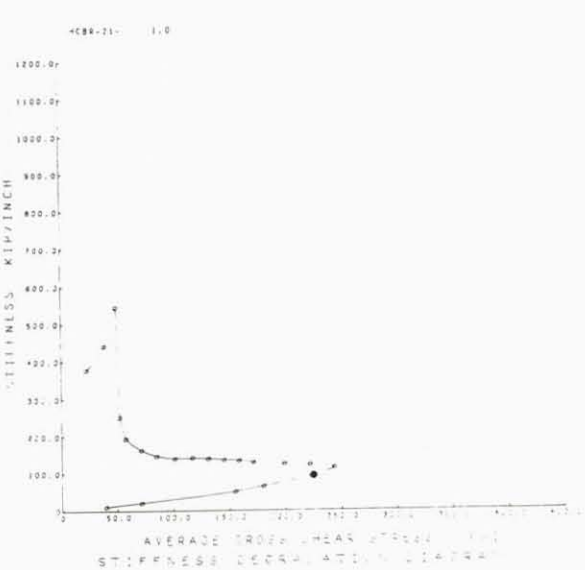

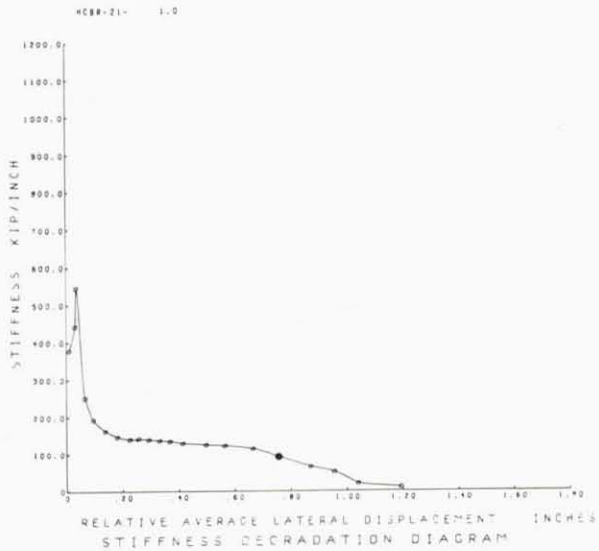

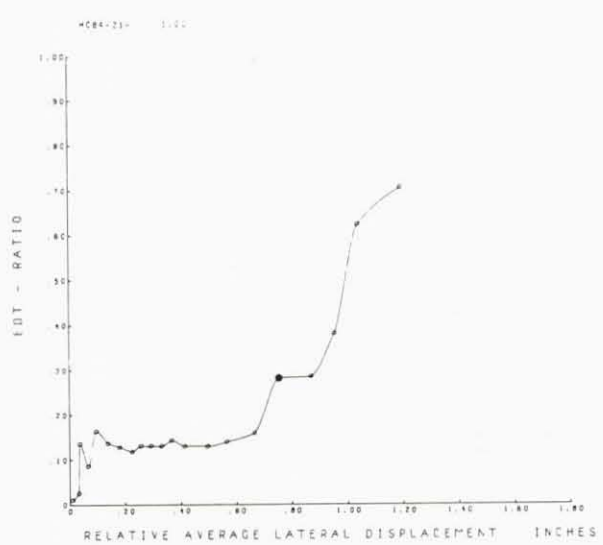

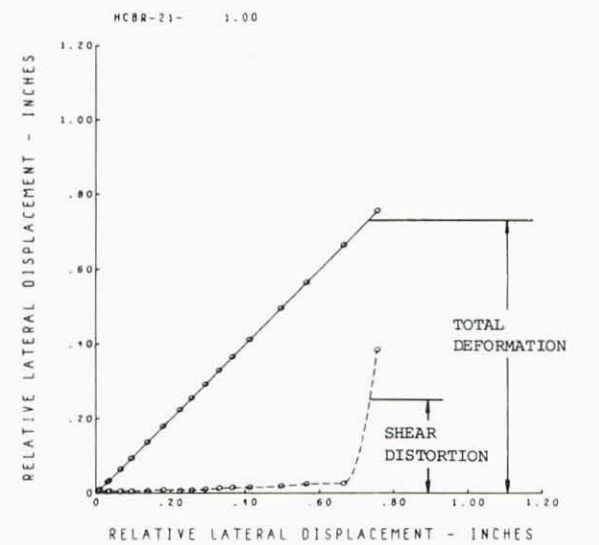

FIG. A.1 CONTINUE HCBR-21-1

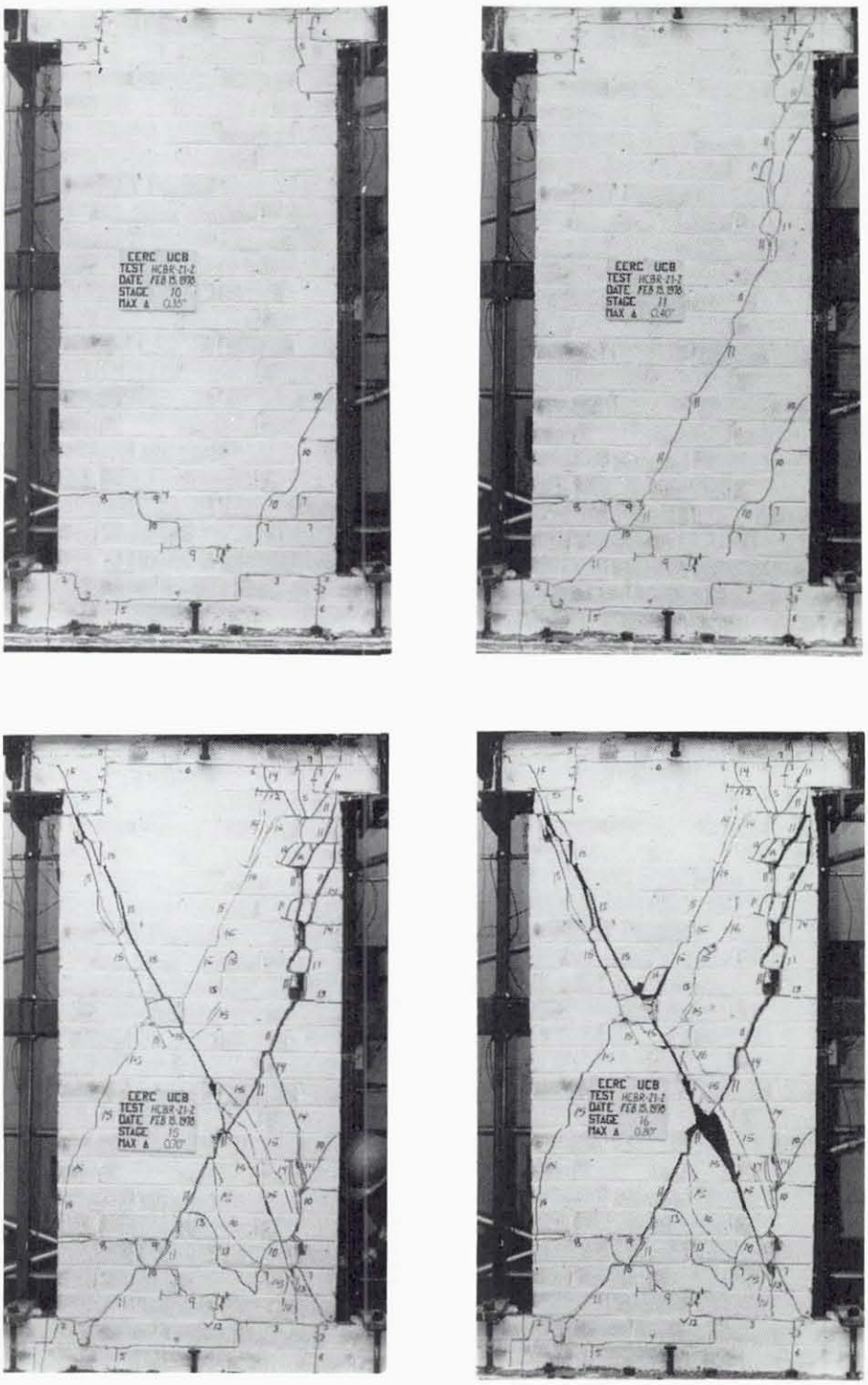

FIG. A.2 SUCCESSIVE CRACK FORMATION
AND EXPERIMENTAL RESULTS
TEST HCBR-21-2

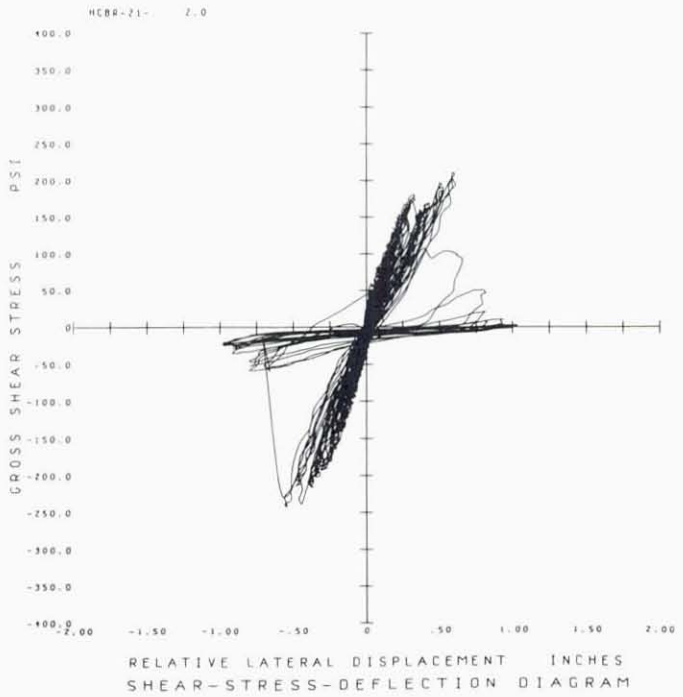

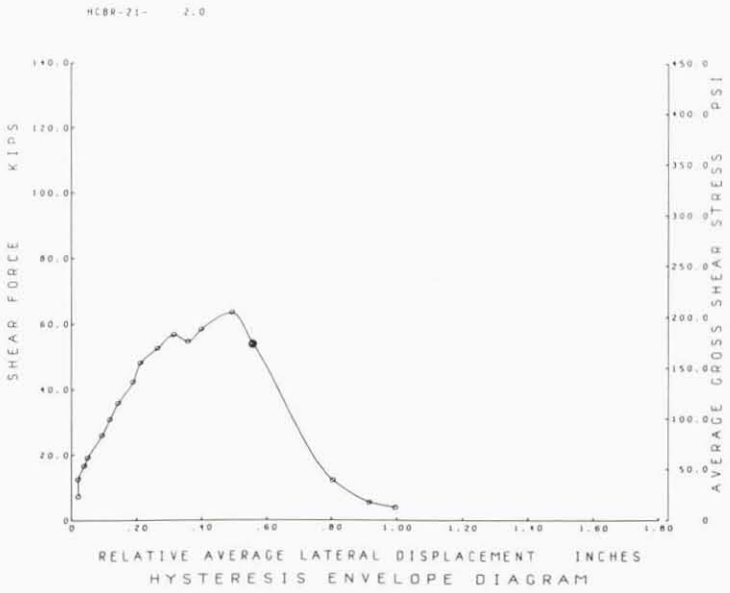

FIG. A.2 CONTINUE HCBR-21-2

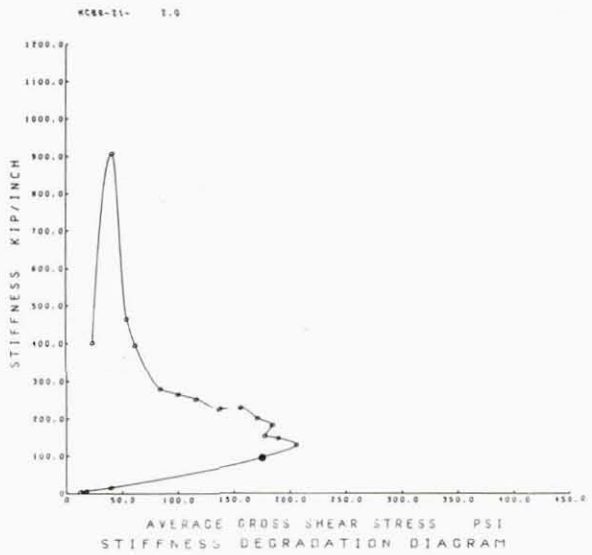

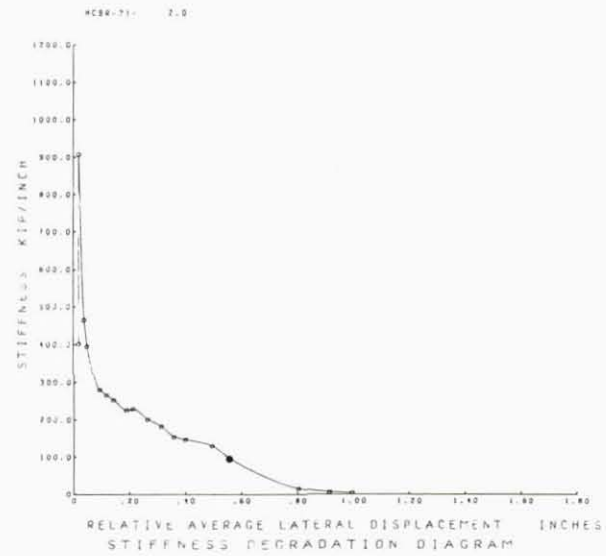

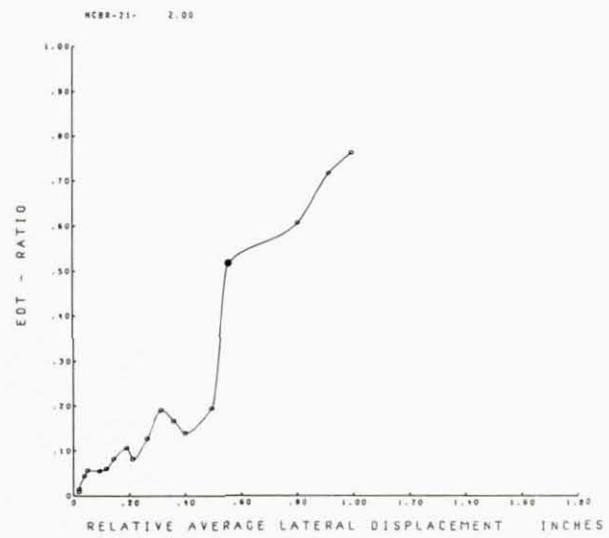

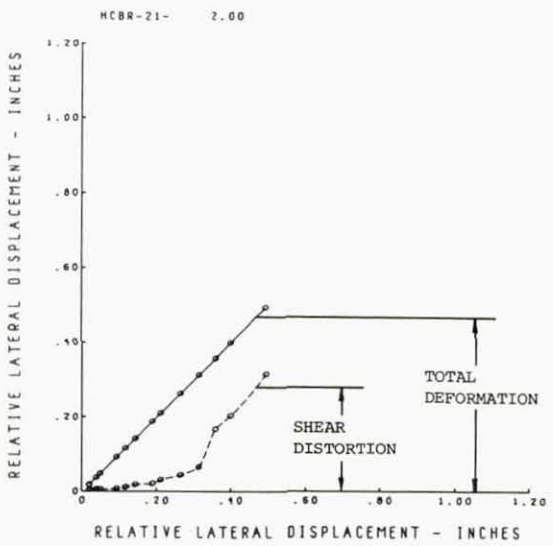

FIG. A.2 CONTINUE HCBR-21-2

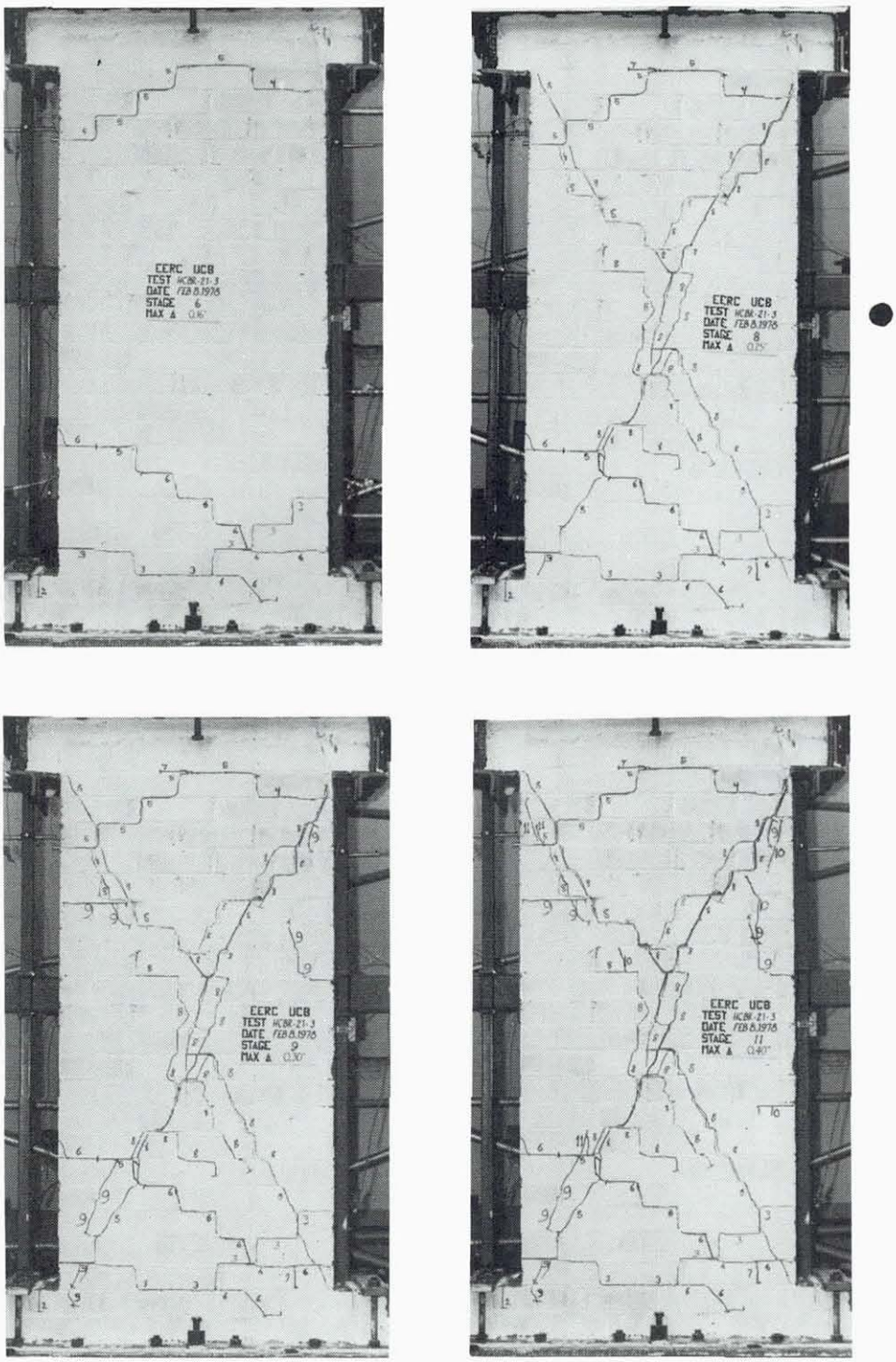

FIG. A.3 SUCCESSIVE CRACK FORMATION
AND EXPERIMENTAL RESULTS
TEST HCBR-21-3

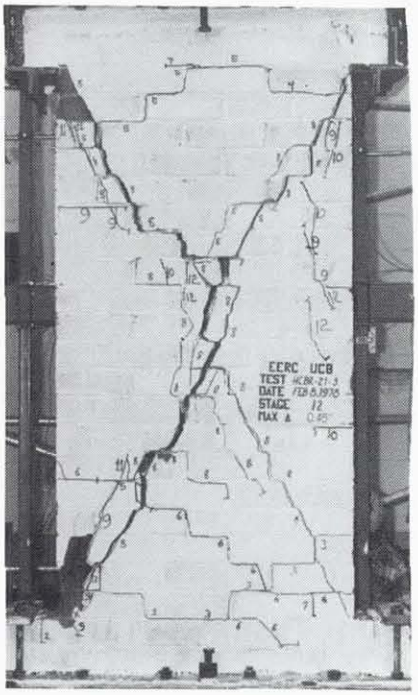

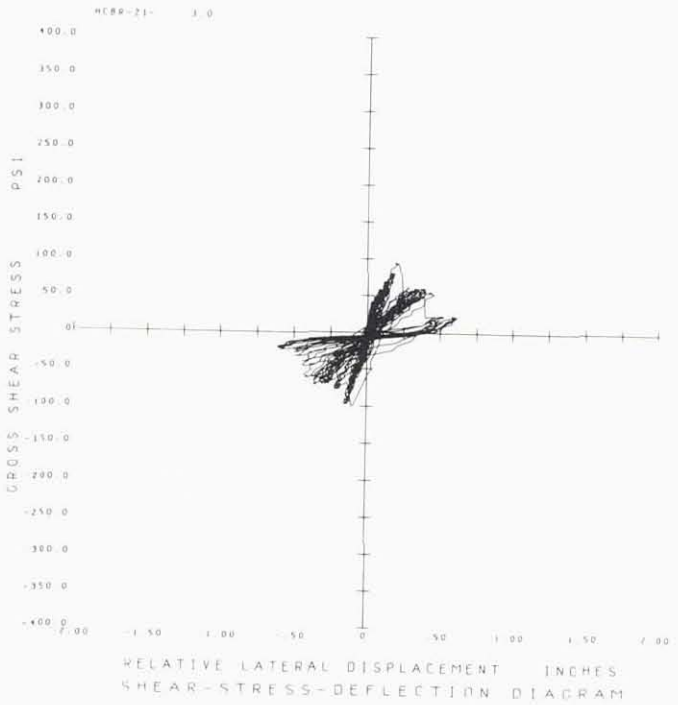

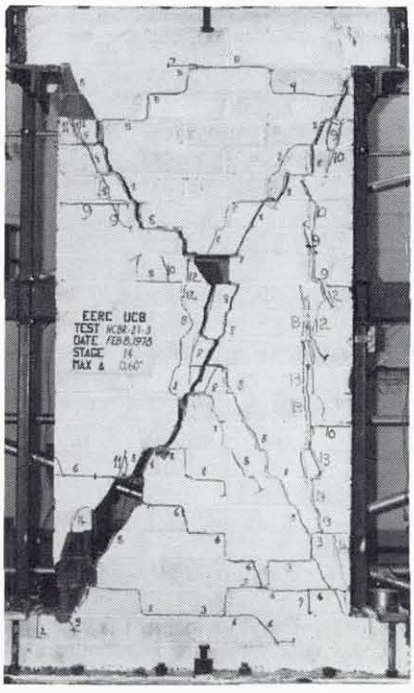

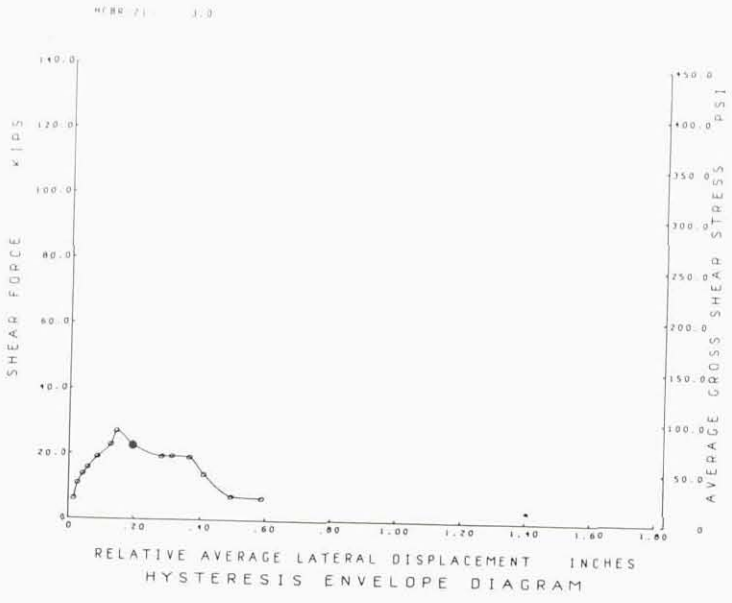

FIG. A.3 CONTINUE HCBR-21-3

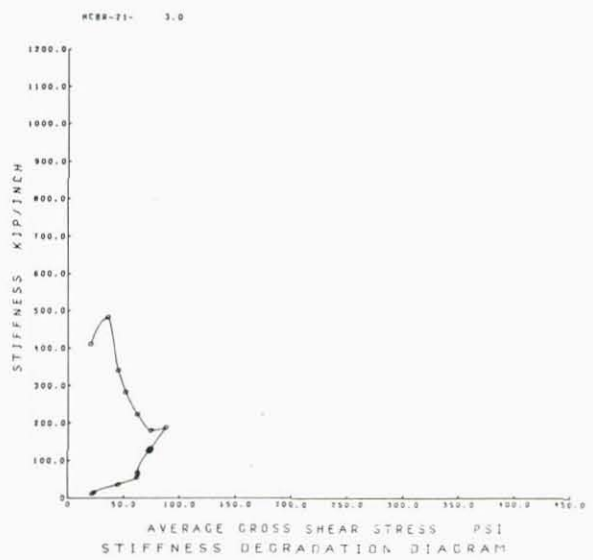

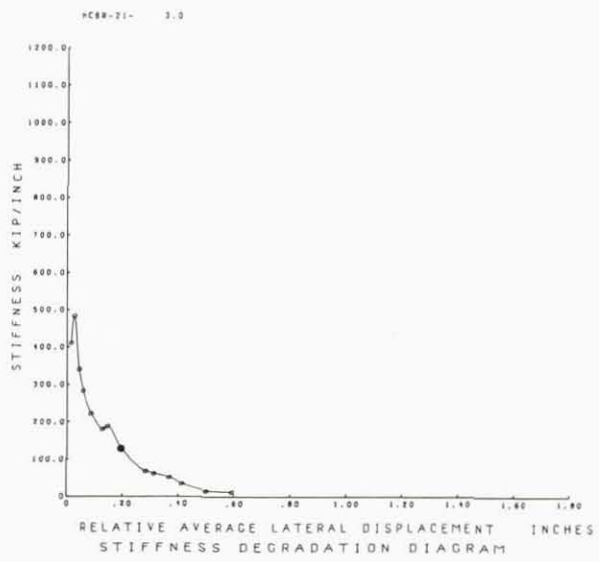

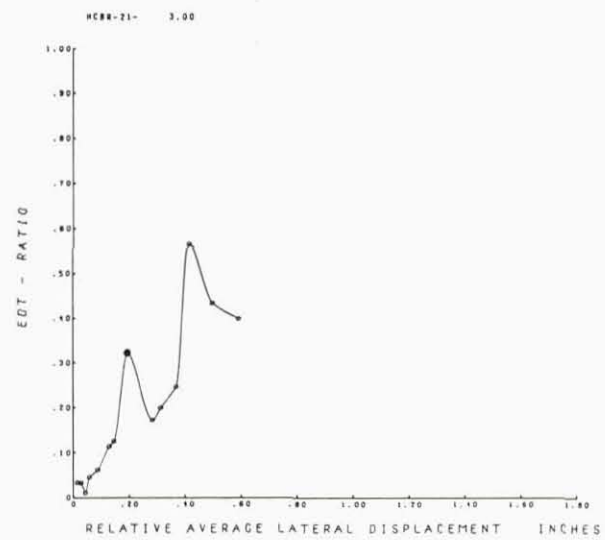

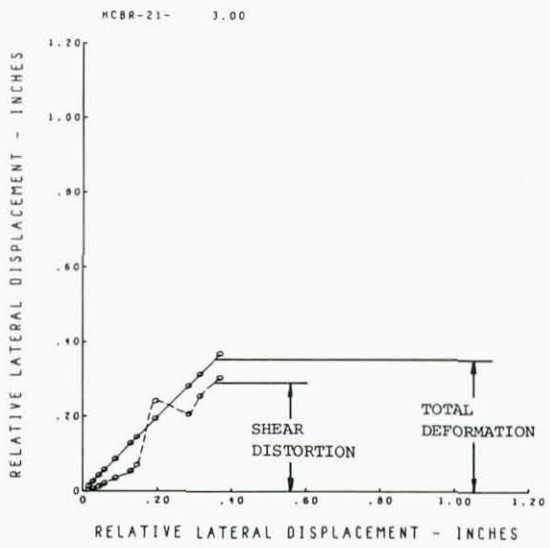

FIG. A.3 CONTINUE HCBR-21-3

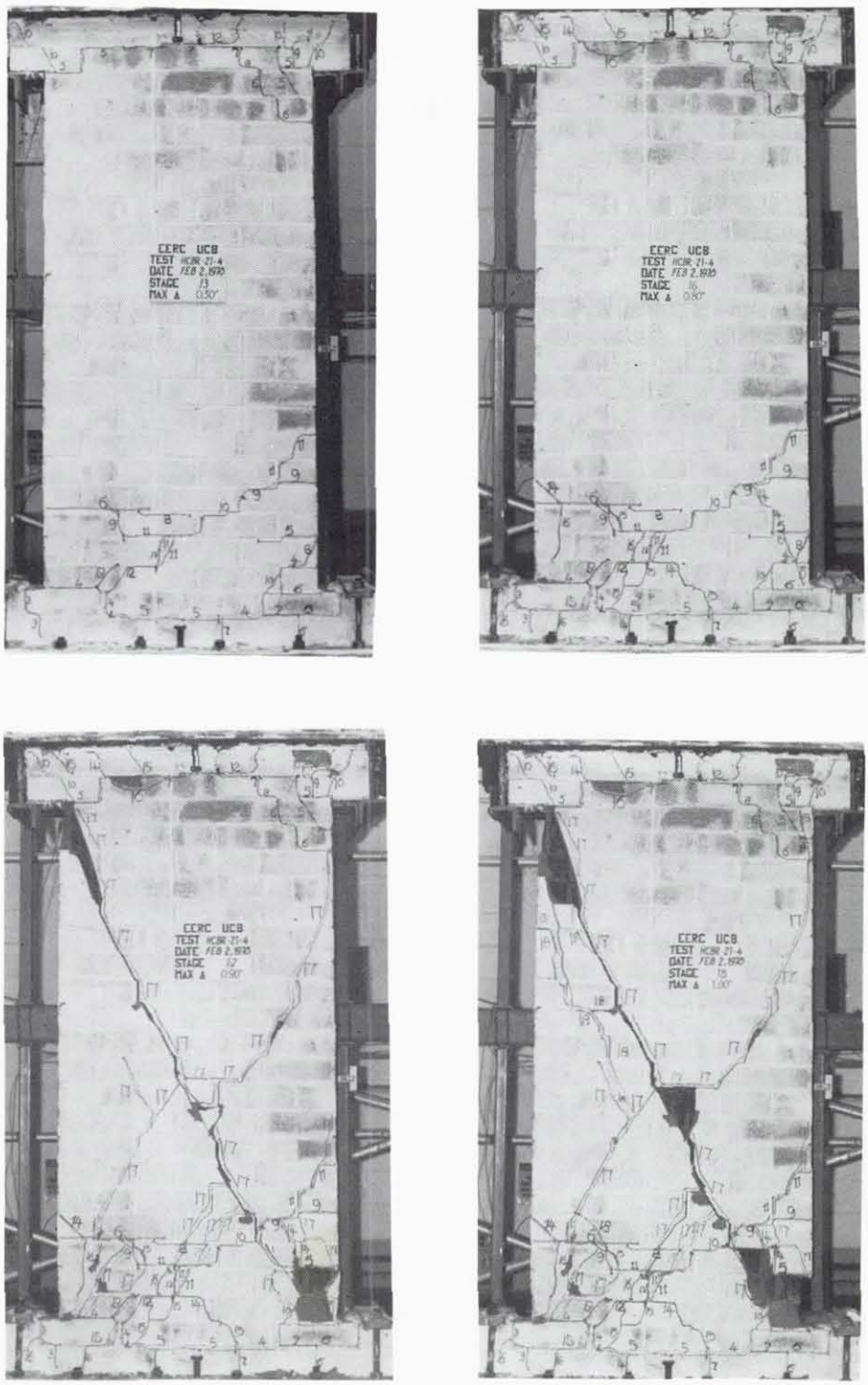

FIG. A.4 SUCCESSIVE CRACK FORMATION
AND EXPERIMENTAL RESULTS
TEST HCBR-21-4

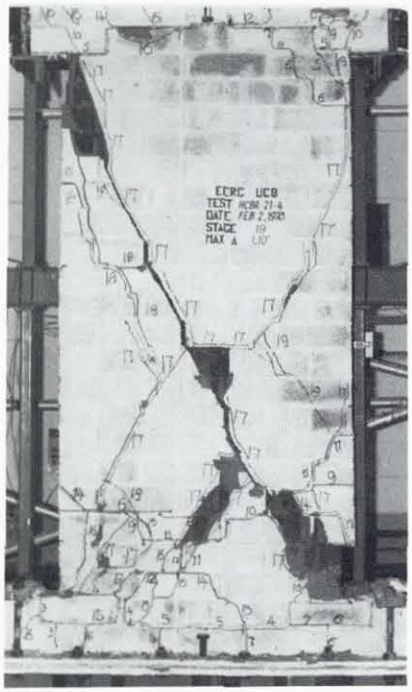

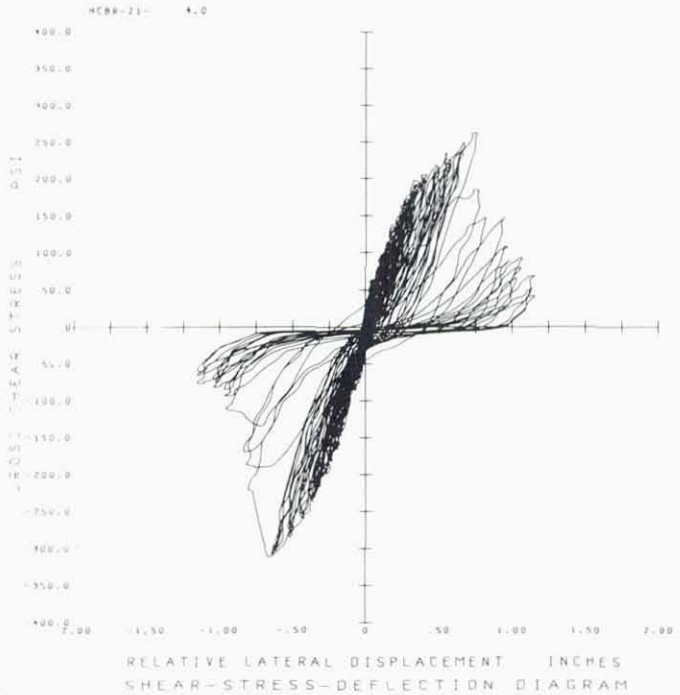

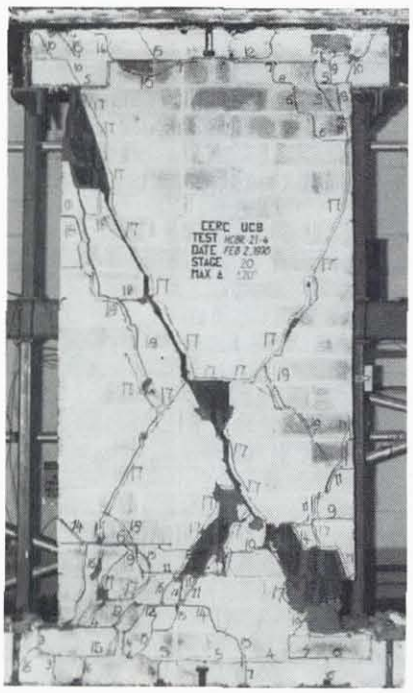

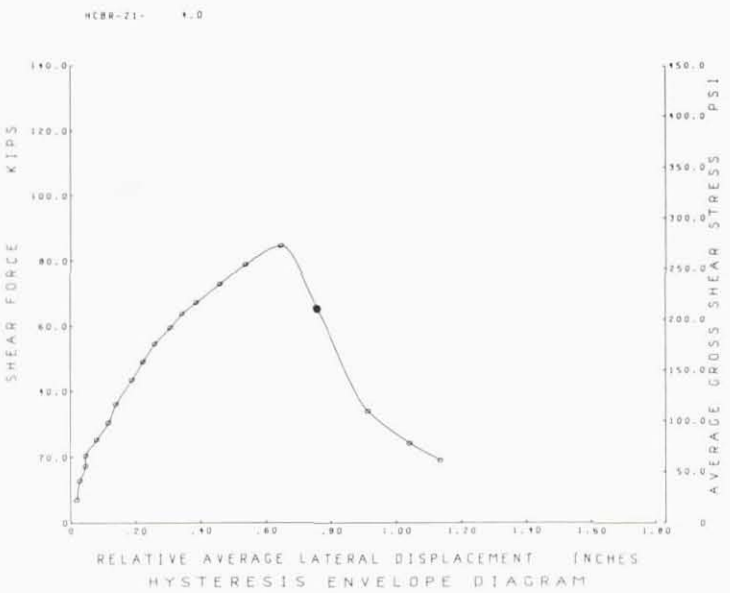

FIG. A.4 CONTINUE HCBR-21-4

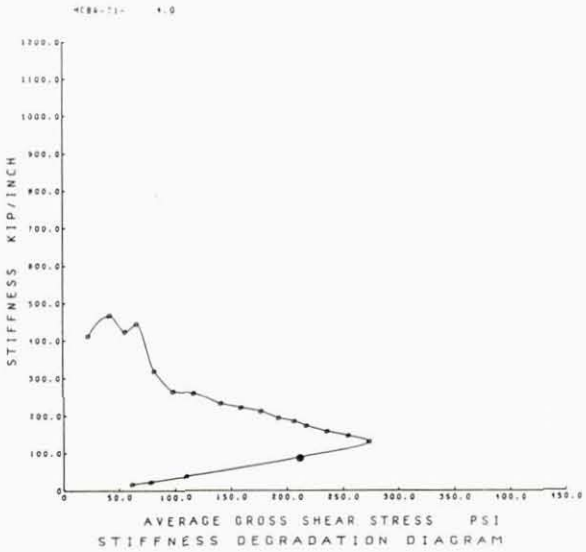

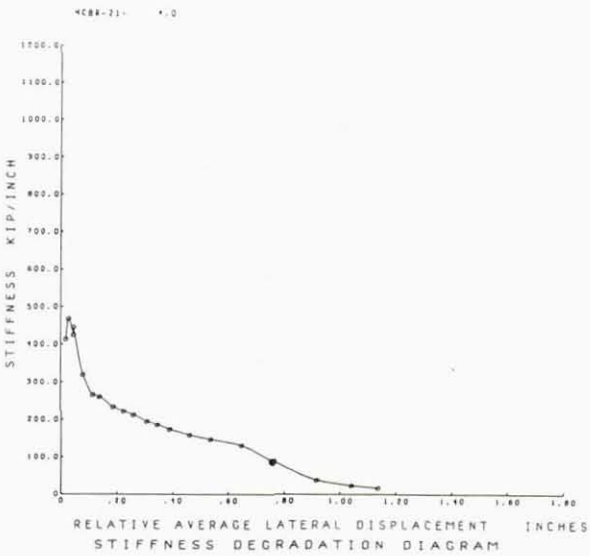

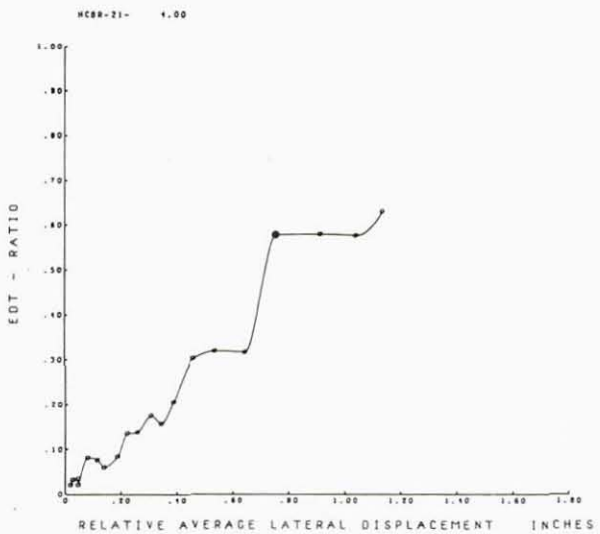

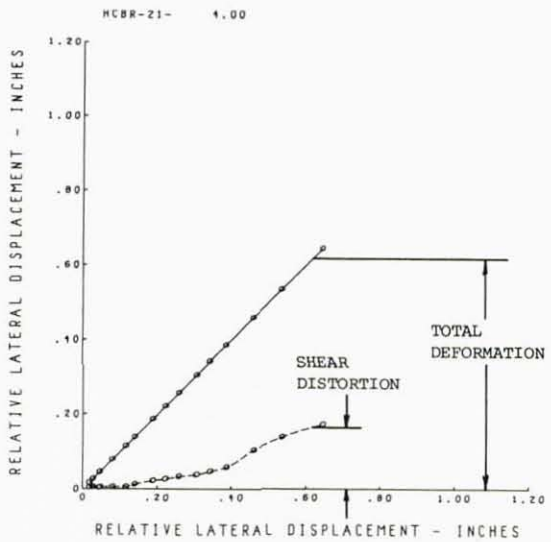

FIG. A.4 CONTINUE HCBR-21-4

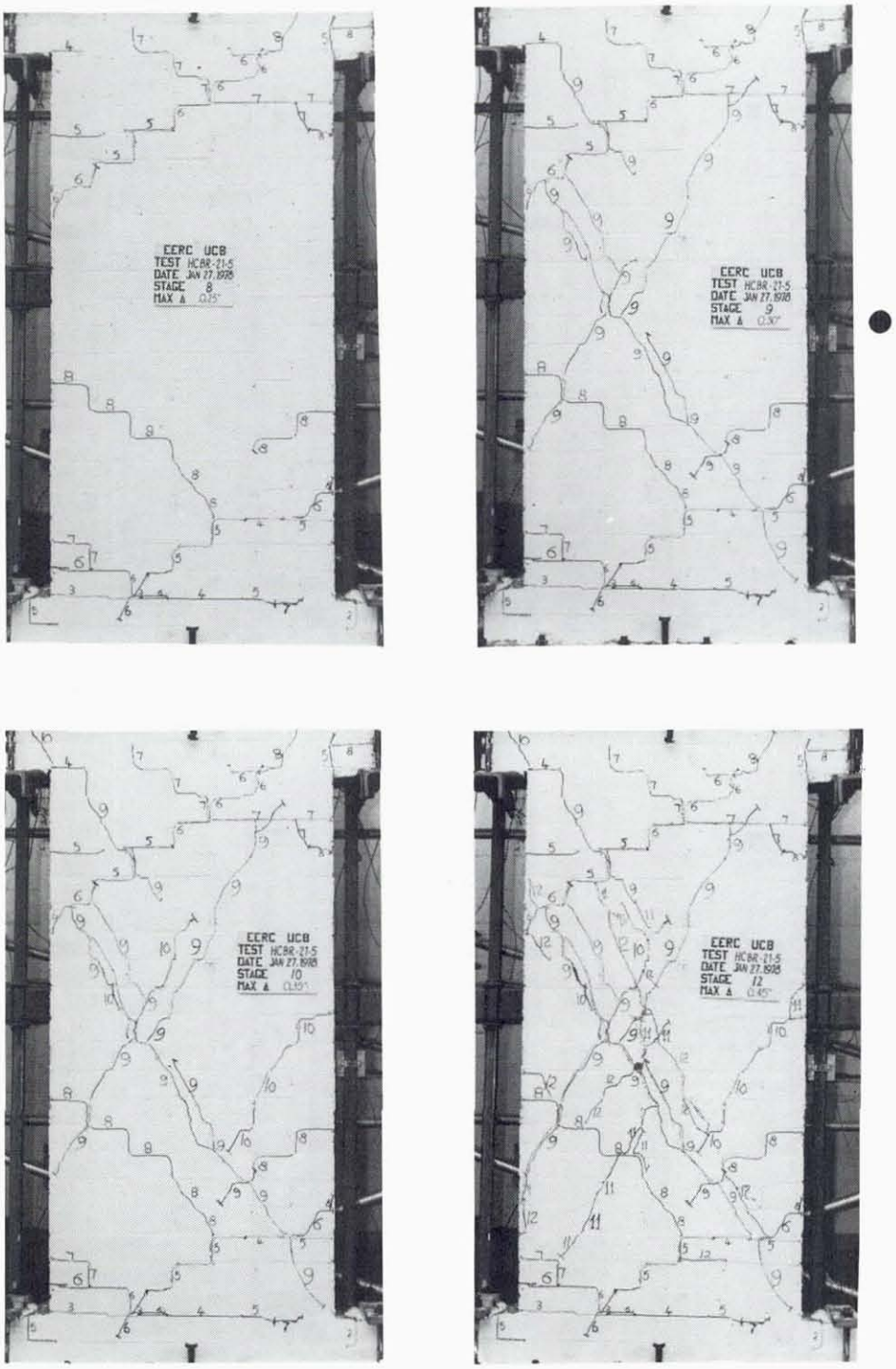

FIG. A.5 SUCCESSIVE CRACK FORMATION
AND EXPERIMENTAL RESULTS
TEST HCBR-21-5

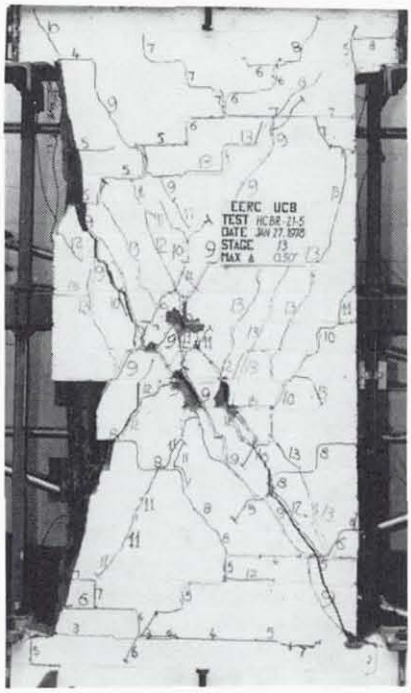

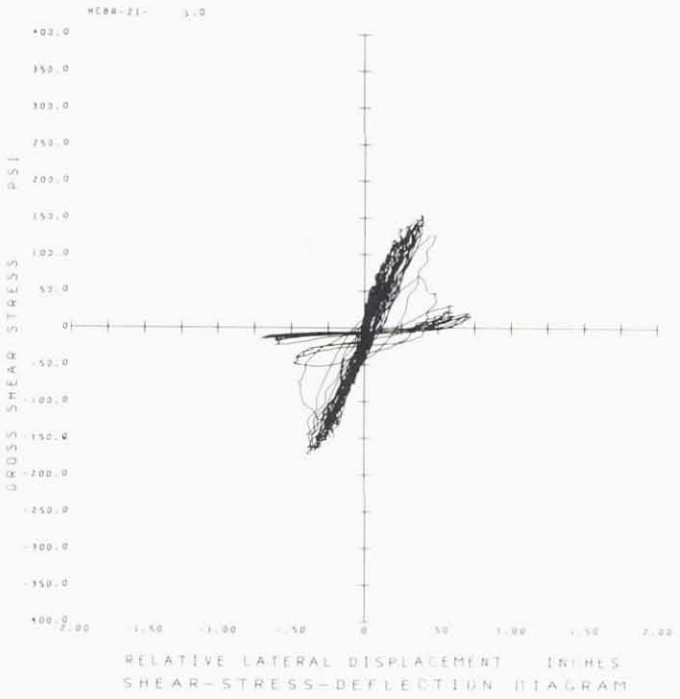

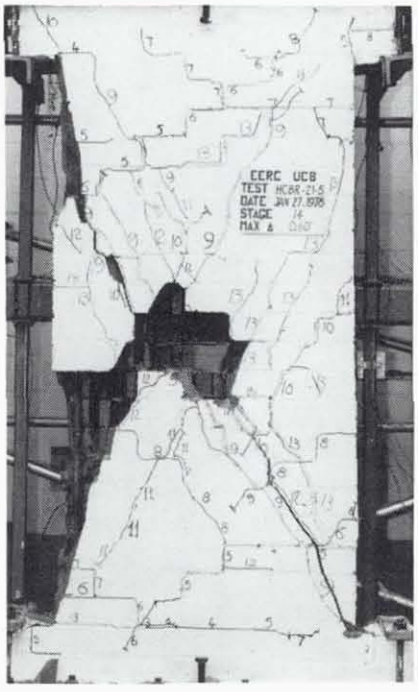

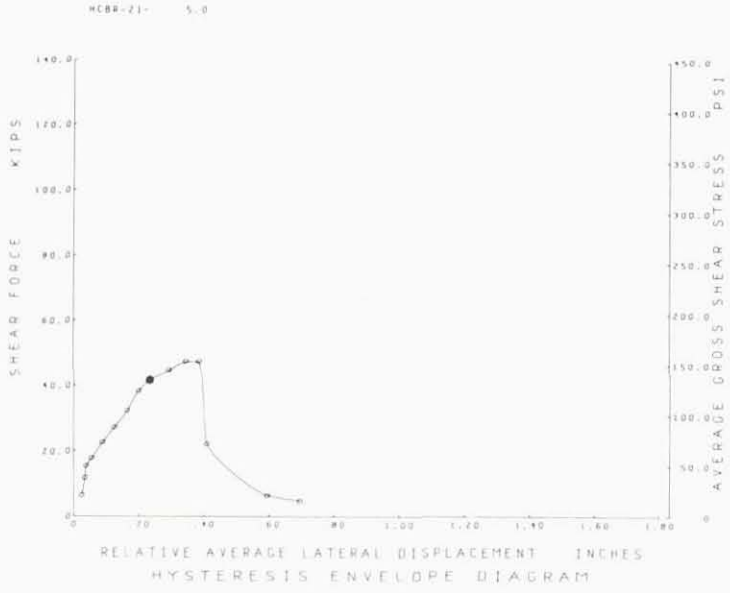

FIG. A.5 CONTINUE HCBR-21-5

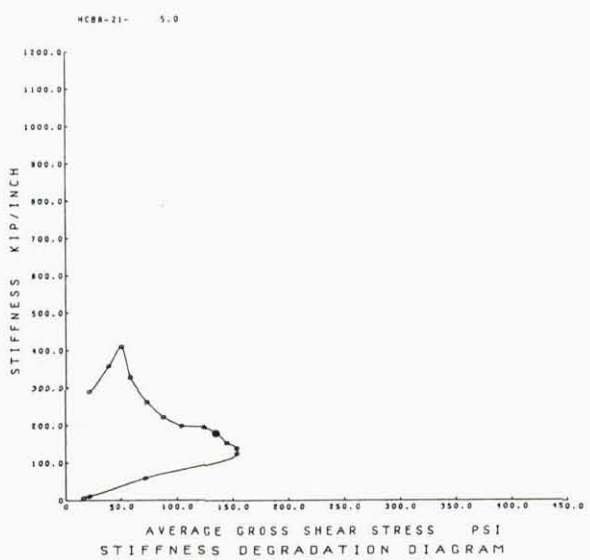

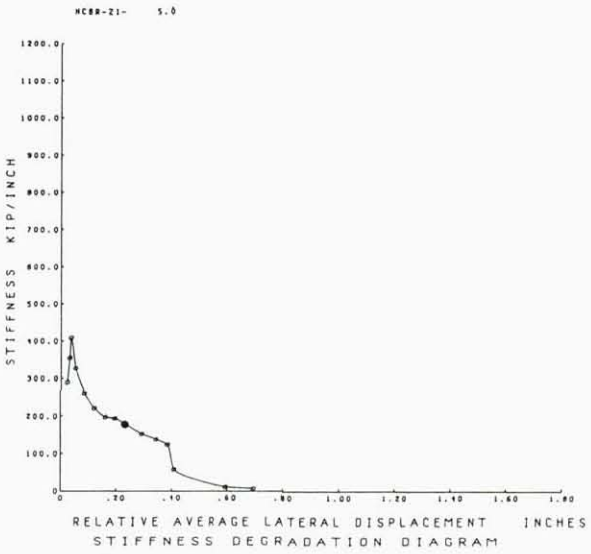

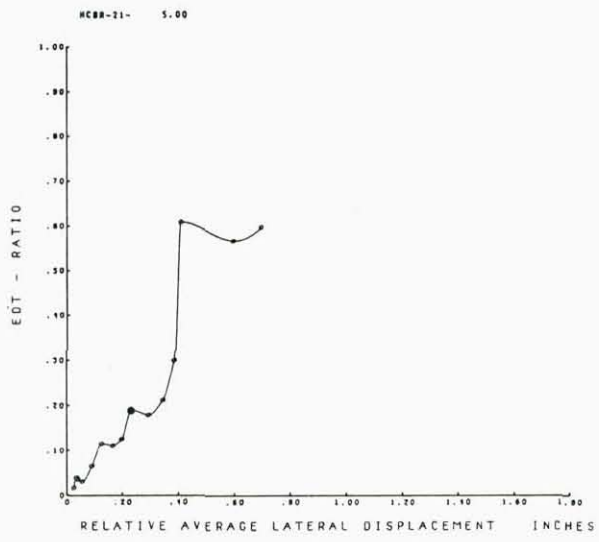

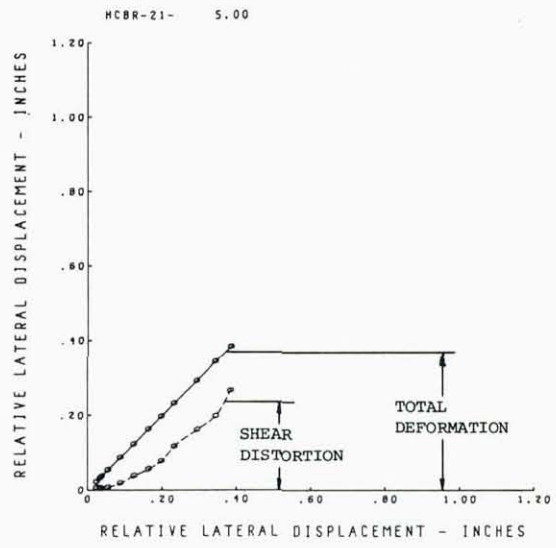

FIG. A.5 CONTINUE HCBR-21-5

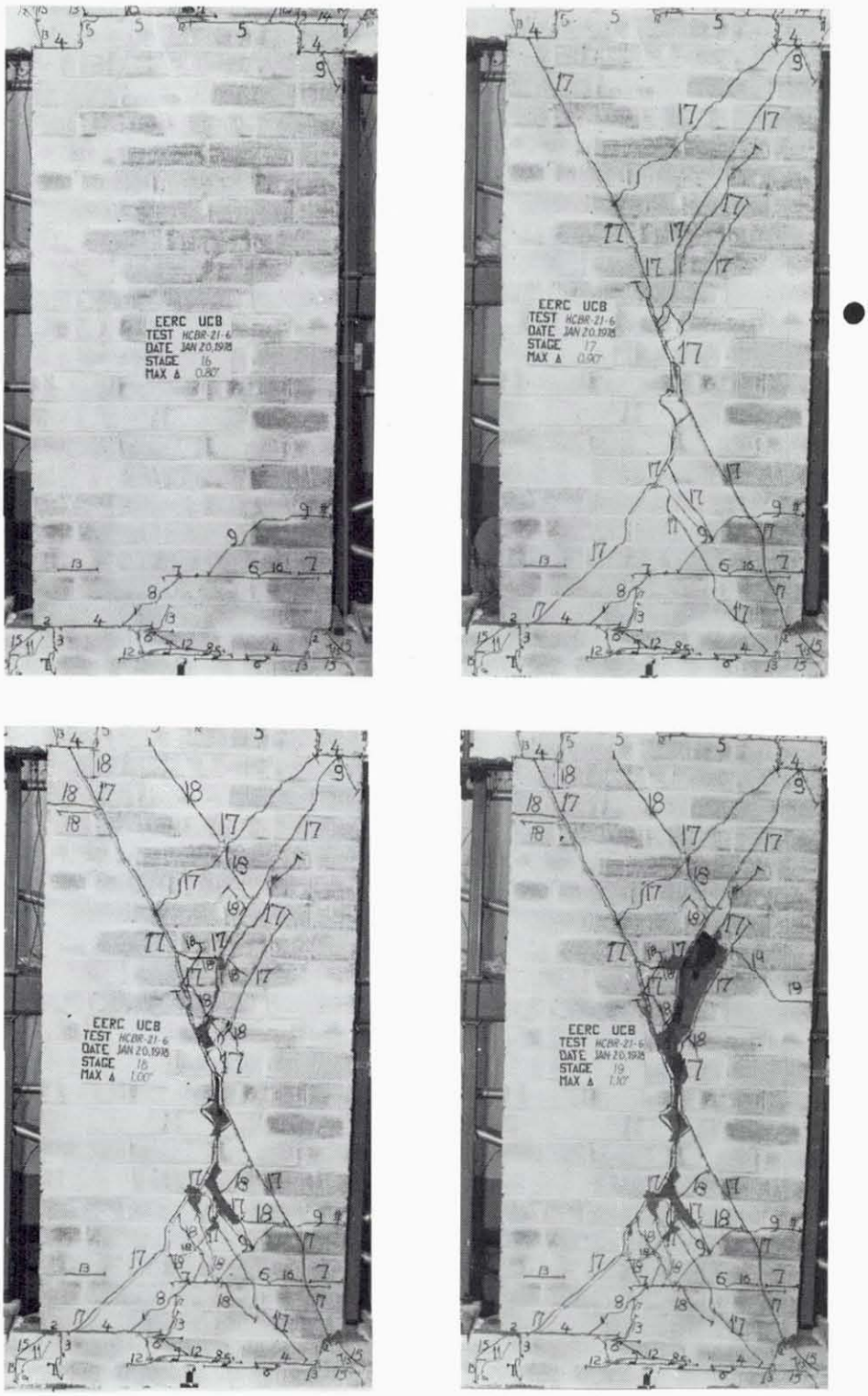

FIG. A.6 SUCCESSIVE CRACK FORMATION
AND EXPERIMENTAL RESULTS
TEST HCBR-21-6

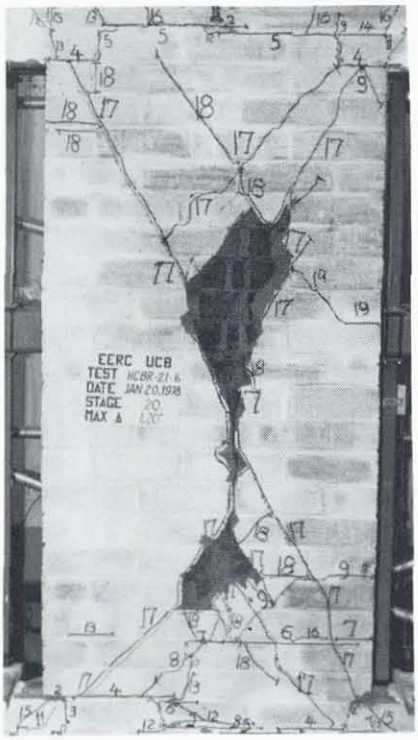

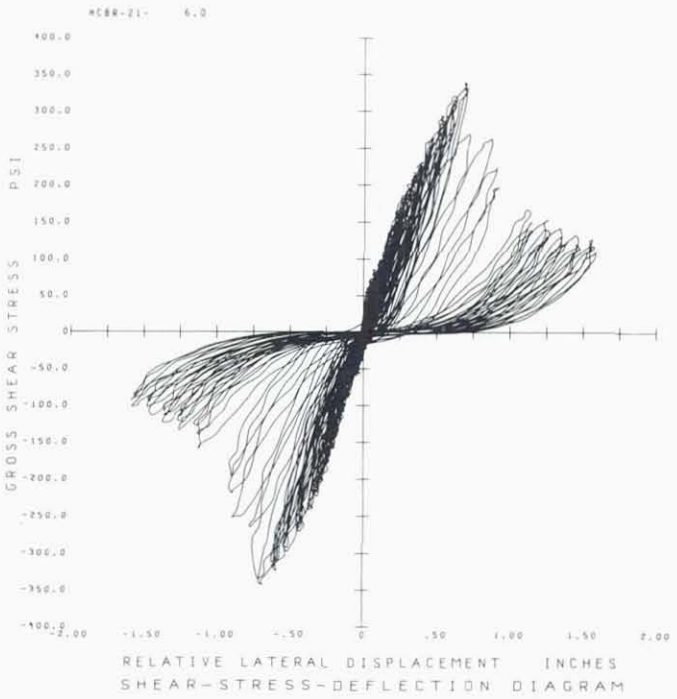

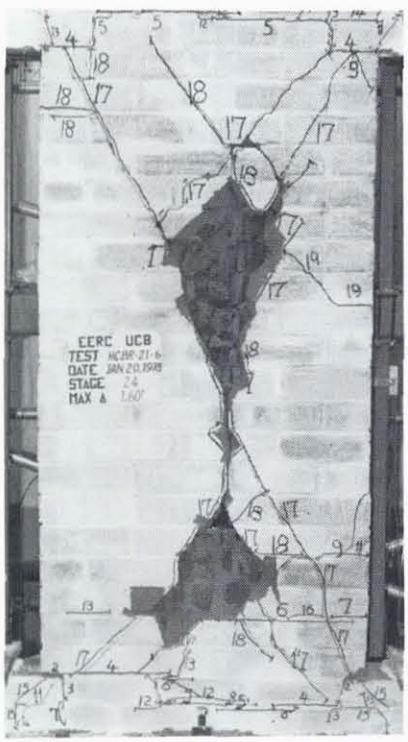

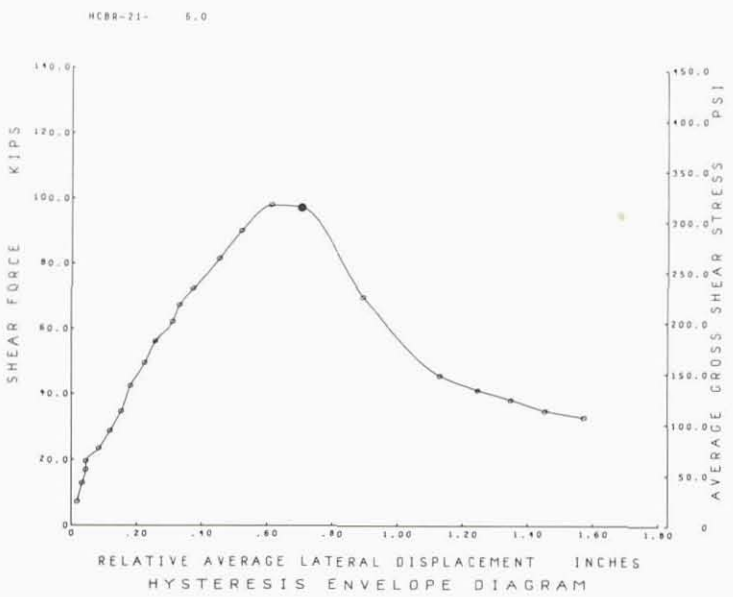

FIG. A.6 CONTINUE HCBR-21-6

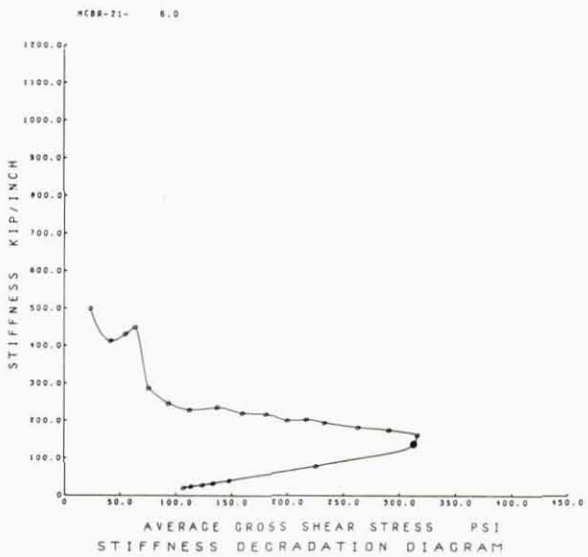

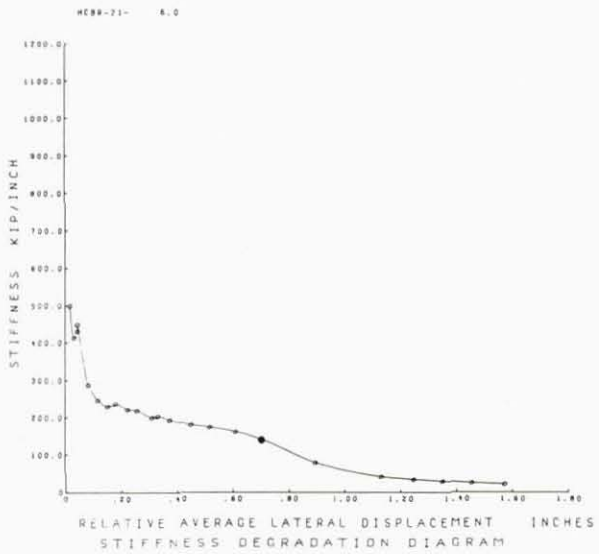

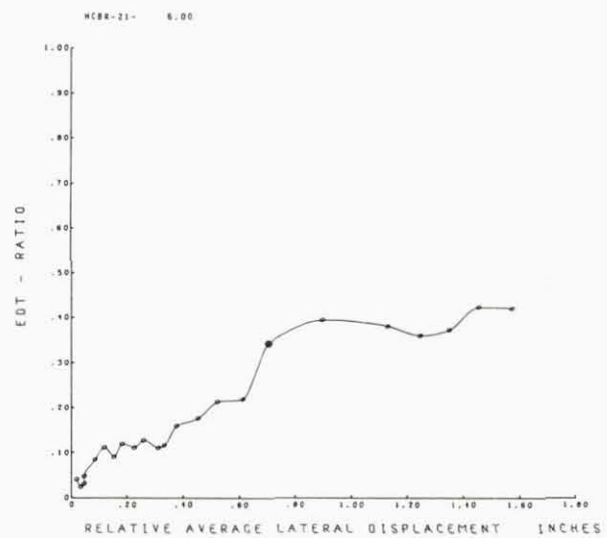

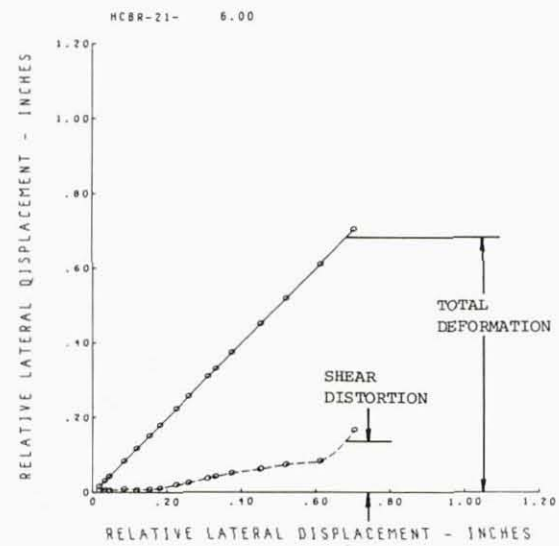

FIG. A.6 CONTINUE HCBR-21-6

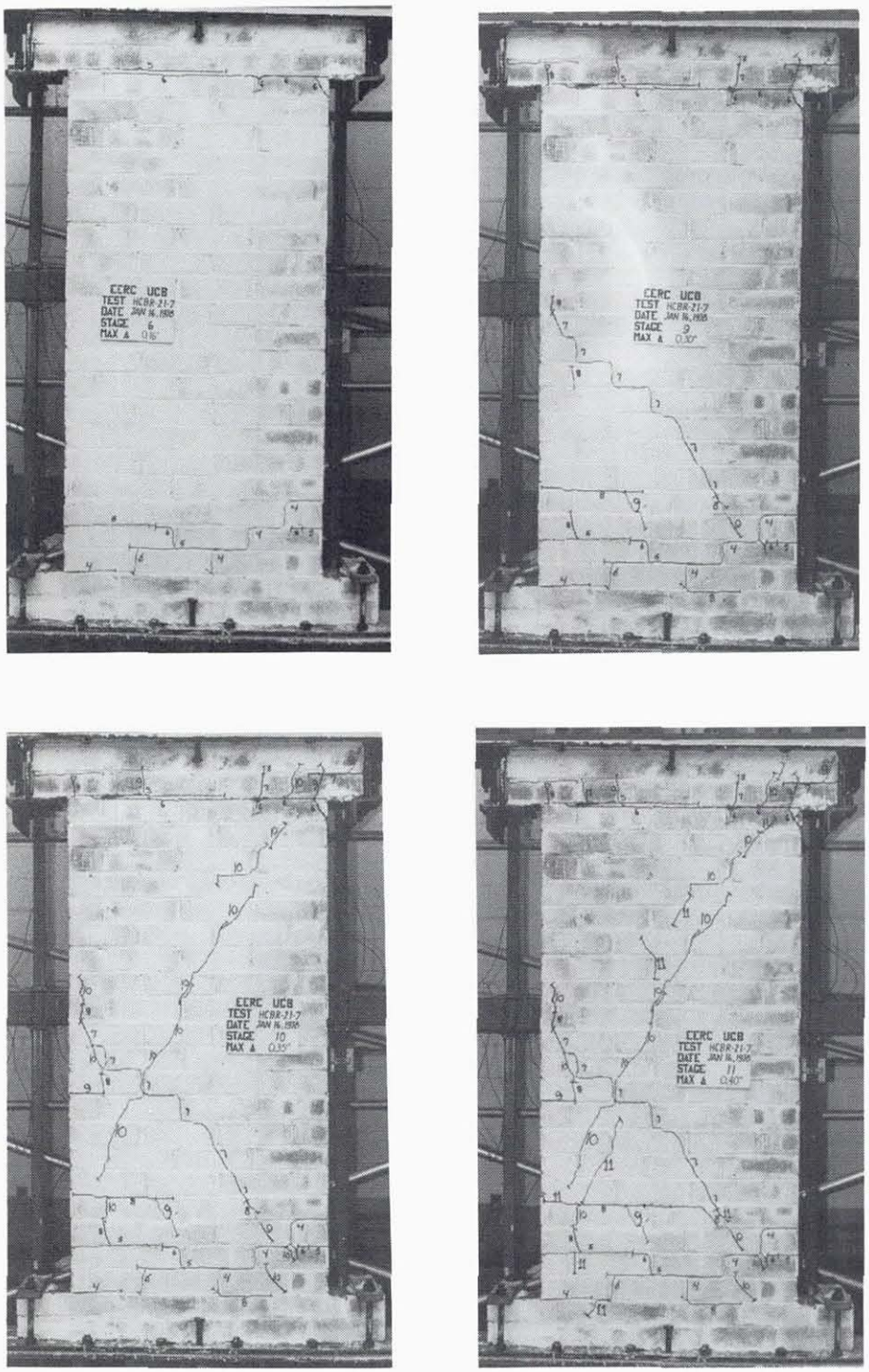

FIG. A.7 SUCCESSIVE CRACK FORMATION
AND EXPERIMENTAL RESULTS
TEST HCBR-21-7

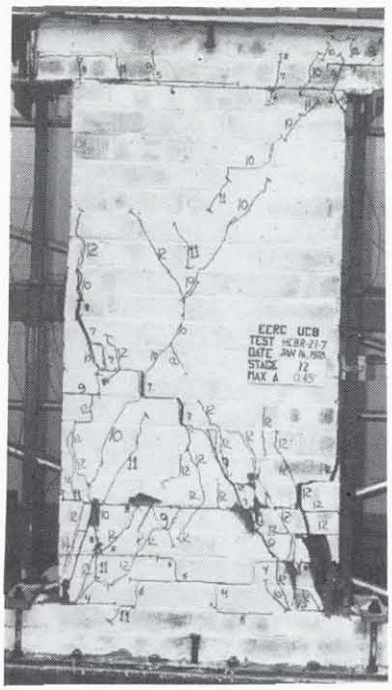

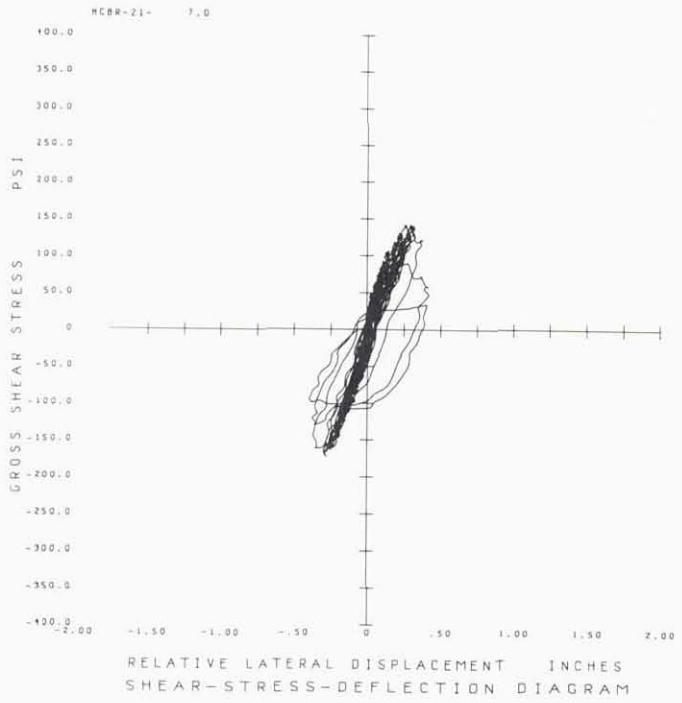

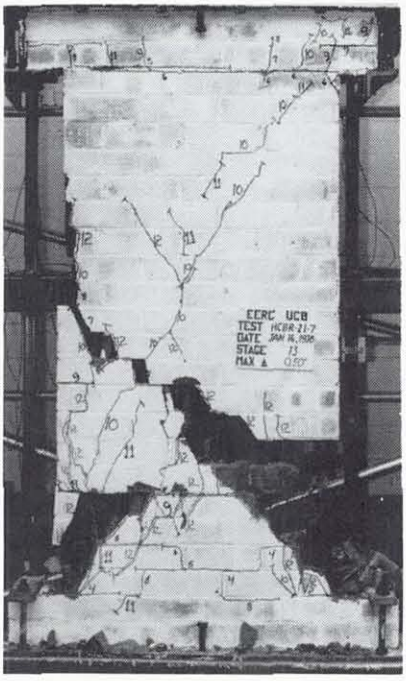

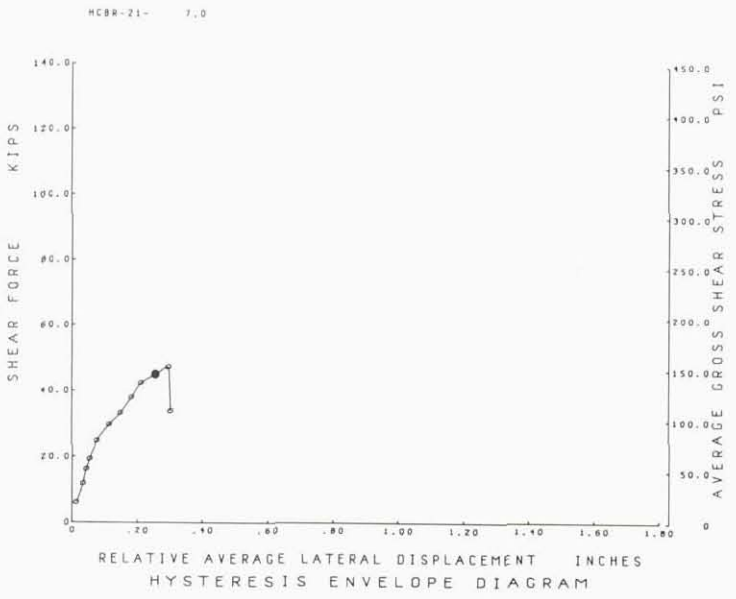

FIG. A.7 CONTINUE HCBR-21-7

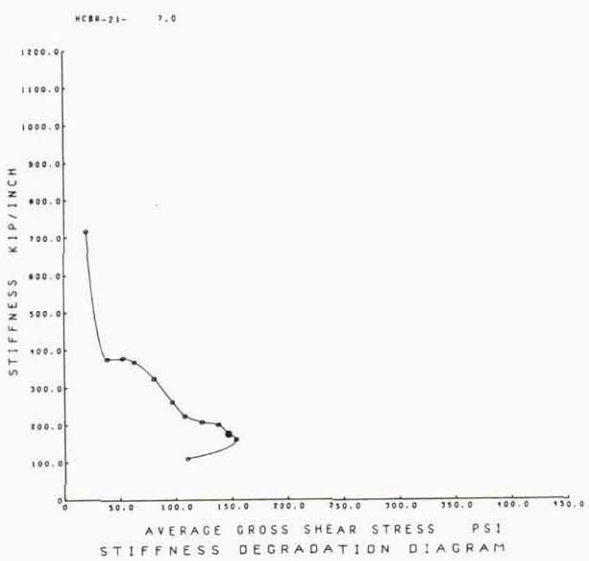

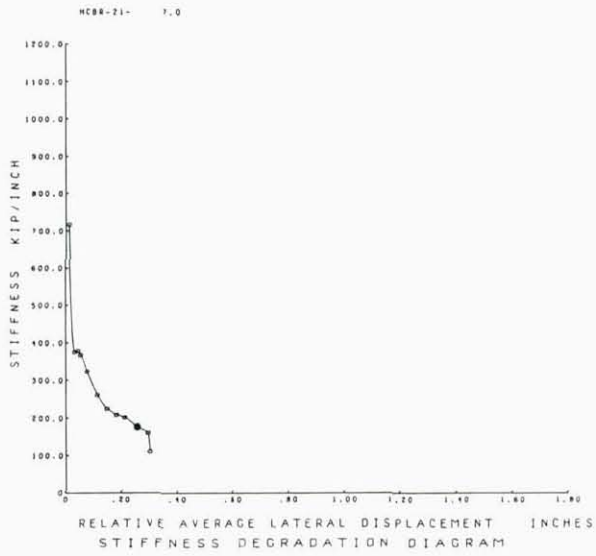

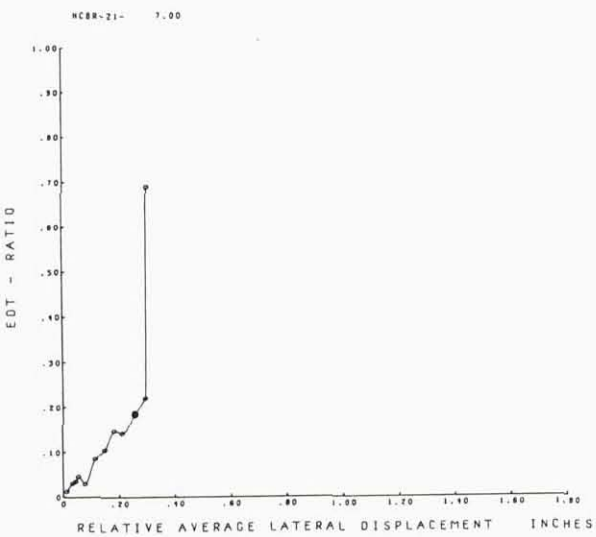

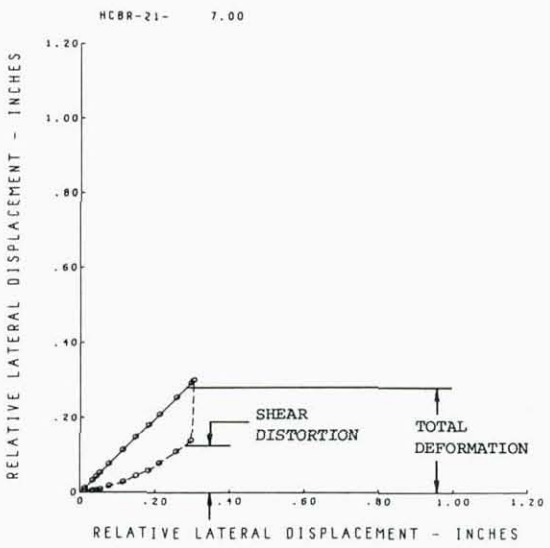

FIG. A.7 CONTINUE HCBR-21-7

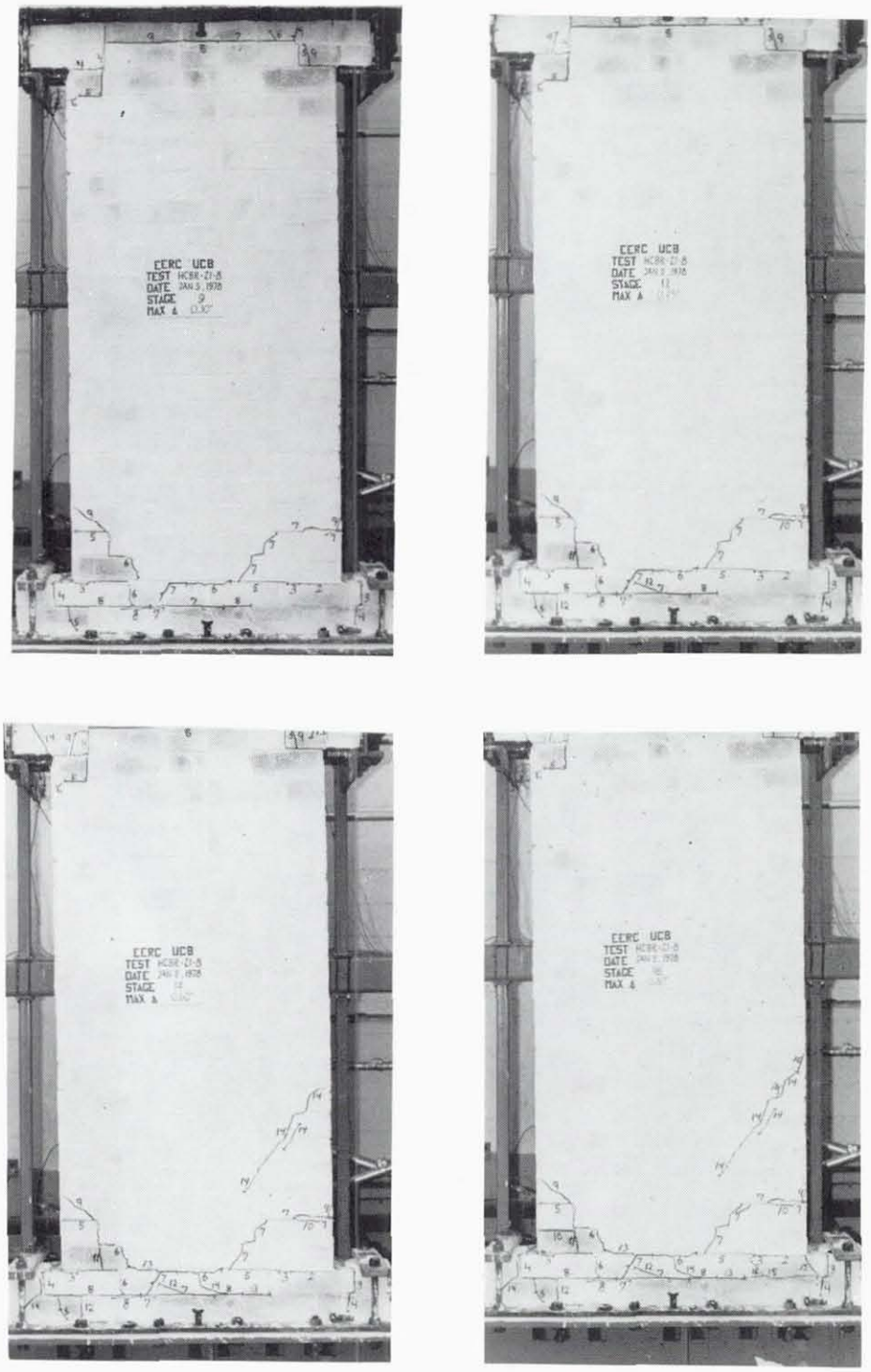

FIG. A.8 SUCCESSIVE CRACK FORMATION
AND EXPERIMENTAL RESULTS
TEST HCBR-21-8

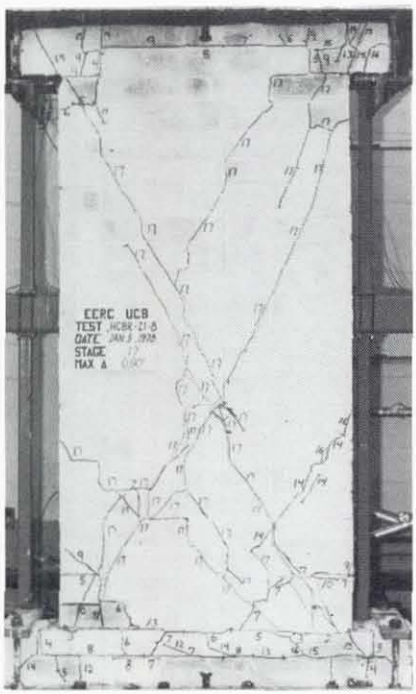

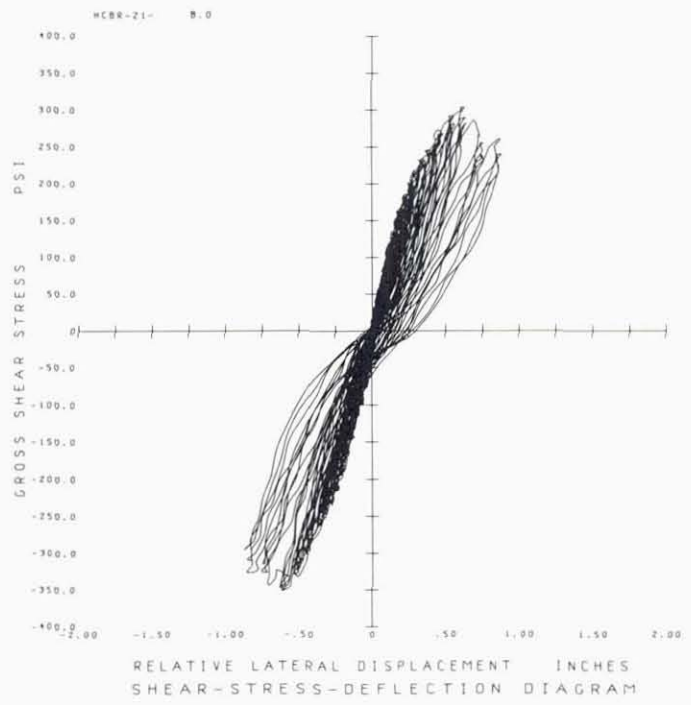

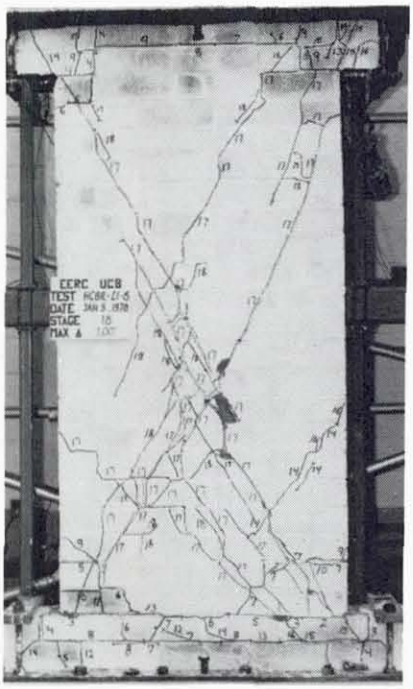

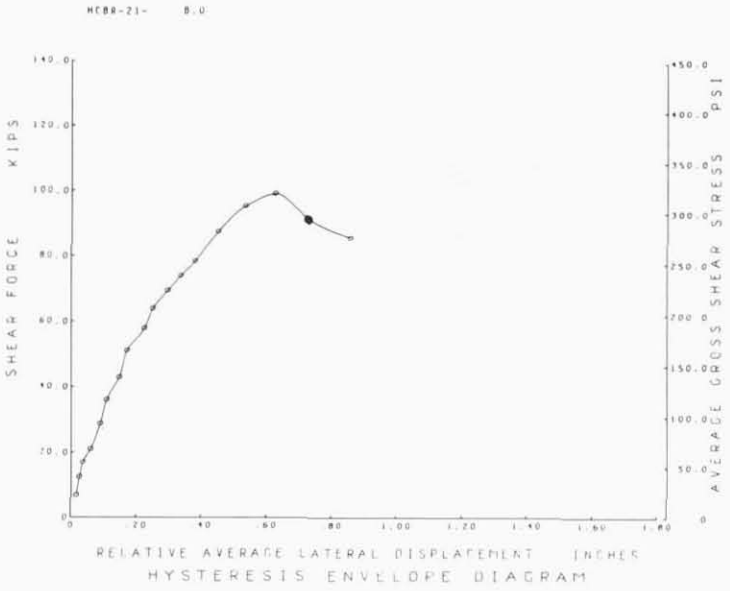

FIG. A.8 CONTINUE HCBR-21-8

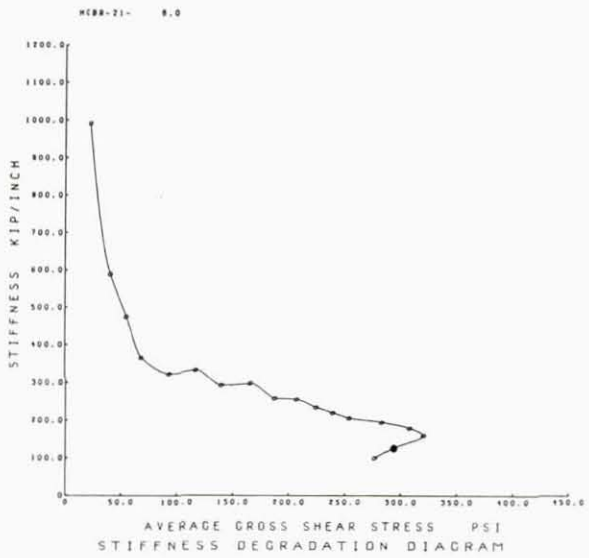

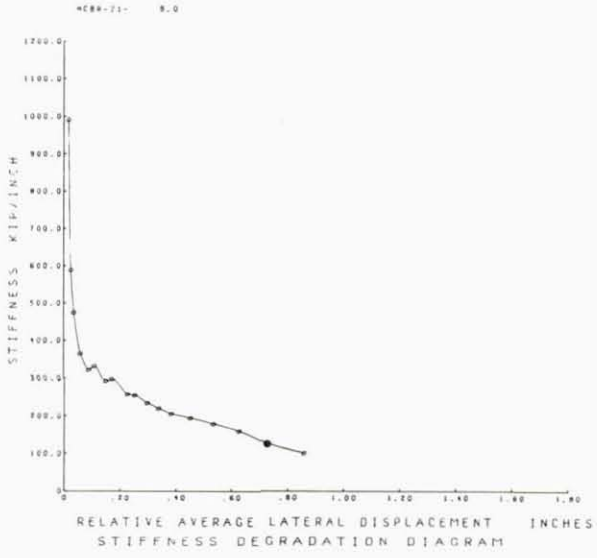

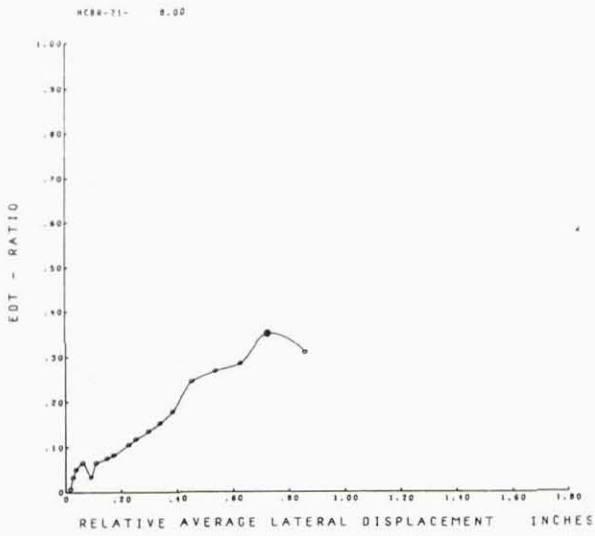

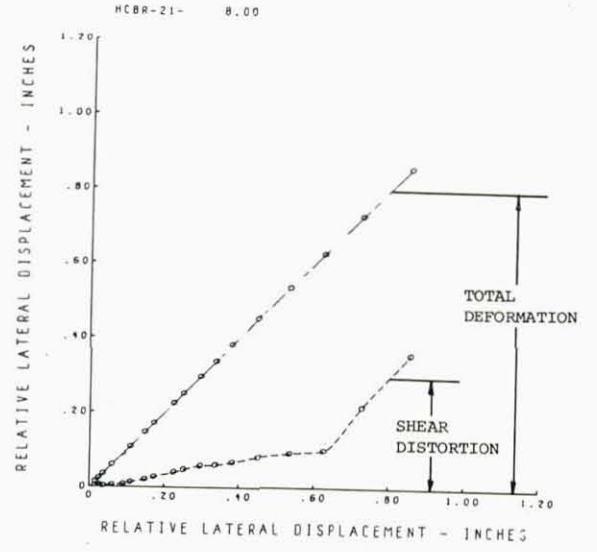

FIG. A.8 CONTINUE HCBR-21-8

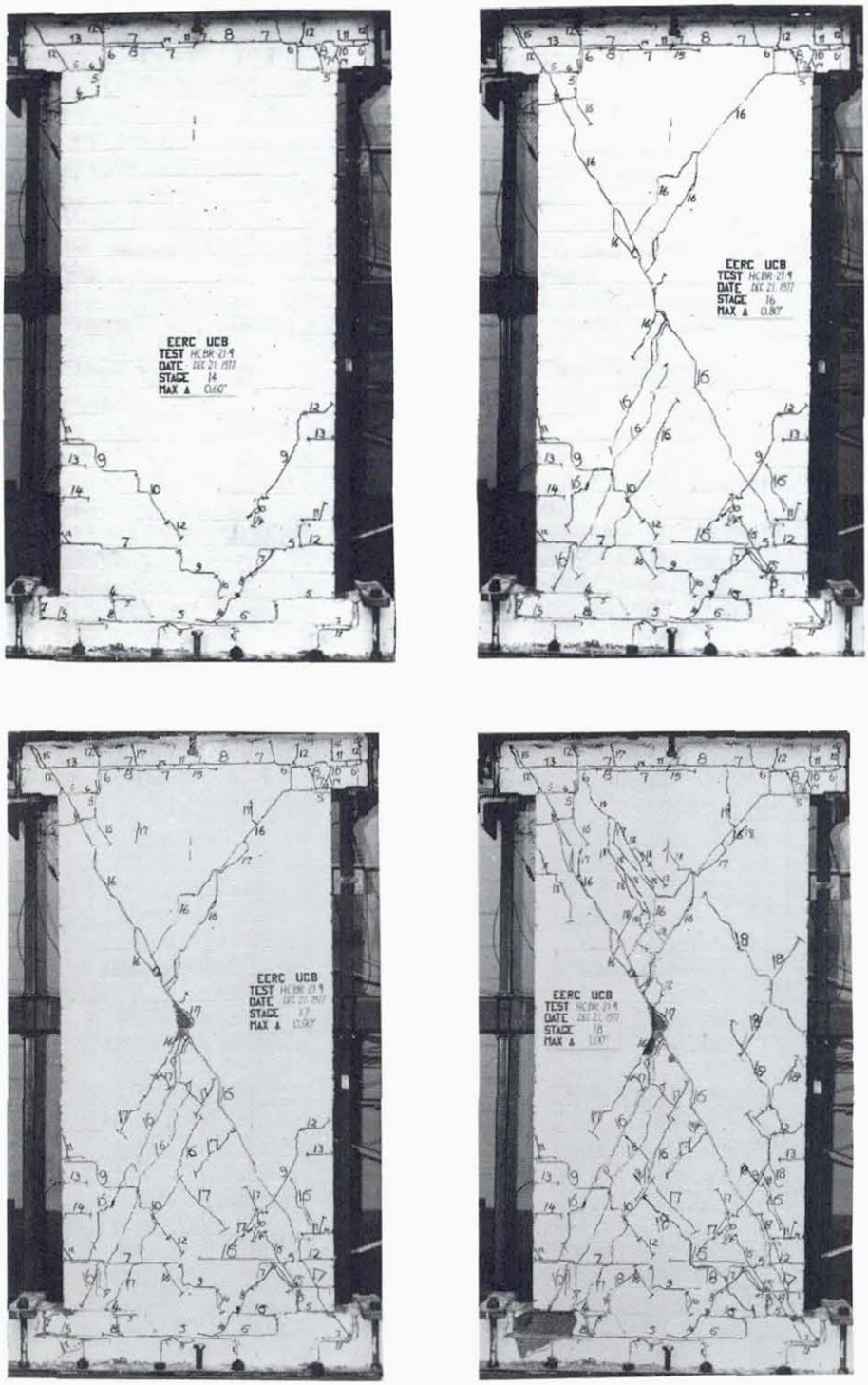

FIG. A.9 SUCCESSIVE CRACK FORMATION
AND EXPERIMENTAL RESULTS
TEST HCBR-21-9

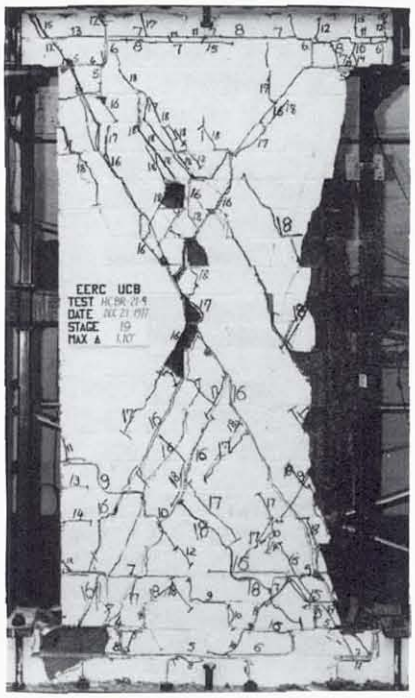

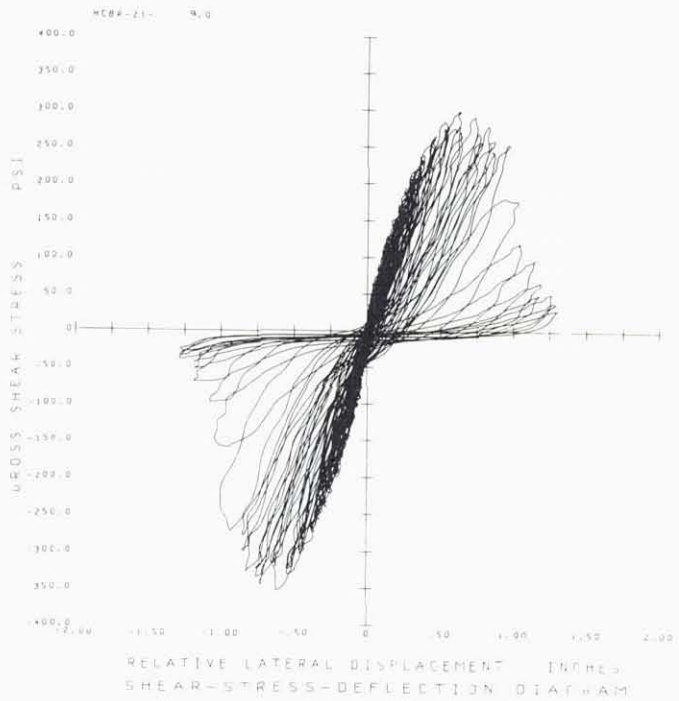

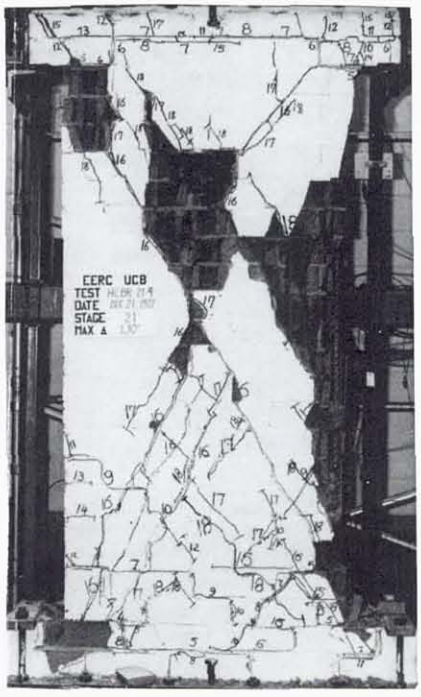

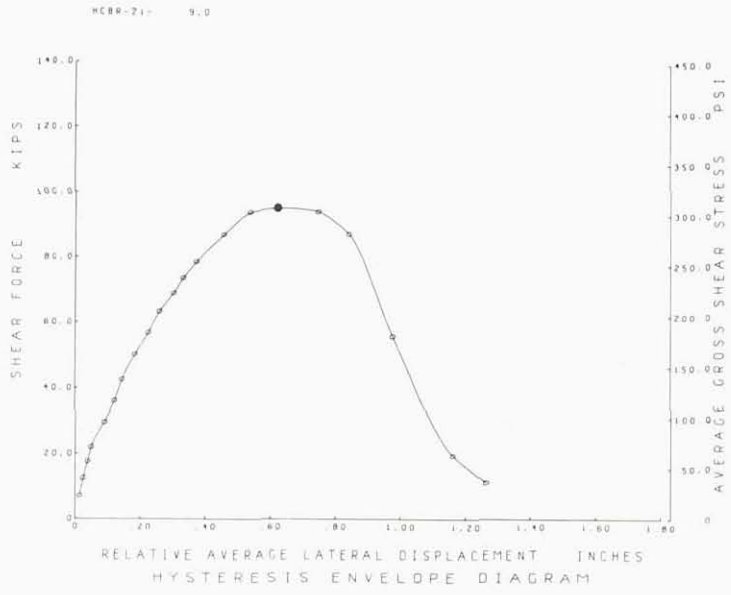

FIG. A.9 CONTINUE HCBR-21-9

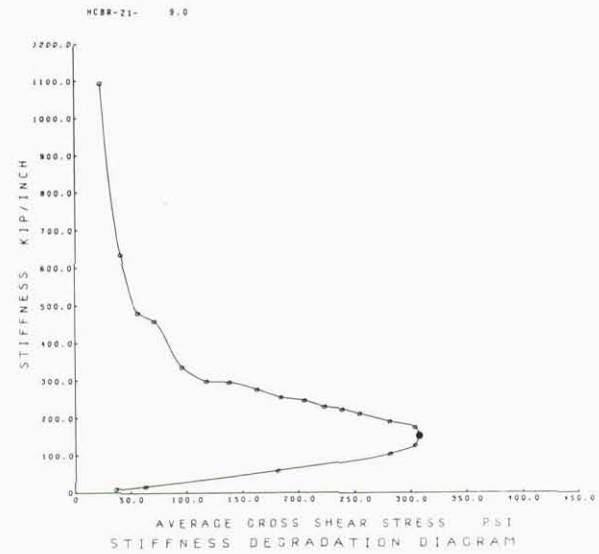

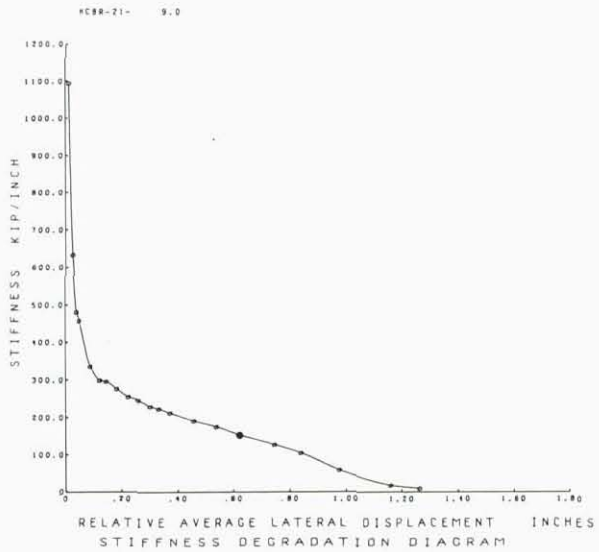

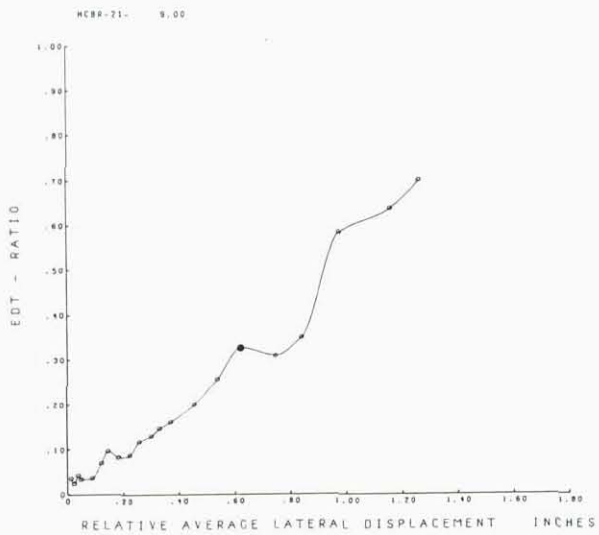

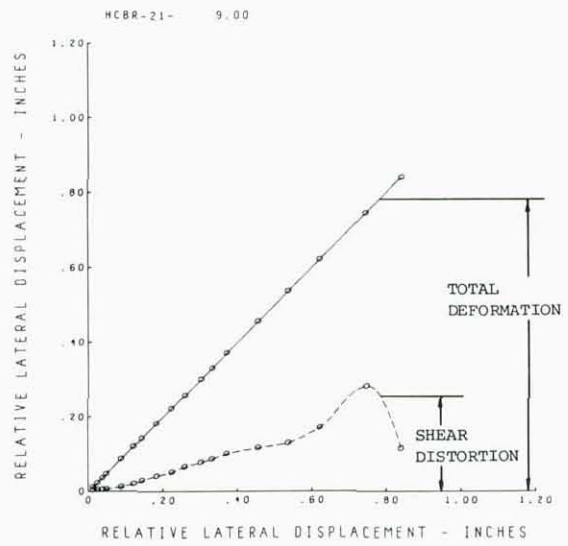

FIG. A.9 CONTINUE HCBR-21-9

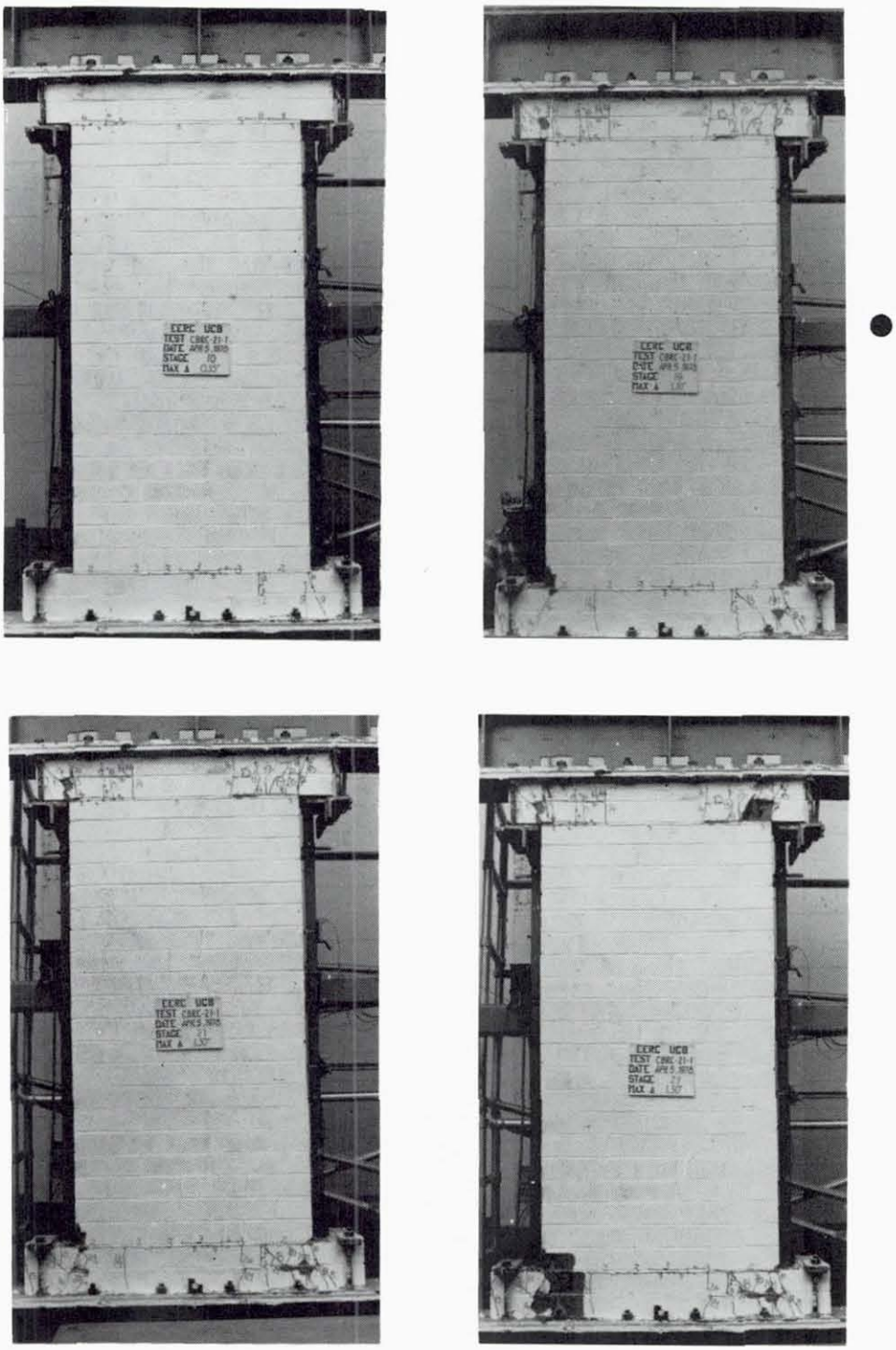

FIG. A.10 SUCCESSIVE CRACK FORMATION
AND EXPERIMENTAL RESULTS
TEST CBRC-21-1

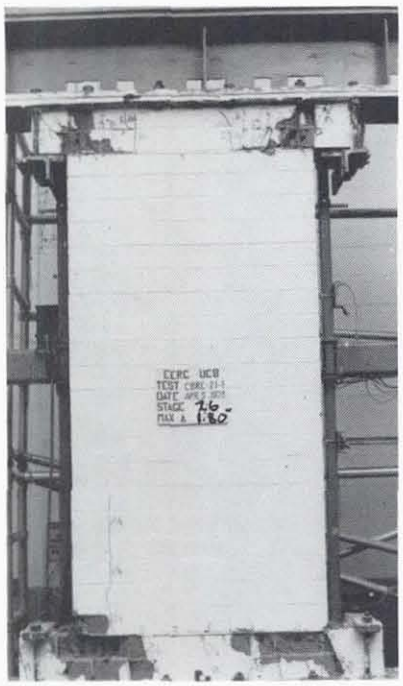

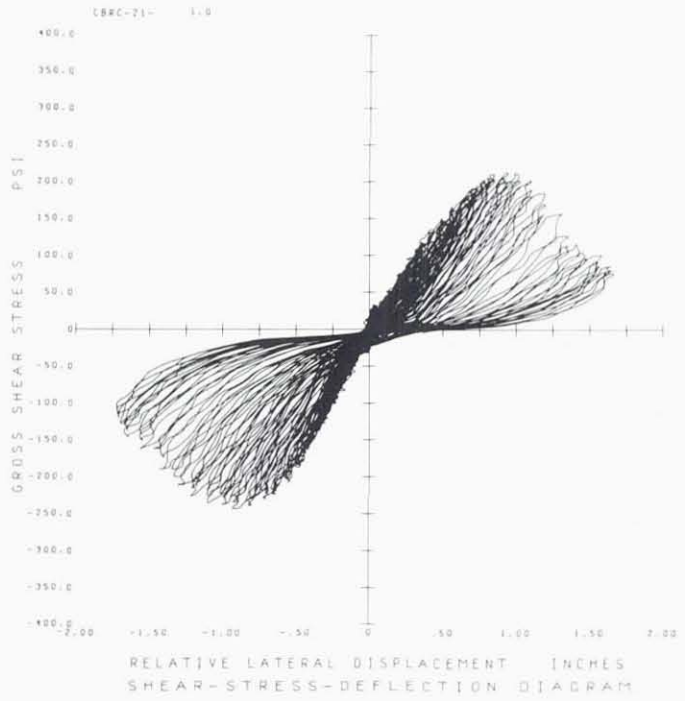

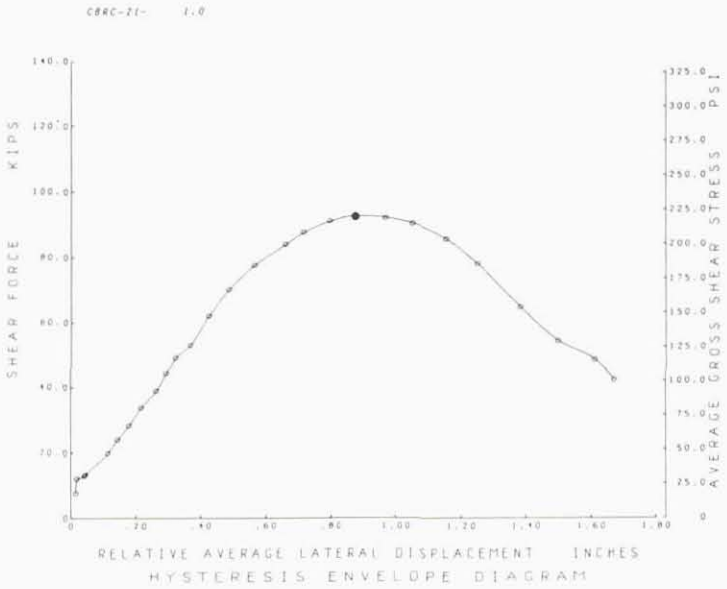

FIG. A.10 CONTINUE CBRC-21-1

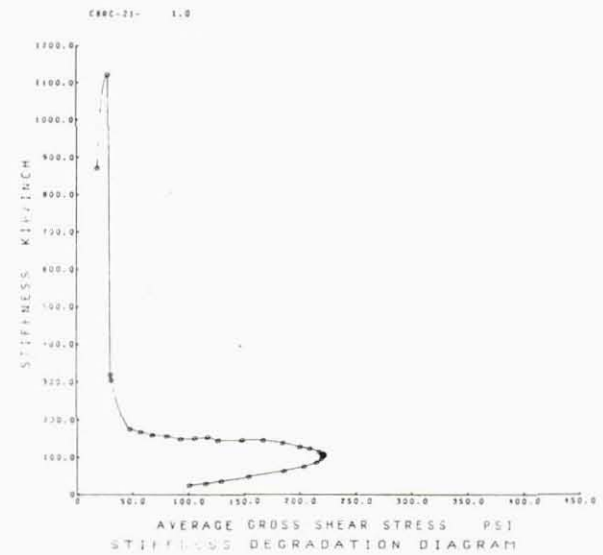

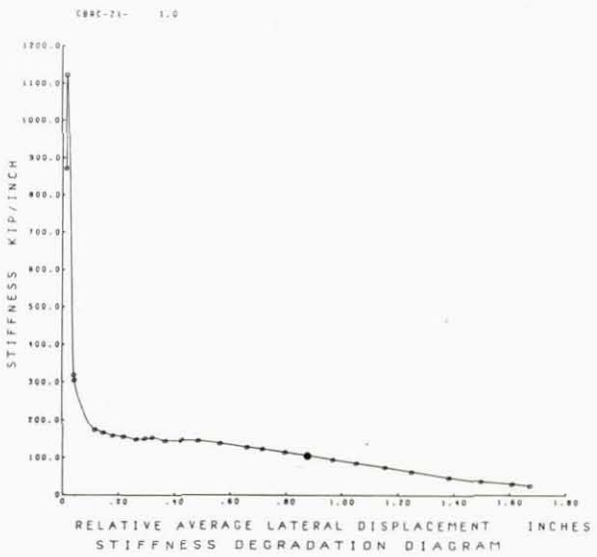

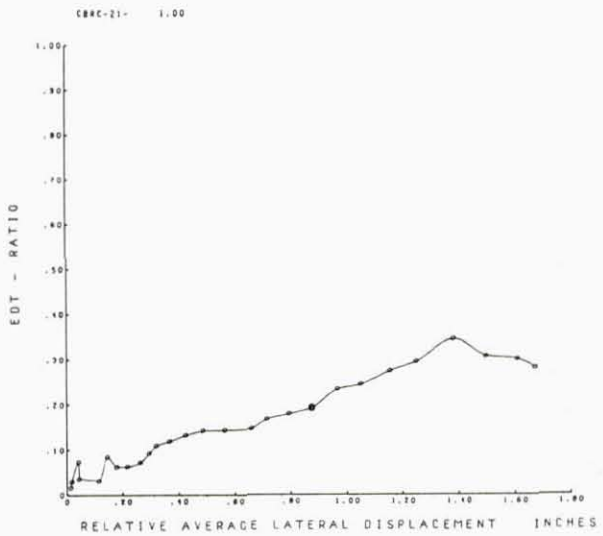

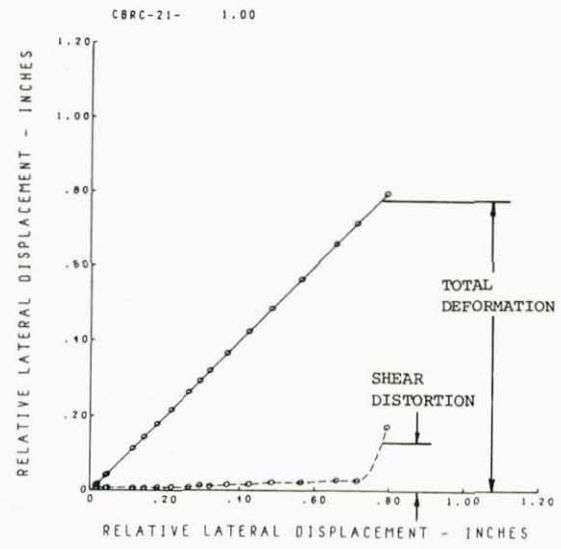

FIG. A.10 CONTINUE CBRC-21-1

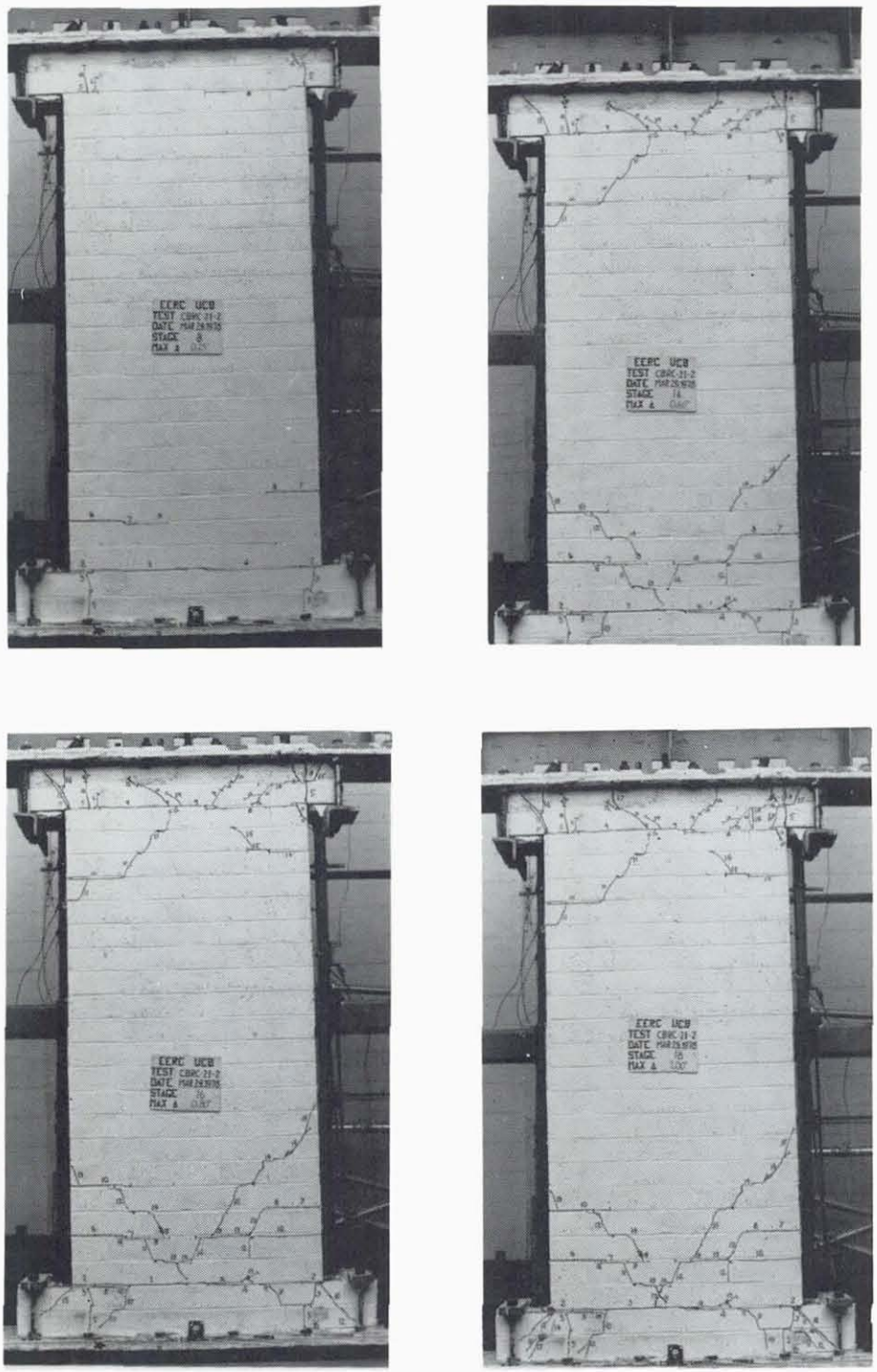

FIG. A.11 SUCCESSIVE CRACK FORMATION
AND EXPERIMENTAL RESULTS
TEST CBRC-21-2

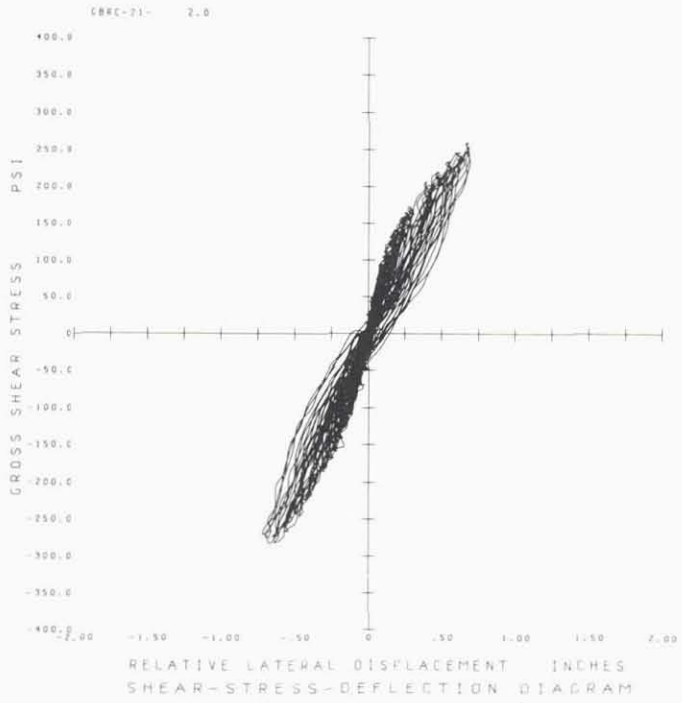

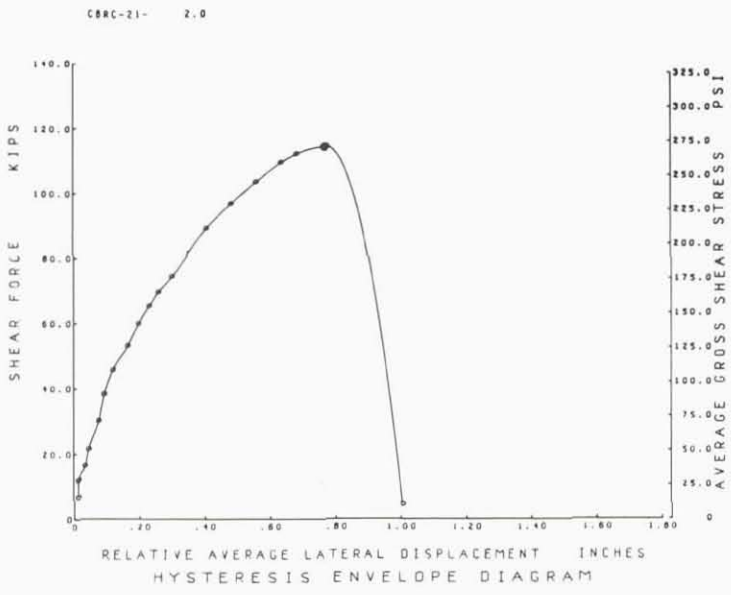

FIG. A.11 CONTINUE CBRC-21-2

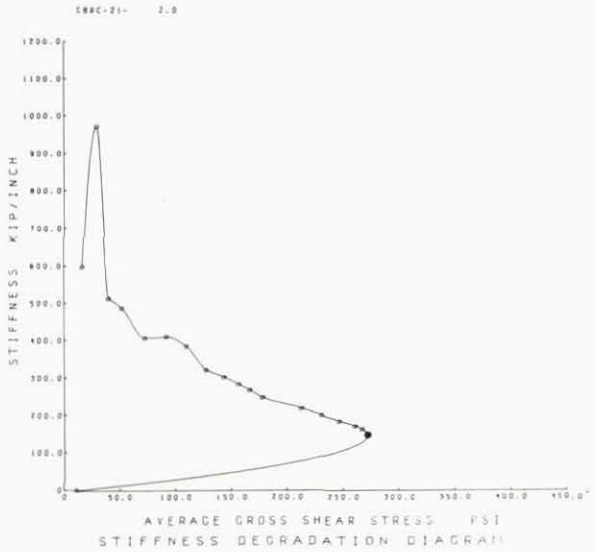

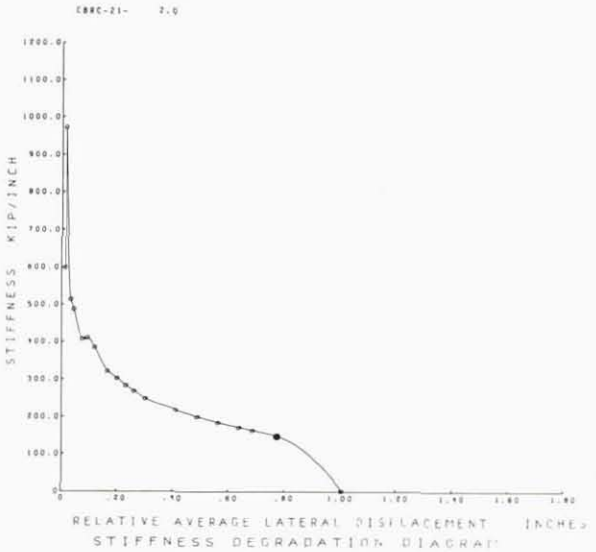

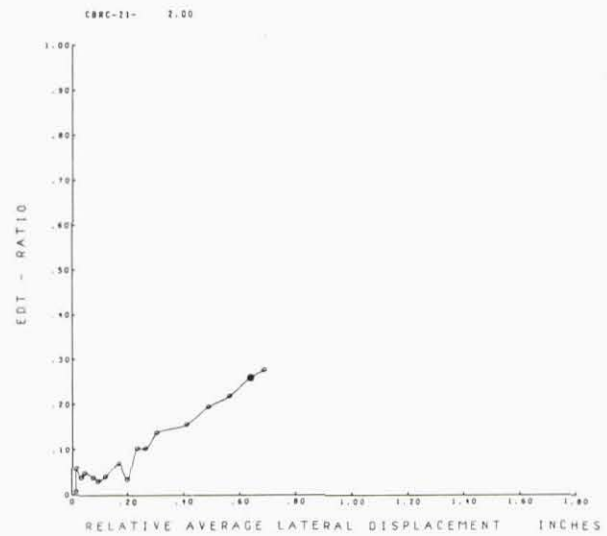

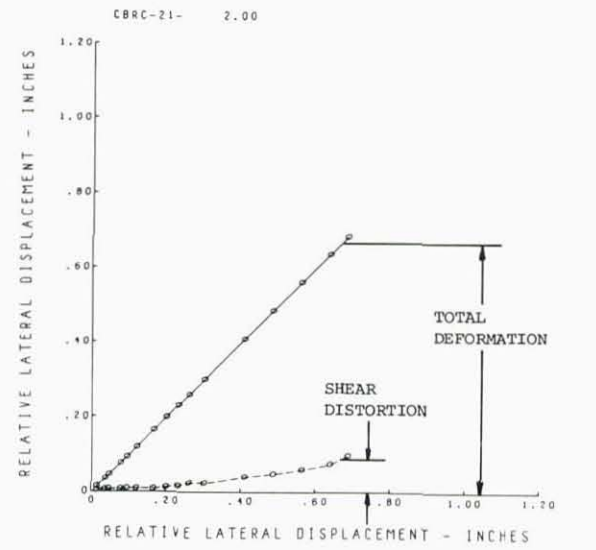

FIG. A.11 CONTINUE CBRC-21-2

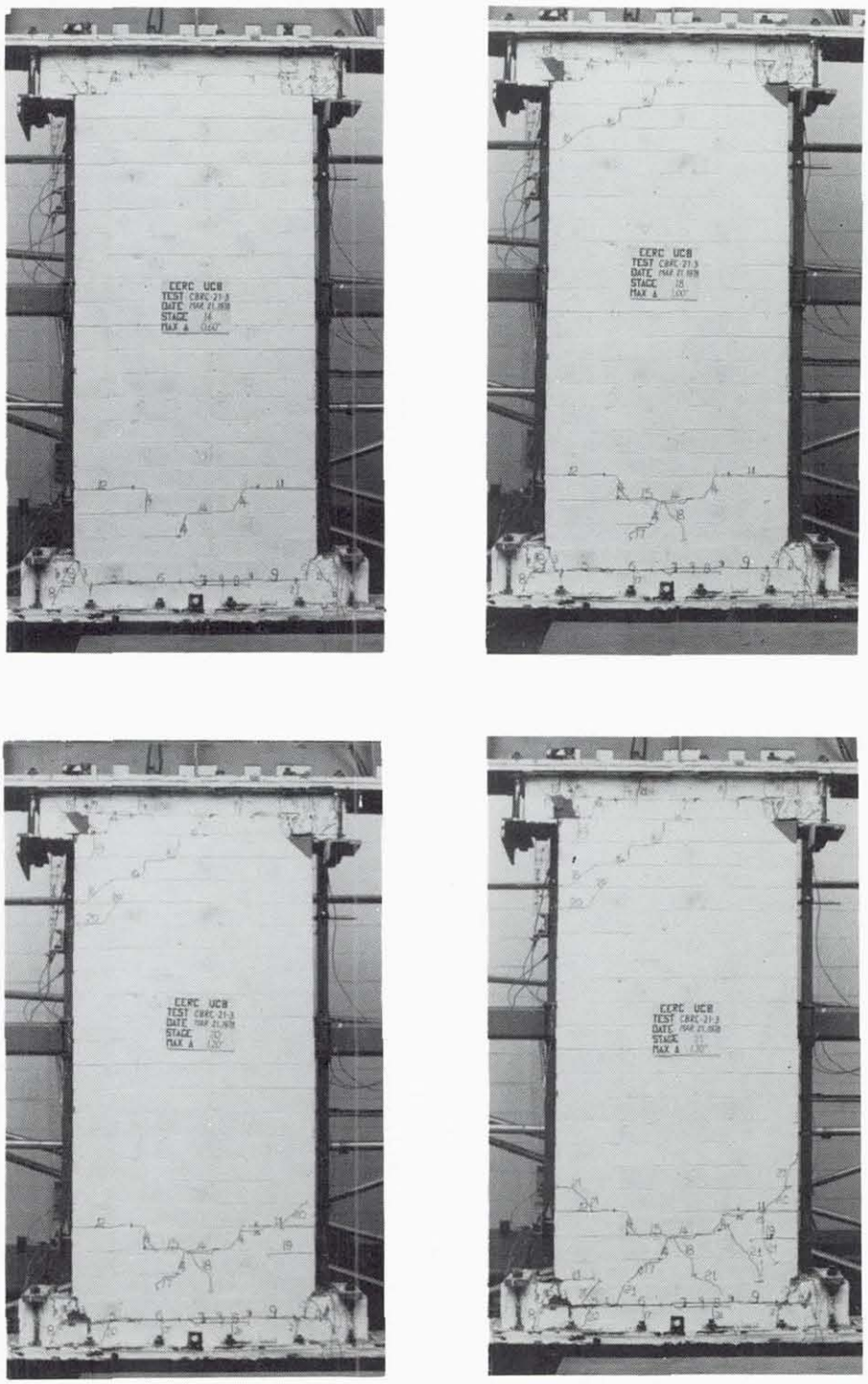

FIG. A.12 SUCCESSIVE CRACK FORMATION
AND EXPERIMENTAL RESULTS
TEST CBRC-21-3

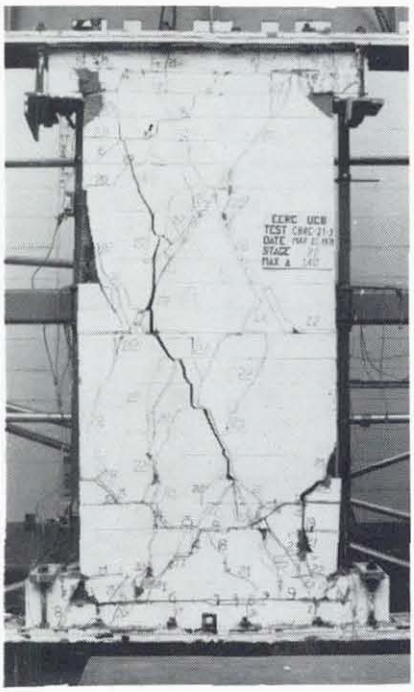

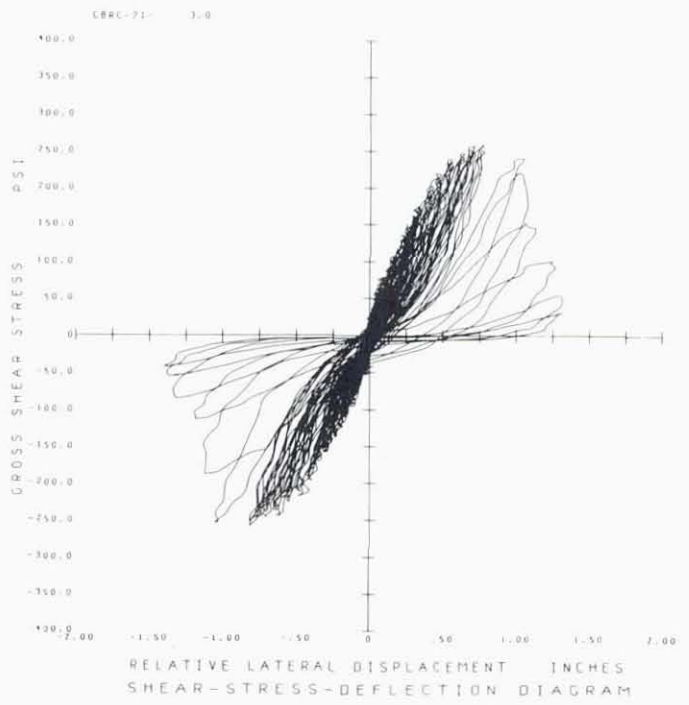

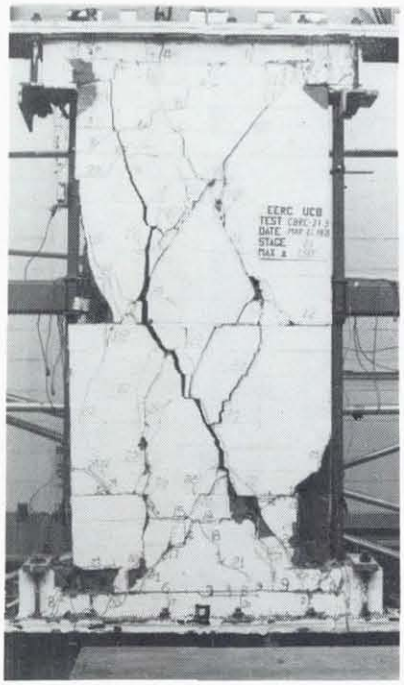

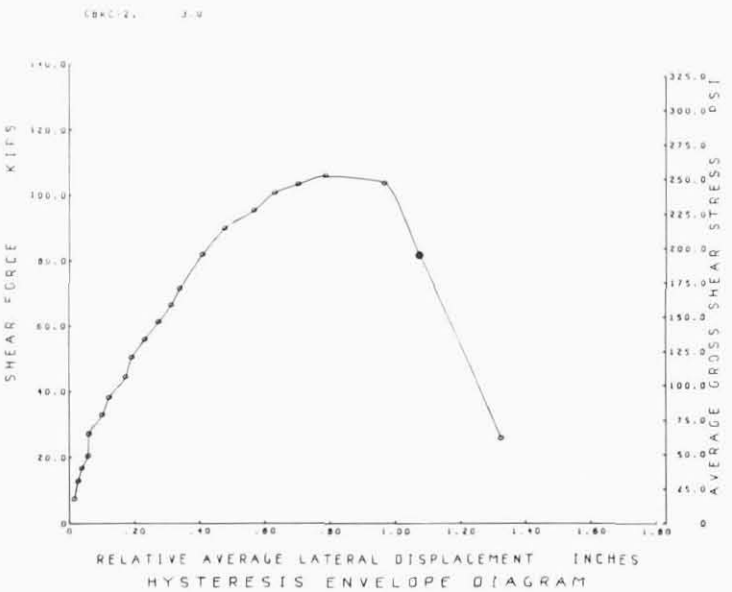

FIG. A.12 CONTINUE CBRC-21-3

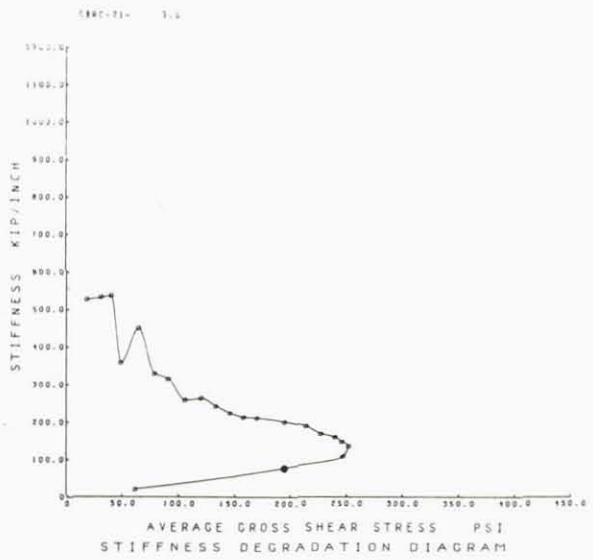

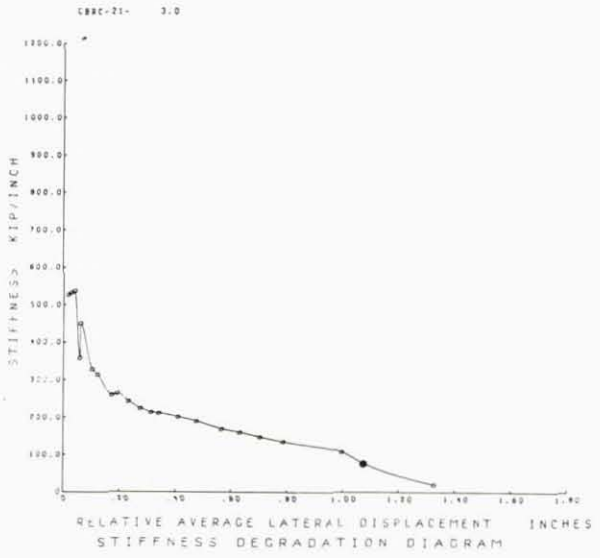

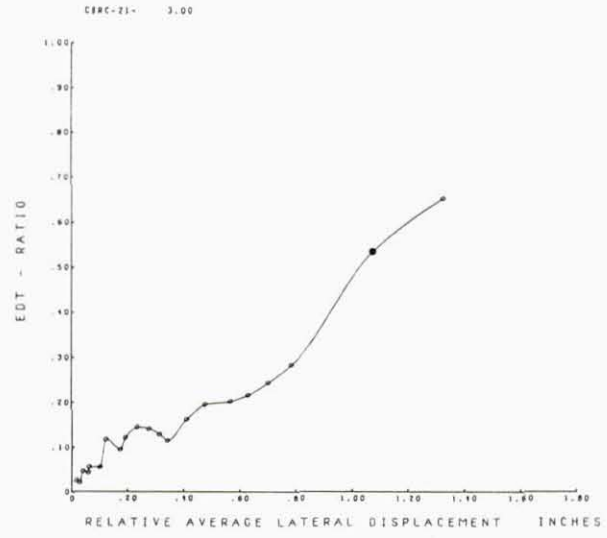

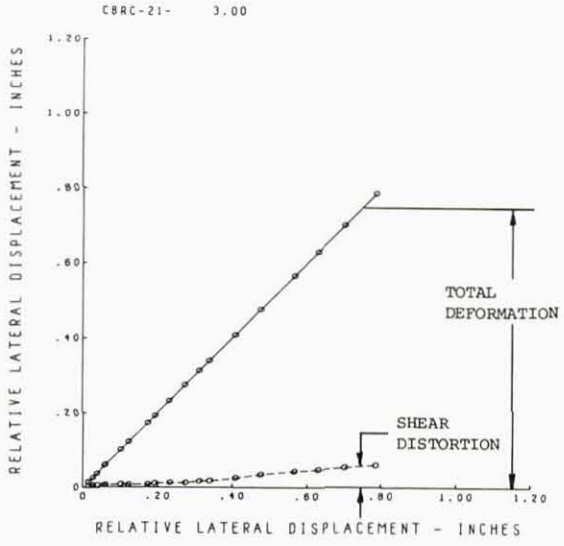

FIG. A.12 CONTINUE CBRC-21-3

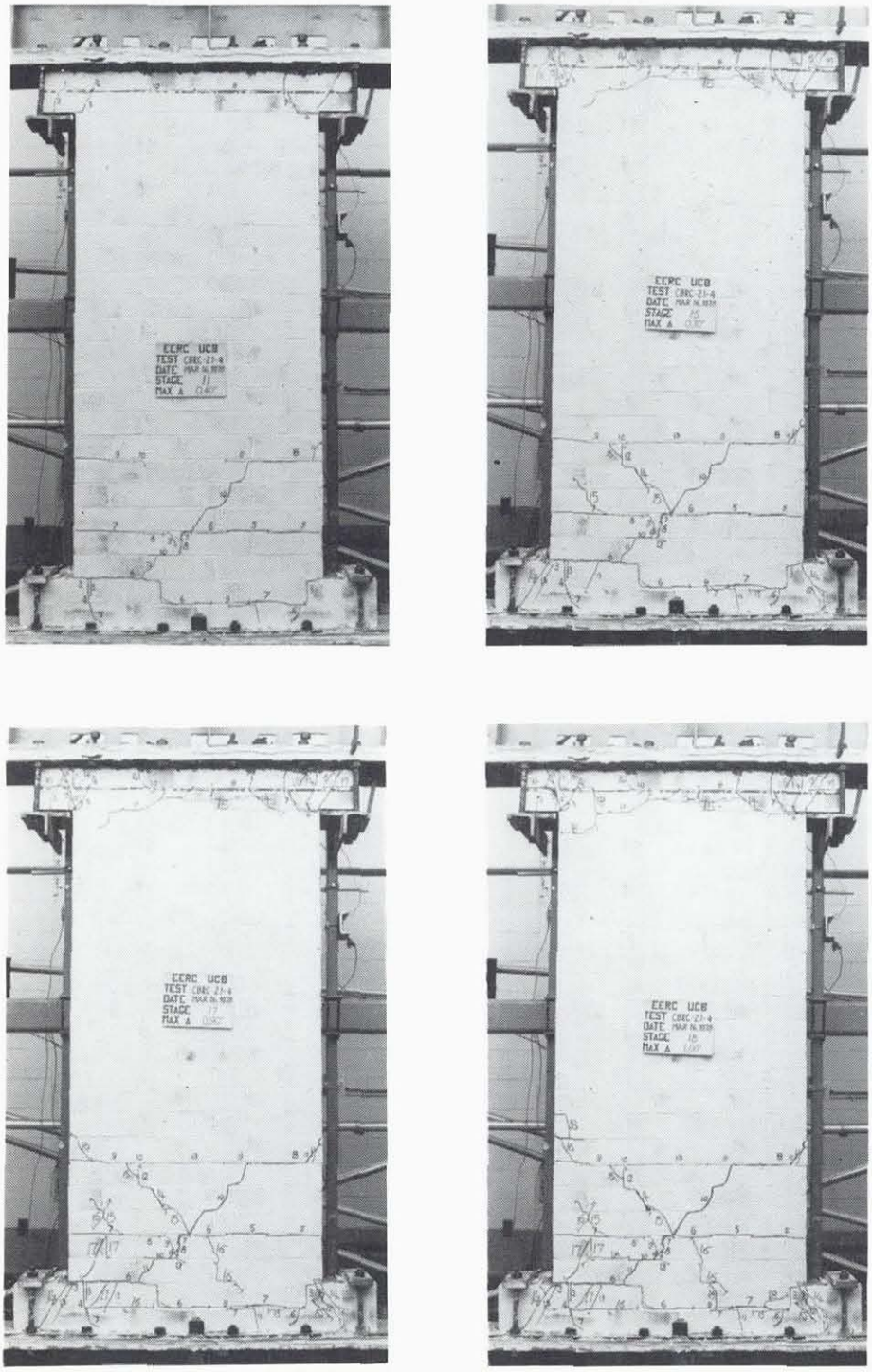

FIG. A.13 SUCCESSIVE CRACK FORMATION
AND EXPERIMENTAL RESULTS
TEST CBRC-21-4

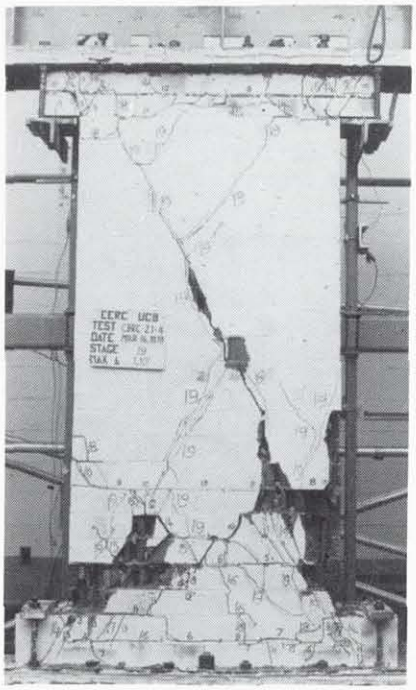

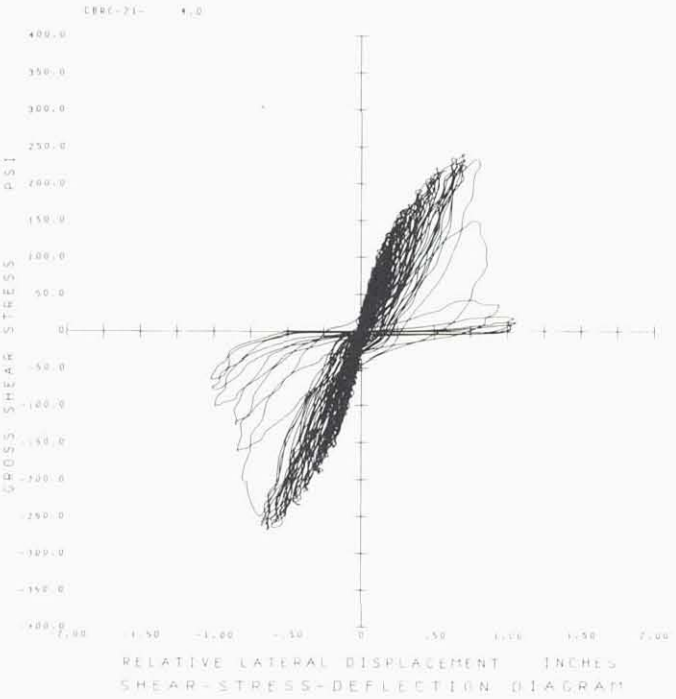

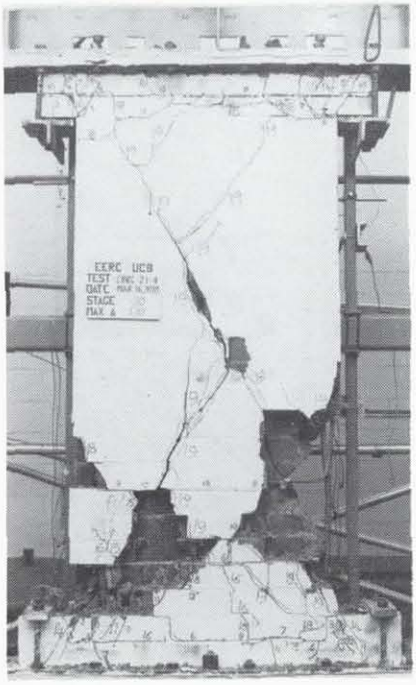

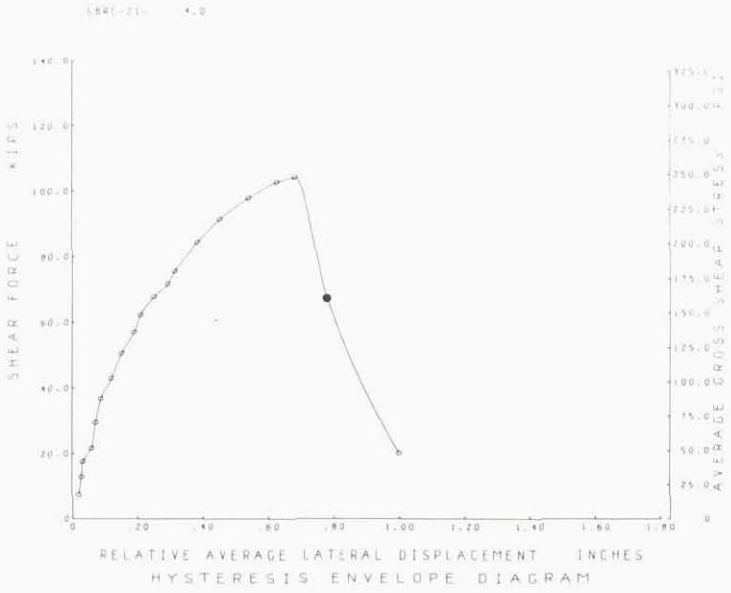

FIG. A.13 CONTINUE CBRC-21-4

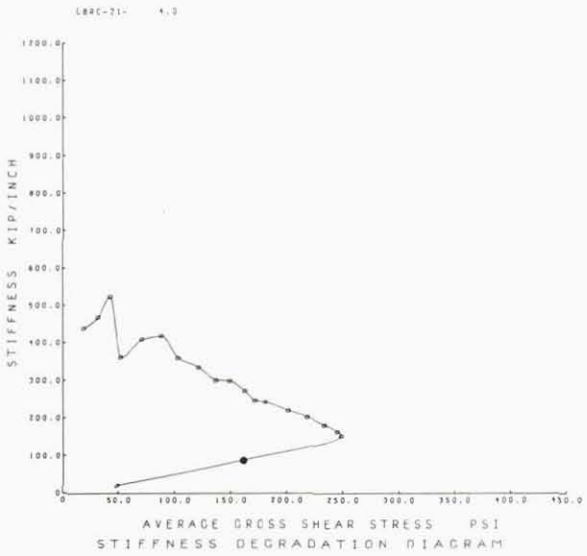

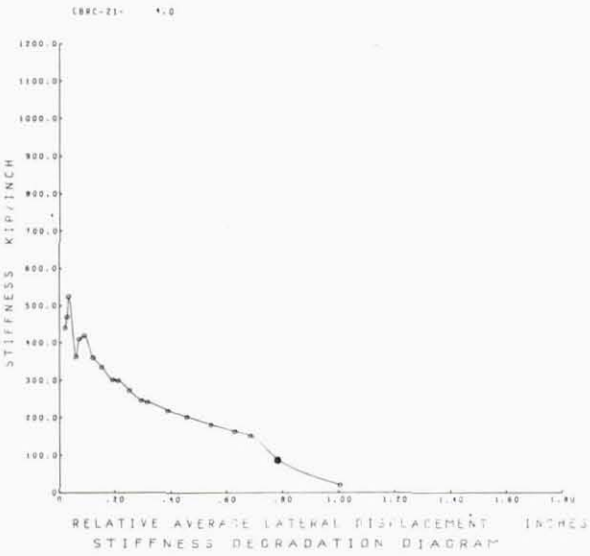

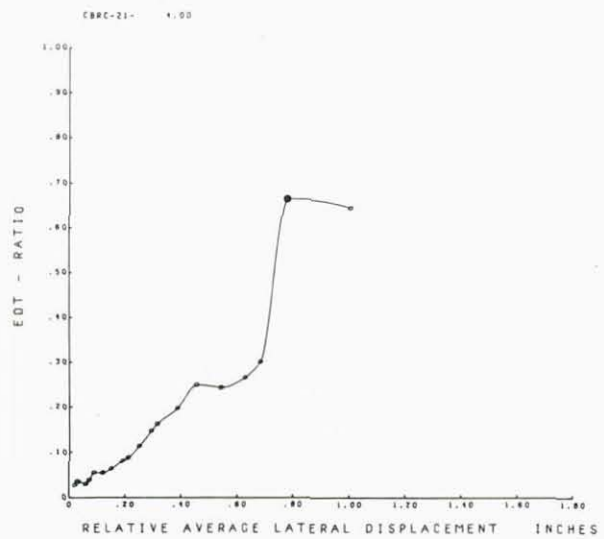

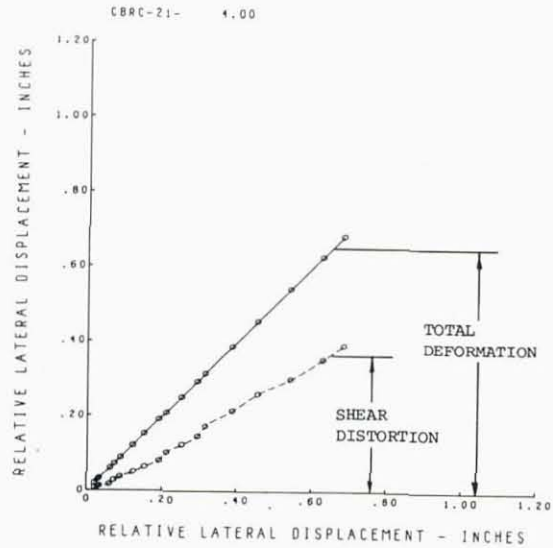

FIG. A.13 CONTINUE CBRC-21-4

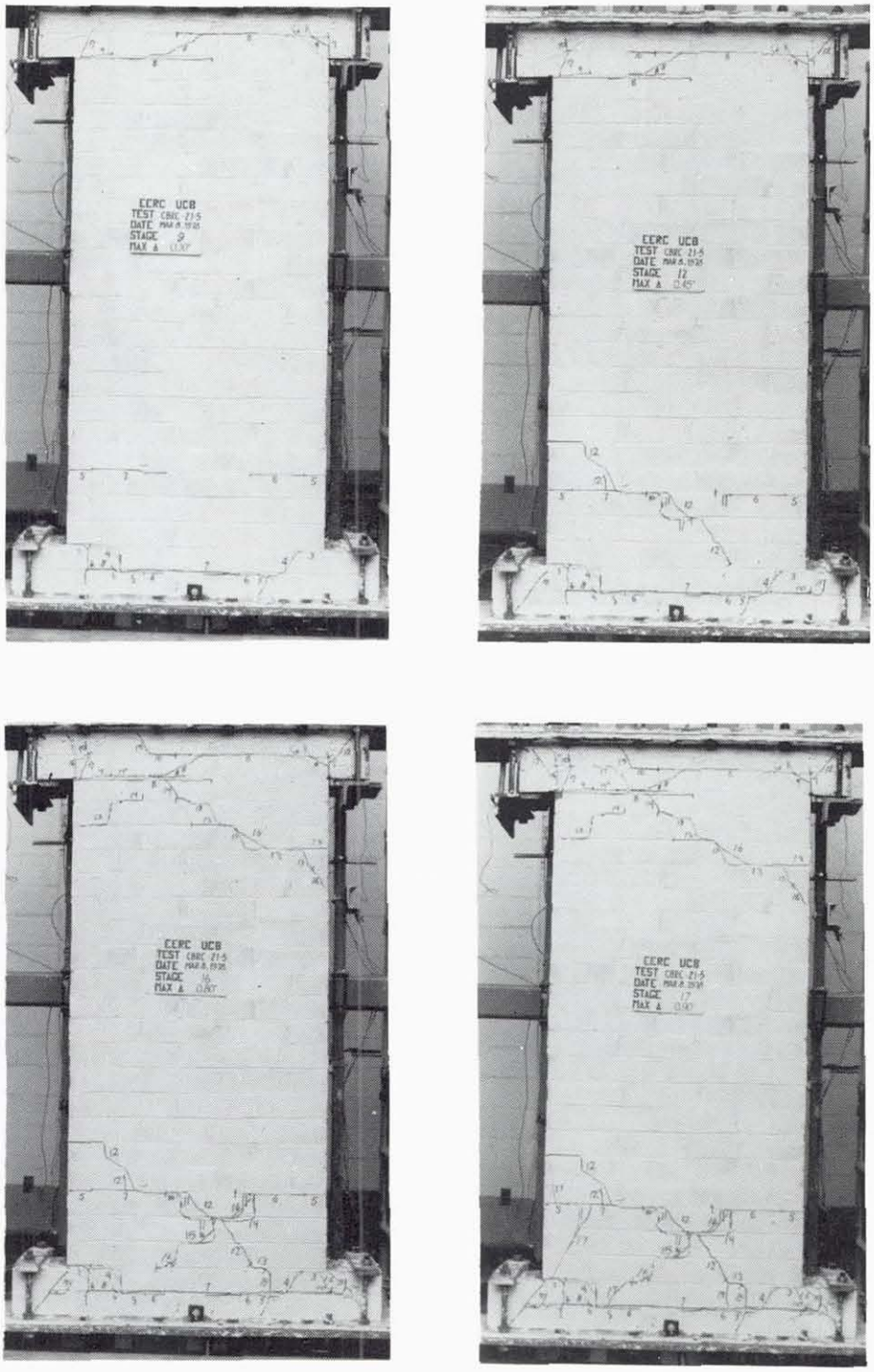

FIG. A.14 SUCCESSIVE CRACK FORMATION
AND EXPERIMENTAL RESULTS
TEST CBRC-21-5

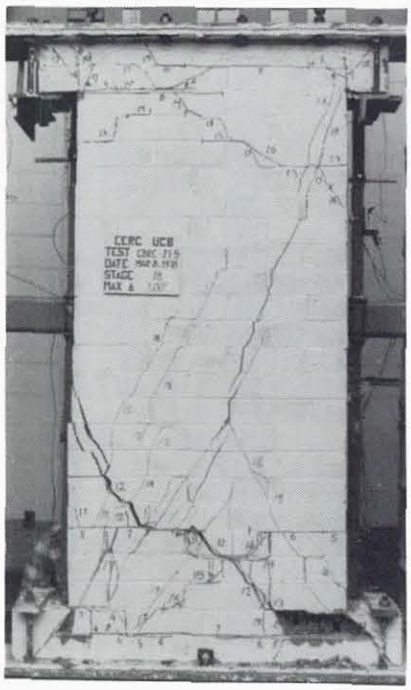

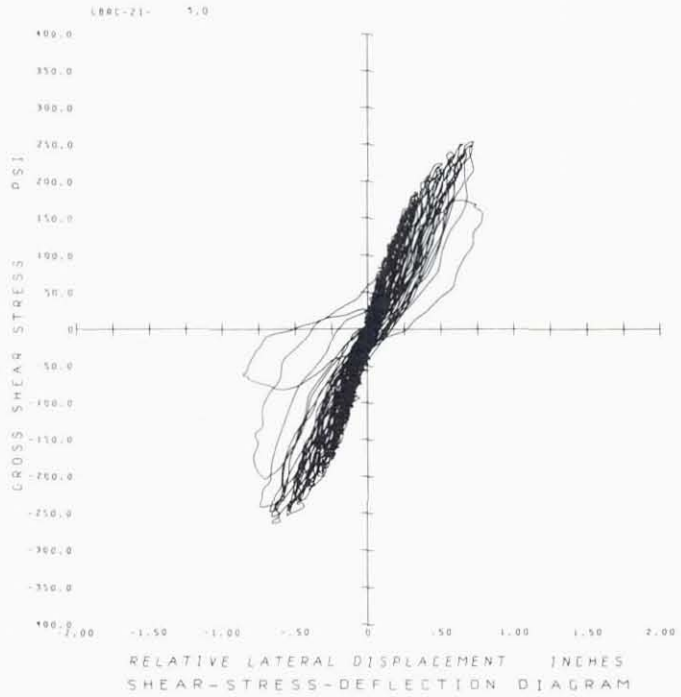

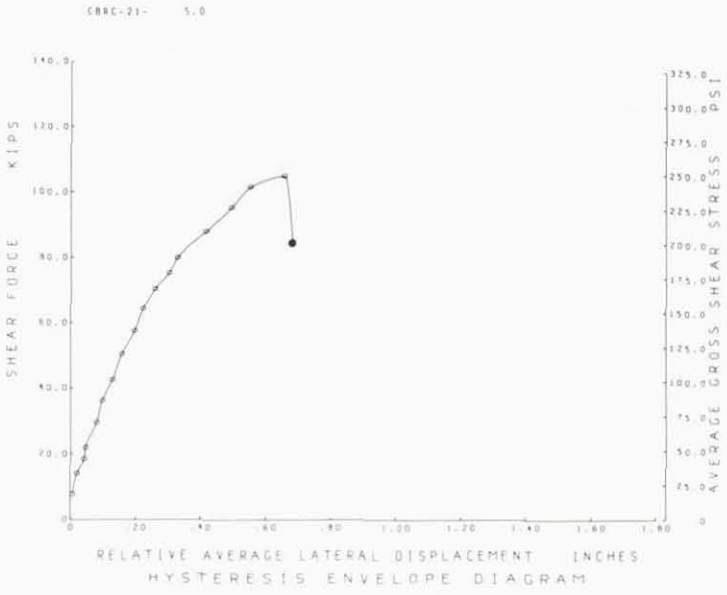

FIG. A.14 CONTINUE CBRC-21-5

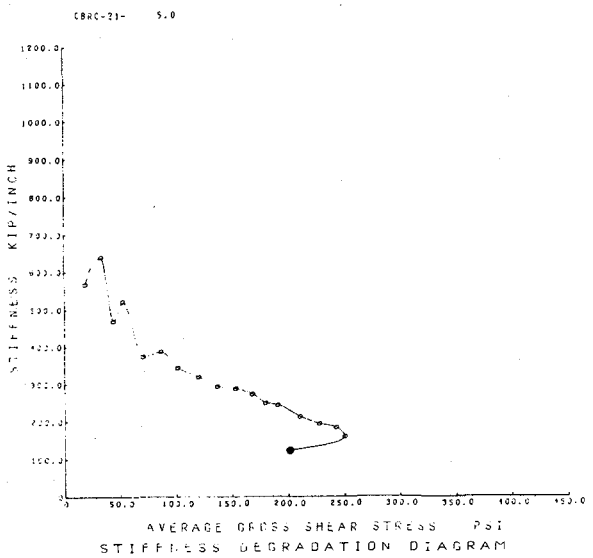

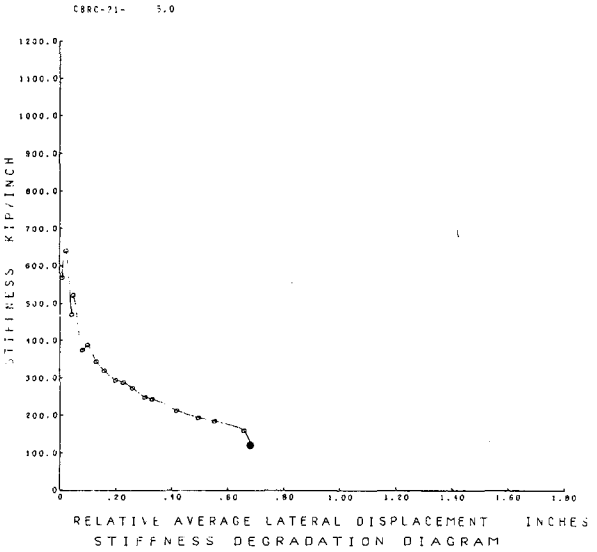

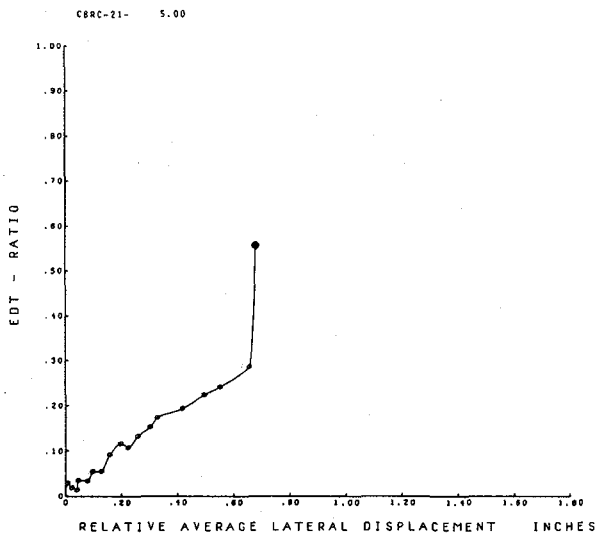

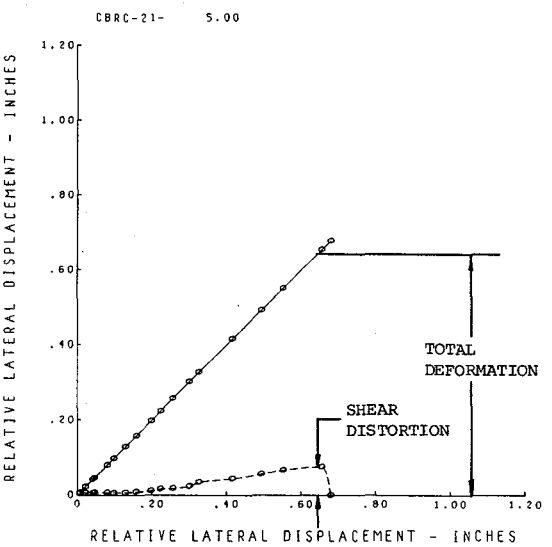

FIG. A.14 CONTINUE CBRC-21-5

EARTHQUAKE ENGINEERING RESEARCH CENTER REPORTS

NOTE: Numbers in parenthesis are Accession Numbers assigned by the National Technical Information Service; these are followed by a price code. Copies of the reports may be ordered from the National Technical Information Service, 5285 Port Royal Road, Springfield, Virginia, 22161. Accession Numbers should be quoted on orders for reports (PB --- ---) and remittance must accompany each order. Reports without this information were not available at time of printing. Upon request, EERC will mail inquirers this information when it becomes available.

EERC 67-1 "Feasibility Study Large-Scale Earthquake Simulator Facility," by J. Penzien, J.G. Bouwkamp, R.W. Clough and D. Rea - 1967 (PB 187 905)A07

EERC 68-1 Unassigned

EERC 68-2 "Inelastic Behavior of Beam-to-Column Subassemblages Under Repeated Loading," by V.V. Bertero - 1968 (PB 184 888)A05

EERC 68-3 "A Graphical Method for Solving the Wave Reflection-Refraction Problem," by H.D. McNiven and Y. Mengi - 1968 (PB 187 943)A03

EERC 68-4 "Dynamic Properties of McKinley School Buildings," by D. Rea, J.G. Bouwkamp and R.W. Clough - 1968 (PB 187 902)A07

EERC 68-5 "Characteristics of Rock Motions During Earthquakes," by H.B. Seed, I.M. Idriss and F.W. Kiefer - 1968 (PB 188 338)A03

EERC 69-1 "Earthquake Engineering Research at Berkeley," - 1969 (PB 187 906)A11

EERC 69-2 "Nonlinear Seismic Response of Earth Structures," by M. Dibaj and J. Penzien - 1969 (PB 187 904)A08

EERC 69-3 "Probabilistic Study of the Behavior of Structures During Earthquakes," by R. Ruiz and J. Penzien - 1969 (PB 187 886)A06

EERC 69-4 "Numerical Solution of Boundary Value Problems in Structural Mechanics by Reduction to an Initial Value Formulation," by N. Distefano and J. Schujman - 1969 (PB 187 942)A02

EERC 69-5 "Dynamic Programming and the Solution of the Biharmonic Equation," by N. Distefano - 1969 (PB 187 941)A03

EERC 69-6 "Stochastic Analysis of Offshore Tower Structures," by A.K. Malhotra and J. Penzien - 1969 (PB 187 903)A08

EERC 69-7 "Rock Motion Accelerograms for High Magnitude Earthquakes," by H.B. Seed and I.M. Idriss - 1969 (PB 187 940)A02

EERC 69-8 "Structural Dynamics Testing Facilities at the University of California, Berkeley," by R.M. Stephen, J.G. Bouwkamp, R.W. Clough and J. Penzien - 1969 (PB 189 111)A04

EERC 69-9 "Seismic Response of Soil Deposits Underlain by Sloping Rock Boundaries," by H. Dezfulian and H.B. Seed 1969 (PB 189 114)A03

EERC 69-10 "Dynamic Stress Analysis of Axisymmetric Structures Under Arbitrary Loading," by S. Ghosh and E.L. Wilson 1969 (PB 189 026)A10

EERC 69-11 "Seismic Behavior of Multistory Frames Designed by Different Philosophies," by J.C. Anderson and V. V. Bertero - 1969 (PB 190 662)A10

EERC 69-12 "Stiffness Degradation of Reinforcing Concrete Members Subjected to Cyclic Flexural Moments," by V.V. Bertero, B. Bresler and H. Ming Liao - 1969 (PB 202 942)A07

EERC 69-13 "Response of Non-Uniform Soil Deposits to Travelling Seismic Waves," by H. Dezfulian and H.B. Seed - 1969 (PB 191 023)A03

EERC 69-14 "Damping Capacity of a Model Steel Structure," by D. Rea, R.W. Clough and J.G. Bouwkamp - 1969 (PB 190 663)A06

EERC 69-15 "Influence of Local Soil Conditions on Building Damage Potential during Earthquakes," by H.B. Seed and I.M. Idriss - 1969 (PB 191 036)A03

EERC 69-16 "The Behavior of Sands Under Seismic Loading Conditions," by M.L. Silver and H.B. Seed - 1969 (AD 714 982)A07

EERC 70-1 "Earthquake Response of Gravity Dams," by A.K. Chopra - 1970 (AD 709 640)A03

EERC 70-2 "Relationships between Soil Conditions and Building Damage in the Caracas Earthquake of July 29, 1967," by H.B. Seed, I.M. Idriss and H. Dezfulian - 1970 (PB 195 762)A05

EERC 70-3 "Cyclic Loading of Full Size Steel Connections," by E.P. Popov and R.M. Stephen - 1970 (PB 213 545)A04

EERC 70-4 "Seismic Analysis of the Charaima Building, Caraballeda, Venezuela," by Subcommittee of the SEAONC Research Committee: V.V. Bertero, P.F. Fratessa, S.A. Mahin, J.H. Sexton, A.C. Scordelis, E.L. Wilson, L.A. Wyllie, H.B. Seed and J. Penzien, Chairman - 1970 (PB 201 455)A06

EERC 70-5 "A Computer Program for Earthquake Analysis of Dams," by A.K. Chopra and P. Chakrabarti - 1970 (AD 723 994)A05

EERC 70-6 "The Propagation of Love Waves Across Non-Horizontally Layered Structures," by J. Lysmer and L.A. Drake 1970 (PB 197 896)A03

EERC 70-7 "Influence of Base Rock Characteristics on Ground Response," by J. Lysmer, H.B. Seed and P.B. Schnabel 1970 (PB 197 897)A03

EERC 70-8 "Applicability of Laboratory Test Procedures for Measuring Soil Liquefaction Characteristics under Cyclic Loading," by H.B. Seed and W.H. Peacock - 1970 (PB 198 016)A03

EERC 70-9 "A Simplified Procedure for Evaluating Soil Liquefaction Potential," by H.B. Seed and I.M. Idriss - 1970 (PB 198 009)A03

EERC 70-10 "Soil Moduli and Damping Factors for Dynamic Response Analysis," by H.B. Seed and I.M. Idriss - 1970 (PB 197 869)A03

EERC 71-1 "Koyna Earthquake of December 11, 1967 and the Performance of Koyna Dam," by A.K. Chopra and P. Chakrabarti 1971 (AD 731 496)A06

EERC 71-2 "Preliminary In-Situ Measurements of Anelastic Absorption in Soils Using a Prototype Earthquake Simulator," by R.D. Borcherdt and P.W. Rodgers - 1971 (PB 201 454)A03

EERC 71-3 "Static and Dynamic Analysis of Inelastic Frame Structures," by F.L. Porter and G.H. Powell - 1971 (PB 210 135)A06

EERC 71-4 "Research Needs in Limit Design of Reinforced Concrete Structures," by V.V. Bertero - 1971 (PB 202 943)A04

EERC 71-5 "Dynamic Behavior of a High-Rise Diagonally Braced Steel Building," by D. Rea, A.A. Shah and J.G. Bouwkamp 1971 (PB 203 584)A06

EERC 71-6 "Dynamic Stress Analysis of Porous Elastic Solids Saturated with Compressible Fluids," by J. Ghaboussi and E. L. Wilson - 1971 (PB 211 396)A06

EERC 71-7 "Inelastic Behavior of Steel Beam-to-Column Subassemblages," by H. Krawinkler, V.V. Bertero and E.P. Popov 1971 (PB 211 335)A14

EERC 71-8 "Modification of Seismograph Records for Effects of Local Soil Conditions," by P. Schnabel, H.B. Seed and J. Lysmer - 1971 (PB 214 450)A03

EERC 72-1 "Static and Earthquake Analysis of Three Dimensional Frame and Shear Wall Buildings," by E.L. Wilson and H.H. Dovey - 1972 (PB 212 904)A05

EERC 72-2 "Accelerations in Rock for Earthquakes in the Western United States," by P.B. Schnabel and H.B. Seed - 1972 (PB 213 100)A03

EERC 72-3 "Elastic-Plastic Earthquake Response of Soil-Building Systems," by T. Minami - 1972 (PB 214 868)A08

EERC 72-4 "Stochastic Inelastic Response of Offshore Towers to Strong Motion Earthquakes," by M.K. Kaul - 1972 (PB 215 713)A05

EERC 72-5 "Cyclic Behavior of Three Reinforced Concrete Flexural Members with High Shear," by E.P. Popov, V.V. Bertero and H. Krawinkler - 1972 (PB 214 555)A05

EERC 72-6 "Earthquake Response of Gravity Dams Including Reservoir Interaction Effects," by P. Chakrabarti and A.K. Chopra - 1972 (AD 762 330)A08

EERC 72-7 "Dynamic Properties of Pine Flat Dam," by D. Rea, C.Y. Liaw and A.K. Chopra - 1972 (AD 763 928)A05

EERC 72-8 "Three Dimensional Analysis of Building Systems," by E.L. Wilson and H.H. Dovey - 1972 (PB 222 438)A06

EERC 72-9 "Rate of Loading Effects on Uncracked and Repaired Reinforced Concrete Members," by S. Mahin, V.V. Bertero, D. Rea and M. Atalay - 1972 (PB 224 520)A08

EERC 72-10 "Computer Program for Static and Dynamic Analysis of Linear Structural Systems," by E.L. Wilson, K.-J. Bathe, J.E. Peterson and H.H.Dovey - 1972 (PB 220 437)A04

EERC 72-11 "Literature Survey - Seismic Effects on Highway Bridges," by T. Iwasaki, J. Penzien and R.W. Clough - 1972 (PB 215 613)A19

EERC 72-12 "SHAKE-A Computer Program for Earthquake Response Analysis of Horizontally Layered Sites," by P.B. Schnabel and J. Lysmer - 1972 (PB 220 207)A06

EERC 73-1 "Optimal Seismic Design of Multistory Frames," by V.V. Bertero and H. Kamil - 1973

EERC 73-2 "Analysis of the Slides in the San Fernando Dams During the Earthquake of February 9, 1971," by H.B. Seed, K.L. Lee, I.M. Idriss and F. Makdisi - 1973 (PB 223 402)A14

EERC 73-3 "Computer Aided Ultimate Load Design of Unbraced Multistory Steel Frames," by M.B. El-Hafez and G.H. Powell 1973 (PB 248 315)A09

EERC 73-4 "Experimental Investigation into the Seismic Behavior of Critical Regions of Reinforced Concrete Components as Influenced by Moment and Shear," by M. Celebi and J. Penzien - 1973 (PB 215 884)A09

EERC 73-5 "Hysteretic Behavior of Epoxy-Repaired Reinforced Concrete Beams," by M. Celebi and J. Penzien - 1973 (PB 239 568)A03

EERC 73-6 "General Purpose Computer Program for Inelastic Dynamic Response of Plane Structures," by A. Kanaan and G.H. Powell - 1973 (PB 221 260)A08

EERC 73-7 "A Computer Program for Earthquake Analysis of Gravity Dams Including Reservoir Interaction," by P. Chakrabarti and A.K. Chopra - 1973 (AD 766 271)A04

EERC 73-8 "Behavior of Reinforced Concrete Deep Beam-Column Subassemblages Under Cyclic Loads," by O. Küstü and J.G. Bouwkamp - 1973 (PB 246 117)A12

EERC 73-9 "Earthquake Analysis of Structure-Foundation Systems," by A.K. Vaish and A.K. Chopra - 1973 (AD 766 272)A07

EERC 73-10 "Deconvolution of Seismic Response for Linear Systems," by R.B. Reimer - 1973 (PB 227 179)A08

EERC 73-11 "SAP IV: A Structural Analysis Program for Static and Dynamic Response of Linear Systems," by K.-J. Bathe, E.L. Wilson and F.E. Peterson - 1973 (PB 221 967)A09

EERC 73-12 "Analytical Investigations of the Seismic Response of Long, Multiple Span Highway Bridges," by W.S. Tseng and J. Penzien - 1973 (PB 227 816)A10

EERC 73-13 "Earthquake Analysis of Multi-Story Buildings Including Foundation Interaction," by A.K. Chopra and J.A. Gutierrez - 1973 (PB 222 970)A03

EERC 73-14 "ADAP: A Computer Program for Static and Dynamic Analysis of Arch Dams," by R.W. Clough, J.M. Raphael and S. Mojtahedi - 1973 (PB 223 763)A09

EERC 73-15 "Cyclic Plastic Analysis of Structural Steel Joints," by R.B. Pinkney and R.W. Clough - 1973 (PB 226 843)A08

EERC 73-16 "QUAD-4: A Computer Program for Evaluating the Seismic Response of Soil Structures by Variable Damping Finite Element Procedures," by I.M. Idriss, J. Lysmer, R. Hwang and H.B. Seed - 1973 (PB 229 424)A05

EERC 73-17 "Dynamic Behavior of a Multi-Story Pyramid Shaped Building," by R.M. Stephen, J.P. Hollings and J.G. Bouwkamp - 1973 (PB 240 718)A06

EERC 73-18 "Effect of Different Types of Reinforcing on Seismic Behavior of Short Concrete Columns," by V.V. Bertero, J. Hollings, O. Küstü, R.M. Stephen and J.G. Bouwkamp - 1973

EERC 73-19 "Olive View Medical Center Materials Studies, Phase I," by B. Bresler and V.V. Bertero - 1973 (PB 235 986)A06

EERC 73-20 "Linear and Nonlinear Seismic Analysis Computer Programs for Long Multiple-Span Highway Bridges," by W.S. Tseng and J. Penzien - 1973

EERC 73-21 "Constitutive Models for Cyclic Plastic Deformation of Engineering Materials," by J.M. Kelly and P.P. Gillis 1973 (PB 226 024)A03

EERC 73-22 "DRAIN - 2D User's Guide," by G.H. Powell - 1973 (PB 227 016)A05

EERC 73-23 "Earthquake Engineering at Berkeley - 1973," (PB 226 033)A11

EERC 73-24 Unassigned

EERC 73-25 "Earthquake Response of Axisymmetric Tower Structures Surrounded by Water," by C.Y. Liaw and A.K. Chopra 1973 (AD 773 052)A09

EERC 73-26 "Investigation of the Failures of the Olive View Stairtowers During the San Fernando Earthquake and Their Implications on Seismic Design," by V.V. Bertero and R.G. Collins - 1973 (PB 235 106)A13

EERC 73-27 "Further Studies on Seismic Behavior of Steel Beam-Column Subassemblages," by V.V. Bertero, H. Krawinkler and E.P. Popov - 1973 (PB 234 172)A06

EERC 74-1 "Seismic Risk Analysis," by C.S. Oliveira - 1974 (PB 235 920)A06

EERC 74-2 "Settlement and Liquefaction of Sands Under Multi-Directional Shaking," by R. Pyke, C.K. Chan and H.B. Seed 1974

EERC 74-3 "Optimum Design of Earthquake Resistant Shear Buildings," by D. Ray, K.S. Pister and A.K. Chopra - 1974 (PB 231 172)A06

EERC 74-4 "LUSH - A Computer Program for Complex Response Analysis of Soil-Structure Systems," by J. Lysmer, T. Udaka, H.B. Seed and R. Hwang - 1974 (PB 236 796)A05

EERC 74-5 "Sensitivity Analysis for Hysteretic Dynamic Systems: Applications to Earthquake Engineering," by D. Ray 1974 (PB 233 213)A06

EERC 74-6 "Soil Structure Interaction Analyses for Evaluating Seismic Response," by H.B. Seed, J. Lysmer and R. Hwang 1974 (PB 236 519)A04

EERC 74-7 Unassigned

EERC 74-8 "Shaking Table Tests of a Steel Frame - A Progress Report," by R.W. Clough and D. Tang - 1974 (PB 240 869)A03

EERC 74-9 "Hysteretic Behavior of Reinforced Concrete Flexural Members with Special Web Reinforcement," by V.V. Bertero, E.P. Popov and T.Y. Wang - 1974 (PB 236 797)A07

EERC 74-10 "Applications of Reliability-Based, Global Cost Optimization to Design of Earthquake Resistant Structures," by E. Vitiello and K.S. Pister - 1974 (PB 237 231)A06

EERC 74-11 "Liquefaction of Gravelly Soils Under Cyclic Loading Conditions," by R.T. Wong, H.B. Seed and C.K. Chan 1974 (PB 242 042)A03

EERC 74-12 "Site-Dependent Spectra for Earthquake-Resistant Design," by H.B. Seed, C. Ugas and J. Lysmer - 1974 (PB 240 953)A03

EERC 74-13 "Earthquake Simulator Study of a Reinforced Concrete Frame," by P. Hidalgo and R.W. Clough - 1974 (PB 241 944)A13

EERC 74-14 "Nonlinear Earthquake Response of Concrete Gravity Dams," by N. Pal - 1974 (AD/A 006 583)A06

EERC 74-15 "Modeling and Identification in Nonlinear Structural Dynamics - I. One Degree of Freedom Models," by N. Distefano and A. Rath - 1974 (PB 241 548)A06

EERC 75-1 "Determination of Seismic Design Criteria for the Dumbarton Bridge Replacement Structure, Vol. I: Description, Theory and Analytical Modeling of Bridge and Parameters," by F. Baron and S.-H. Pang - 1975 (PB 259 407)A15

EERC 75-2 "Determination of Seismic Design Criteria for the Dumbarton Bridge Replacement Structure, Vol. II: Numerical Studies and Establishment of Seismic Design Criteria," by F. Baron and S.-H. Pang - 1975 (PB 259 408)A11 (For set of EERC 75-1 and 75-2 (PB 259 406))

EERC 75-3 "Seismic Risk Analysis for a Site and a Metropolitan Area," by C.S. Oliveira - 1975 (PB 248 134)A09

EERC 75-4 "Analytical Investigations of Seismic Response of Short, Single or Multiple-Span Highway Bridges," by M.-C. Chen and J. Penzien - 1975 (PB 241 454)A09

EERC 75-5 "An Evaluation of Some Methods for Predicting Seismic Behavior of Reinforced Concrete Buildings," by S.A. Mahin and V.V. Bertero - 1975 (PB 246 306)A16

EERC 75-6 "Earthquake Simulator Study of a Steel Frame Structure, Vol. I: Experimental Results," by R.W. Clough and D.T. Tang - 1975 (PB 243 981)A13

EERC 75-7 "Dynamic Properties of San Bernardino Intake Tower," by D. Rea, C.-Y. Liaw and A.K. Chopra - 1975 (AD/A008 406) A05

EERC 75-8 "Seismic Studies of the Articulation for the Dumbarton Bridge Replacement Structure, Vol. I: Description, Theory and Analytical Modeling of Bridge Components," by F. Baron and R.E. Hamati - 1975 (PB 251 539)A07

EERC 75-9 "Seismic Studies of the Articulation for the Dumbarton Bridge Replacement Structure, Vol. 2: Numerical Studies of Steel and Concrete Girder Alternates," by F. Baron and R.E. Hamati - 1975 (PB 251 540)A10

EERC 75-10 "Static and Dynamic Analysis of Nonlinear Structures," by D.P. Mondkar and G.H. Powell - 1975 (PB 242 434)A08

EERC 75-11 "Hysteretic Behavior of Steel Columns," by E.P. Popov, V.V. Bertero and S. Chandramouli - 1975 (PB 252 365)A11

EERC 75-12 "Earthquake Engineering Research Center Library Printed Catalog," - 1975 (PB 243 711)A26

EERC 75-13 "Three Dimensional Analysis of Building Systems (Extended Version)," by E.L. Wilson, J.P. Hollings and H.H. Dovey - 1975 (PB 243 989)A07

EERC 75-14 "Determination of Soil Liquefaction Characteristics by Large-Scale Laboratory Tests," by P. De Alba, C.K. Chan and H.B. Seed - 1975 (NUREG 0027)A08

EERC 75-15 "A Literature Survey - Compressive, Tensile, Bond and Shear Strength of Masonry," by R.L. Mayes and R.W. Clough - 1975 (PB 246 292)A10

EERC 75-16 "Hysteretic Behavior of Ductile Moment Resisting Reinforced Concrete Frame Components," by V.V. Bertero and E.P. Popov - 1975 (PB 246 388)A05

EERC 75-17 "Relationships Between Maximum Acceleration, Maximum Velocity, Distance from Source, Local Site Conditions for Moderately Strong Earthquakes," by H.B. Seed, R. Murarka, J. Lysmer and I.M. Idriss - 1975 (PB 248 172)A03

EERC 75-18 "The Effects of Method of Sample Preparation on the Cyclic Stress-Strain Behavior of Sands," by J. Mulilis, C.K. Chan and H.B. Seed - 1975 (Summarized in EERC 75-28)

EERC 75-19 "The Seismic Behavior of Critical Regions of Reinforced Concrete Components as Influenced by Moment, Shear and Axial Force," by M.B. Atalay and J. Penzien - 1975 (PB 258 842)A11

EERC 75-20 "Dynamic Properties of an Eleven Story Masonry Building," by R.M. Stephen, J.P. Hollings, J.G. Bouwkamp and D. Jurukovski - 1975 (PB 246 945)A04

EERC 75-21 "State-of-the-Art in Seismic Strength of Masonry - An Evaluation and Review," by R.L. Mayes and R.W. Clough 1975 (PB 249 040)A07

EERC 75-22 "Frequency Dependent Stiffness Matrices for Viscoelastic Half-Plane Foundations," by A.K. Chopra, P. Chakrabarti and G. Dasgupta - 1975 (PB 248 121)A07

EERC 75-23 "Hysteretic Behavior of Reinforced Concrete Framed Walls," by T.Y. Wong, V.V. Bertero and E.P. Popov - 1975

EERC 75-24 "Testing Facility for Subassemblages of Frame-Wall Structural Systems," by V.V. Bertero, E.P. Popov and T. Endo - 1975

EERC 75-25 "Influence of Seismic History on the Liquefaction Characteristics of Sands," by H.B. Seed, K. Mori and C.K. Chan - 1975 (Summarized in EERC 75-28)

EERC 75-26 "The Generation and Dissipation of Pore Water Pressures during Soil Liquefaction," by H.B. Seed, P.P. Martin and J. Lysmer - 1975 (PB 252 648)A03

EERC 75-27 "Identification of Research Needs for Improving Aseismic Design of Building Structures," by V.V. Bertero 1975 (PB 248 136)A05

EERC 75-28 "Evaluation of Soil Liquefaction Potential during Earthquakes," by H.B. Seed, I. Arango and C.K. Chan - 1975 (NUREG 0026)A13

EERC 75-29 "Representation of Irregular Stress Time Histories by Equivalent Uniform Stress Series in Liquefaction Analyses," by H.B. Seed, I.M. Idriss, F. Makdisi and N. Banerjee - 1975 (PB 252 635)A03

EERC 75-30 "FLUSH - A Computer Program for Approximate 3-D Analysis of Soil-Structure Interaction Problems," by J. Lysmer, T. Udaka, C.-F. Tsai and H.B. Seed - 1975 (PB 259 332)A07

EERC 75-31 "ALUSH - A Computer Program for Seismic Response Analysis of Axisymmetric Soil-Structure Systems," by E. Berger, J. Lysmer and H.B. Seed - 1975

EERC 75-32 "TRIP and TRAVEL - Computer Programs for Soil-Structure Interaction Analysis with Horizontally Travelling Waves," by T. Udaka, J. Lysmer and H.B. Seed - 1975

EERC 75-33 "Predicting the Performance of Structures in Regions of High Seismicity," by J. Penzien - 1975 (PB 248 130)A03

EERC 75-34 "Efficient Finite Element Analysis of Seismic Structure - Soil - Direction," by J. Lysmer, H.B. Seed, T. Udaka, R.N. Hwang and C.-F. Tsai - 1975 (PB 253 570)A03

EERC 75-35 "The Dynamic Behavior of a First Story Girder of a Three-Story Steel Frame Subjected to Earthquake Loading," by R.W. Clough and L.-Y. Li - 1975 (PB 248 841)A05

EERC 75-36 "Earthquake Simulator Study of a Steel Frame Structure, Volume II - Analytical Results," by D.T. Tang - 1975 (PB 252 926)A10

EERC 75-37 "ANSR-I General Purpose Computer Program for Analysis of Non-Linear Structural Response," by D.P. Mondkar and G.H. Powell - 1975 (PB 252 386)A08

EERC 75-38 "Nonlinear Response Spectra for Probabilistic Seismic Design and Damage Assessment of Reinforced Concrete Structures," by M. Murakami and J. Penzien - 1975 (PB 259 530)A05

EERC 75-39 "Study of a Method of Feasible Directions for Optimal Elastic Design of Frame Structures Subjected to Earthquake Loading," by N.D. Walker and K.S. Pister - 1975 (PB 257 781)A06

EERC 75-40 "An Alternative Representation of the Elastic-Viscoelastic Analogy," by G. Dasgupta and J.L. Sackman - 1975 (PB 252 173)A03

EERC 75-41 "Effect of Multi-Directional Shaking on Liquefaction of Sands," by H.B. Seed, R. Pyke and G.R. Martin - 1975 (PB 258 781)A03

EERC 76-1 "Strength and Ductility Evaluation of Existing Low-Rise Reinforced Concrete Buildings - Screening Method," by T. Okada and B. Bresler - 1976 (PB 257 906)A11

EERC 76-2 "Experimental and Analytical Studies on the Hysteretic Behavior of Reinforced Concrete Rectangular and T-Beams," by S.-Y.M. Ma, E.P. Popov and V.V. Bertero - 1976 (PB 260 843)A12

EERC 76-3 "Dynamic Behavior of a Multistory Triangular-Shaped Building," by J. Petrovski, R.M. Stephen, E. Gartenbaum and J.G. Bouwkamp - 1976

EERC 76-4 "Earthquake Induced Deformations of Earth Dams," by N. Serff and H.B. Seed - 1976

EERC 76-5 "Analysis and Design of Tube-Type Tall Building Structures," by H. de Clercq and G.H. Powell - 1976 (PB 252 220) A10

EERC 76-6 "Time and Frequency Domain Analysis of Three-Dimensional Ground Motions, San Fernando Earthquake," by T. Kubo and J. Penzien (PB 260 556)A11

EERC 76-7 "Expected Performance of Uniform Building Code Design Masonry Structures," by R.L. Mayes, Y. Omote, S.W. Chen and R.W. Clough - 1976

EERC 76-8 "Cyclic Shear Tests on Concrete Masonry Piers," Part I - Test Results," by R.L. Mayes, Y. Omote and R.W. Clough - 1976 (PB 264 424)A06

EERC 76-9 "A Substructure Method for Earthquake Analysis of Structure - Soil Interaction," by J.A. Gutierrez and A.K. Chopra - 1976 (PB 257 783)A08

EERC 76-10 "Stabilization of Potentially Liquefiable Sand Deposits using Gravel Drain Systems," by H.B. Seed and J.R. Booker - 1976 (PB 258 820)A04

EERC 76-11 "Influence of Design and Analysis Assumptions on Computed Inelastic Response of Moderately Tall Frames," by G.H. Powell and D.G. Row - 1976

EERC 76-12 "Sensitivity Analysis for Hysteretic Dynamic Systems: Theory and Applications," by D. Ray, K.S. Pister and E. Polak - 1976 (PB 262 859)A04

EERC 76-13 "Coupled Lateral Torsional Response of Buildings to Ground Shaking," by C.L. Kan and A.K. Chopra - 1976 (PB 257 907)A09

EERC 76-14 "Seismic Analyses of the Banco de America," by V.V. Bertero, S.A. Mahin and J.A. Hollings - 1976

EERC 76-15 "Reinforced Concrete Frame 2: Seismic Testing and Analytical Correlation," by R.W. Clough and J. Gidwani - 1976 (PB 261 323)A08

EERC 76-16 "Cyclic Shear Tests on Masonry Piers, Part II - Analysis of Test Results," by R.L. Mayes, Y. Omote and R.W. Clough - 1976

EERC 76-17 "Structural Steel Bracing Systems: Behavior Under Cyclic Loading," by E.P. Popov, K. Takanashi and C.W. Roeder - 1976 (PB 260 715)A05

EERC 76-18 "Experimental Model Studies on Seismic Response of High Curved Overcrossings," by D. Williams and W.G. Godden - 1976

EERC 76-19 "Effects of Non-Uniform Seismic Disturbances on the Dumbarton Bridge Replacement Structure," by F. Baron and R.E. Hamati - 1976

EERC 76-20 "Investigation of the Inelastic Characteristics of a Single Story Steel Structure Using System Identification and Shaking Table Experiments," by V.C. Matzen and H.D. McNiven - 1976 (PB 258 453)A07

EERC 76-21 "Capacity of Columns with Splice Imperfections," by E.P. Popov, R.M. Stephen and R. Philbrick - 1976 (PB 260 378)A04

EERC 76-22 "Response of the Olive View Hospital Main Building during the San Fernando Earthquake," by S. A. Mahin, R. Collins, A.K. Chopra and V.V. Bertero - 1976

EERC 76-23 "A Study on the Major Factors Influencing the Strength of Masonry Prisms," by N.M. Mostaghel, R.L. Mayes, R. W. Clough and S.W. Chen - 1976

EERC 76-24 "GADFLEA - A Computer Program for the Analysis of Pore Pressure Generation and Dissipation during Cyclic or Earthquake Loading," by J.R. Booker, M.S. Rahman and H.B. Seed - 1976 (PB 263 947)A04

EERC 76-25 "Rehabilitation of an Existing Building: A Case Study," by B. Bresler and J. Axley - 1976

EERC 76-26 "Correlative Investigations on Theoretical and Experimental Dynamic Behavior of a Model Bridge Structure," by K. Kawashima and J. Penzien - 1976 (PB 263 388)A11

EERC 76-27 "Earthquake Response of Coupled Shear Wall Buildings," by T. Srichatrapimuk - 1976 (PB 265 157)A07

EERC 76-28 "Tensile Capacity of Partial Penetration Welds," by E.P. Popov and R.M. Stephen - 1976 (PB 262 899)A03

EERC 76-29 "Analysis and Design of Numerical Integration Methods in Structural Dynamics," by H.M. Hilber - 1976 (PB 264 410)A06

EERC 76-30 "Contribution of a Floor System to the Dynamic Characteristics of Reinforced Concrete Buildings," by L.J. Edgar and V.V. Bertero - 1976

EERC 76-31 "The Effects of Seismic Disturbances on the Golden Gate Bridge," by F. Baron, M. Arikan and R.E. Hamati - 1976

EERC 76-32 "Infilled Frames in Earthquake Resistant Construction," by R.E. Klingner and V.V. Bertero - 1976 (PB 265 892)A13

UCB/EERC-77/01 "PLUSH - A Computer Program for Probabilistic Finite Element Analysis of Seismic Soil-Structure Interaction," by M.P. Romo Organista, J. Lysmer and H.B. Seed - 1977

UCB/EERC-77/02 "Soil-Structure Interaction Effects at the Humboldt Bay Power Plant in the Ferndale Earthquake of June 7, 1975," by J.E. Valera, H.B. Seed, C.F. Tsai and J. Lysmer - 1977 (PB 265 795)A04

UCB/EERC-77/03 "Influence of Sample Disturbance on Sand Response to Cyclic Loading," by K. Mori, H.B. Seed and C.K. Chan - 1977 (PB 267 352)A04

UCB/EERC-77/04 "Seismological Studies of Strong Motion Records," by J. Shoja-Taheri - 1977 (PB 269 655)A10

UCB/EERC-77/05 "Testing Facility for Coupled-Shear Walls," by L. Li-Hyung, V.V. Bertero and E.P. Popov - 1977

UCB/EERC-77/06 "Developing Methodologies for Evaluating the Earthquake Safety of Existing Buildings," by No. 1 - B. Bresler; No. 2 - B. Bresler, T. Okada and D. Zisling; No. 3 - T. Okada and B. Bresler; No. 4 - V.V. Bertero and B. Bresler - 1977 (PB 267 354)A08

UCB/EERC-77/07 "A Literature Survey - Transverse Strength of Masonry Walls," by Y. Omote, R.L. Mayes, S.W. Chen and R.W. Clough - 1977 (PB 277 933)A07

UCB/EERC-77/08 "DRAIN-TABS: A Computer Program for Inelastic Earthquake Response of Three Dimensional Buildings," by R. Guendelman-Israel and G.H. Powell - 1977 (PB 270 693)A07

UCB/EERC-77/09 "SUBWALL: A Special Purpose Finite Element Computer Program for Practical Elastic Analysis and Design of Structural Walls with Substructure Option," by D.Q. Le, H. Peterson and E.P. Popov - 1977 (PB 270 567)A05

UCB/EERC-77/10 "Experimental Evaluation of Seismic Design Methods for Broad Cylindrical Tanks," by D.P. Clough (PB 272 280)A13

UCB/EERC-77/11 "Earthquake Engineering Research at Berkeley - 1976," - 1977 (PB 273 507)A09

UCB/EERC-77/12 "Automated Design of Earthquake Resistant Multistory Steel Building Frames," by N.D. Walker, Jr. - 1977 (PB 276 526)A09

UCB/EERC-77/13 "Concrete Confined by Rectangular Hoops Subjected to Axial Loads," by J. Vallenas, V.V. Bertero and E.P. Popov - 1977 (PB 275 165)A06

UCB/EERC-77/14 "Seismic Strain Induced in the Ground During Earthquakes," by Y. Sugimura - 1977 (PB 284 201)A04

UCB/EERC-77/15 "Bond Deterioration under Generalized Loading," by V.V. Bertero, E.P. Popov and S. Viwathanatepa - 1977

UCB/EERC-77/16 "Computer Aided Optimum Design of Ductile Reinforced Concrete Moment Resisting Frames," by S.W. Zagajeski and V.V. Bertero - 1977 (PB 280 137)A07

UCB/EERC-77/17 "Earthquake Simulation Testing of a Stepping Frame with Energy-Absorbing Devices," by J.M. Kelly and D.F. Tsztoo - 1977 (PB 273 506)A04

UCB/EERC-77/18 "Inelastic Behavior of Eccentrically Braced Steel Frames under Cyclic Loadings," by C.W. Roeder and E.P. Popov - 1977 (PB 275 526)A15

UCB/EERC-77/19 "A Symplified Procedure for Estimating Earthquake-Induced Deformations in Dams and Embankments," by F.I. Makdisi and H.B. Seed - 1977 (PB 276 820) A04

UCB/EERC-77/20 "The Performance of Earth Dams during Earthquakes," by H.B. Seed, F.I. Makdisi and P. de Alba - 1977 (PB 276 821)A04

UCB/EERC-77/21 "Dynamic Plastic Analysis Using Stress Resultant Finite Element Formulation," by P. Lukkunapvasit and J.M. Kelly - 1977 (PB 275 453)A04

UCB/EERC-77/22 "Preliminary Experimental Study of Seismic Uplift of a Steel Frame," by R.W. Clough and A.A. Huckelbridge 1977 (PB 278 769)A08

UCB/EERC-77/23 "Earthquake Simulator Tests of a Nine-Story Steel Frame with Columns Allowed to Uplift," by A.A. Huckelbridge - 1977 (PB 277 944)A09

UCB/EERC-77/24 "Nonlinear Soil-Structure Interaction of Skew Highway Bridges," by M.-C. Chen and J. Penzien - 1977 (PB 276 176)A07

UCB/EERC-77/25 "Seismic Analysis of an Offshore Structure Supported on Pile Foundations," by D.D.-N. Liou and J. Penzien 1977 (PB 283 180)A06

UCB/EERC-77/26 "Dynamic Stiffness Matrices for Homogeneous Viscoelastic Half-Planes," by G. Dasgupta and A.K. Chopra - 1977 (PB 279 654)A06

UCB/EERC-77/27 "A Practical Soft Story Earthquake Isolation System," by J.M. Kelly and J.M. Eidinger - 1977 (PB 276 814)A07

UCB/EERC-77/28 "Seismic Safety of Existing Buildings and Incentives for Hazard Mitigation in San Francisco: An Exploratory Study," by A.J. Meltsner - 1977 (PB 281 970)A05

UCB/EERC-77/29 "Dynamic Analysis of Electrohydraulic Shaking Tables," by D. Rea, S. Abedi-Hayati and Y. Takahashi 1977 (PB 282 569)A04

UCB/EERC-77/30 "An Approach for Improving Seismic - Resistant Behavior of Reinforced Concrete Interior Joints," by B. Galunic, V.V. Bertero and E.P. Popov - 1977

UCB/EERC-78/01 "The Development of Energy-Absorbing Devices for Aseismic Base Isolation Systems," by J.M. Kelly and D.F. Tsztoo 1978 (PB 284 978)A04

UCB/EERC-78/02 "Effect of Tensile Prestrain on the Cyclic Response of Structural Steel Connections," by J.G. Bouwkamp and A. Mukhopadhyay - 1978

UCB/EERC-78/03 "Experimental Results of an Earthquake Isolation System using Natural Rubber Bearings," by J.M. Eidinger and J.M. Kelly - 1978

UCB/EERC-78/04 "Seismic Behavior of Tall Liquid Storage Tanks," by A. Niwa 1978

UCB/EERC-78/05 "Hysteretic Behavior of Reinforced Concrete Columns Subjected to High Axial and Cyclic Shear Forces," by S.W. Zagajeski, V.V. Bertero and J.G. Bouwkamp - 1978

UCB/EERC-78/06 "Inelastic Beam-Column Elements for the ANSR-I Program," by A. Riahi, D.G. Row and G.H. Powell - 1978

UCB/EERC-78/07 "Studies of Structural Response to Earthquake Ground Motion," by O.A. Lopez and A.K. Chopra - 1978

UCB/EERC-78/08 "A Laboratory Study of the Fluid-Structure Interaction of Submerged Tanks and Caissons in Earthquakes," by R.C. Byrd - 1978 (PB 284 957)A08

UCB/EERC-78/09 "Models for Evaluating Damageability of Structures," by I. Sakamoto and B. Bresler - 1978

UCB/EERC-78/10 "Seismic Performance of Secondary Structural Elements," by I. Sakamoto - 1978

UCB/EERC-78/11 Case Study--Seismic Safety Evaluation of a Reinforced Concrete School Building," by J. Axley and B. Bresler 1978

UCB/EERC-78/12 "Potential Damageability in Existing Buildings," by T. Blejwas and B. Bresler - 1978

UCB/EERC-78/13 "Dynamic Behavior of a Pedestal Base Multistory Building," by R. M. Stephen, E. L. Wilson, J. G. Bouwkamp and M. Button - 1978

UCB/EERC-78/14 "Seismic Response of Bridges - Case Studies," by R.A. Imbsen, V. Nutt and J. Penzien - 1978

UCB/EERC-78/15 "A Substructure Technique for Nonlinear Static and Dynamic Analysis," by D.G. Row and G.H. Powell - 1978

UCB/EERC-78/16 "Seismic Performance of Nonstructural and Secondary Structural Elements," by Isao Sakamoto - 1978

UCB/EERC-78/17 "Model for Evaluating Damageability of Structures," by Isao Sakamoto and B. Bresler - 1978

UCB/EERC-78/18 "Response of K-Braced Steel Frame Models to Lateral Loads," by J.G. Bouwkamp, R.M. Stephen and E.P. Popov - 1978

UCB/EERC-78/19 "Rational Design Methods for Light Equipment in Structures Subjected to Ground Motion," by Jerome L. Sackman and James M. Kelly - 1978

UCB/EERC-78/20 "Testing of a Wind Restraint for Aseismic Base Isolation," by James M. Kelly and Daniel E. Chitty - 1978

UCB/EERC-78/21 "APOLLO A Computer Program for the Analysis of Pore Pressure Generation and Dissipation in Horizontal Sand Layers During Cyclic or Earthquake Loading," by Philippe P. Martin and H. Bolton Seed - 1978

UCB/EERC-78/22 "Optimal Design of an Earthquake Isolation System," by M.A. Bhatti, K.S. Pister and E. Polak - 1978

UCB/EERC-78/23 "MASH A Computer Program for the Non-Linear Analysis of Vertically Propagating Shear Waves in Horizontally Layered Deposits," by Philippe P. Martin and H. Bolton Seed - 1978

UCB/EERC-78/24 "Investigation of the Elastic Characteristics of a Three Story Steel Frame Using System Identification," by Izak Kaya and Hugh D. McNiven - 1978

UCB/EERC-78/25 "Investigation of the Nonlinear Characteristics of a Three-Story Steel Frame Using System Identification," by I. Kaya and H.D. McNiven - 1978

UCB/EERC-78/26 "Studies of Strong Ground Motion in Taiwan," by Y.M. Hsiung, B.A. Bolt and J. Penzien - 1978

UCB/EERC-78/27 "Cyclic Loading Tests of Masonry Single Piers Volume 1 - Height to Width Ratio of 2," by P.A. Hidalgo, R.L. Mayes, H.D. McNiven & R.W. Clough - 1978